

DOCTORAL THESIS

Design Optimization Methods of Additively Manufactured Switched Reluctance Motor

Ekaterina Andriushchenko

TALLINN UNIVERSITY OF TECHNOLOGY
DOCTORAL THESIS
16/2023

Design Optimization Methods of Additively Manufactured Switched Reluctance Motor

EKATERINA ANDRIUSHCHENKO



TALLINN UNIVERSITY OF TECHNOLOGY

School of Engineering

Department of Electrical Power Engineering and Mechatronics

This dissertation was accepted for the defence of the degree 12/05/2023

Supervisor:

Prof. Ants Kallaste
School of Engineering
Tallinn University of Technology
Tallinn, Estonia

Co-supervisor:

PhD Toomas Vaimann
School of Engineering
Tallinn University of Technology
Tallinn, Estonia

Opponents:

Dr. Jenni Pippuri-Mäkeläinen
VTT Technical Research Centre of Finland
Espoo, Finland

Dr. Nick Simpson
University of Bristol
Bristol, United Kingdom

Defence of the thesis: 12/06/2023, Tallinn

Declaration:

Hereby I declare that this doctoral thesis, my original investigation and achievement, submitted for the doctoral degree at Tallinn University of Technology has not been submitted for doctoral or equivalent academic degree.

Ekaterina Andriushchenko

signature



European Union
European Regional
Development Fund



Investing
in your future

Copyright: Ekaterina Andriushchenko, 2023

ISSN 2585-6898 (publication)

ISBN 978-9949-83-983-4 (publication)

ISSN 2585-6901 (PDF)

ISBN 978-9949-83-984-1 (PDF)

Printed by Joon

TALLINNA TEHNIKAÜLIKOOL
DOKTORITÖÖ
16/2023

Kihtlisandustehnoloogia abil toodetud samm-mootori optimeerimise meetodid

EKATERINA ANDRIUSHCHENKO



Contents

| | |
|--|-----|
| Contents..... | 4 |
| List of Publications | 6 |
| Author’s Contribution to the Publications | 7 |
| 1 Introduction | 8 |
| 1.1 The Motivation of the Study | 8 |
| 1.2 The Objectives of the Study | 8 |
| 1.3 The Novelty of the Study..... | 9 |
| 2 State of the art of optimization and additive manufacturing of switched reluctance motor | 11 |
| 2.1 Switched Reluctance Motor-Drive | 11 |
| 2.1.1 Design and Control of Switched Reluctance Motors..... | 11 |
| 2.1.2 Challenges of Switched Reluctance Motors Application..... | 14 |
| 2.2 Optimization Environment..... | 15 |
| 2.2.1 Optimization Models..... | 15 |
| 2.2.2 Optimization Algorithms | 24 |
| 2.2.3 Optimization Methods | 25 |
| 2.2.4 Optimization Types and Model/Algorithm Selection..... | 25 |
| 2.3 Additive Manufacturing of Switched Reluctance Motor..... | 26 |
| 3 Optimization and Additive Manufacturing of Switched Reluctance Motor..... | 28 |
| 3.1 Design of Switched Reluctance Motor | 28 |
| 3.2 Proposed optimization method | 31 |
| 3.2.1 Initial Design Optimization | 32 |
| 3.2.2 Sensitivity Analysis | 37 |
| 3.2.3 Topology optimization | 45 |
| 4 Conclusion..... | 49 |
| 5 Future studies | 50 |
| References | 51 |
| Acknowledgements..... | 57 |
| Abstract..... | 58 |
| Lühikokkuvõte..... | 59 |
| Appendix | 61 |
| Curriculum vitae..... | 122 |
| Elulookirjeldus..... | 123 |

List of Publications

The list of author's publications, on the basis of which the thesis has been prepared:

- I **Andriushchenko E.**, Mohammadi M. H., Lowther D. A., Heidari H., Kallaste A. (2022). Topology optimization of a 3D-printed switched reluctance motor. 2022 International Conference on Electrical Machines (ICEM), Valencia, Spain, pp. 1976–1980, 2022.
- II **Andriushchenko E.**, Kallaste A., Mohammadi M. H., Lowther D. A., Heidari H. (2022). Sensitivity analysis for multi-objective optimization of switched reluctance motors. MDPI Machines 10(7), 559.
- III **Andriushchenko E.**, Kallaste A., Belahcen A., Vaimann T., Rassolkin A., Heidari H., Tiismus H. (2021). Optimization of a 3D-printed permanent magnet coupling using genetic algorithm and Taguchi method. MDPI Electronics 10(4), 494.
- IV **Andriushchenko E.**, Kaska J., Kallaste A., Belahcen A., Vaimann T., Rassolkin A. (2021). Design optimization of a permanent magnet clutch with Artap framework. Periodica Polytechnica Electrical Engineering and Computer Science, 65(2), pp. 106–112, 2021.
- V **Andriushchenko E.**, Kallaste A., Heidari H., Belahcen A., Vaimann T., Rassolkin A. (2020). Design optimization of permanent magnet clutch. 2020 International Conference on Electrical Machines (ICEM), pp. 436–440, 2020.

Author's Contribution to the Publications

Contribution to the papers in this thesis are:

- I **Ekaterina Andriushchenko**, as the main author, has carried out the topology optimization of the motor and analysed the results. The paper was written by her.
- II **Ekaterina Andriushchenko**, as the main author, has carried out the sensitivity analysis of the motor and discussed the results. The paper was written by her.
- III **Ekaterina Andriushchenko**, as the main author, has carried out the shape optimization of the permanent magnet clutch using genetic algorithm and Taguchi methods. Ekaterina analysed the results of the optimizations and compared two methods. The paper was written by her.
- IV **Ekaterina Andriushchenko**, as the main author, has carried out the shape optimization of the permanent magnet clutch in collaboration with Jan Kaska and analysed the results. The paper was written by her.
- V **Ekaterina Andriushchenko**, as the main author, has carried out the shape optimization of the permanent magnet clutch and analysed the results. The paper was written by her.

1 Introduction

To date, electrical machines (EMs) and drives have been incorporated into a vast number of industrial processes and applications. Electrical motors are the major users of electrical energy. They consume more than 50% of the global electrical power [1], [2]. Therefore, the efficiency of the electric motors is crucial for sustainable industry development. Optimization is one of the promising approaches to enhancing the efficiency of electric motors [3].

Often, motor optimization can lead to intricate design geometries which cannot be produced using conventional manufacturing techniques [4]. Additive manufacturing (AM) provides wider production possibilities for complex optimized designs and opens new ground for motor efficiency improvement [5].

In this work, the optimization of a Switched Reluctance Motor (SRM) is studied and a novel multi-level optimization methodology is proposed and implemented. Major elements of optimization are reviewed such as optimization models, optimization methods, and algorithms. In the meanwhile, key steps of the SRM design and optimization are presented. Lastly, additive manufacturing possibilities are explored and the initial and optimal designs of the motor are manufactured.

1.1 The Motivation of the Study

SRM has been invented nearly two centuries ago, but there has not been a motivation for its development, due to its low efficiency and loud noise production [6]. Thanks to the rapid growth of advanced power electronics and various control possibilities, the SRMs have now the opportunity to be implemented in the industry [7]. However, not all the problems can be solved by applying power electronic devices to the SRM drive. SR motors have a lot of potentials, yet they own design complications due to their salient nature [8]. Literature shows that optimization of SRMs can help to overcome the SRMs' design issues and considerably improve their performance. On another hand, AM is strong support of motor optimization. Due to the vast design opportunities that AM provides for motor manufacturing, optimization can be carried out at a more delicate level [9]. Hence, this thesis was motivated by the optimization of an additively manufactured SRM using sophisticated optimization techniques.

1.2 The Objectives of the Study

The objective of the study is to carry out SRM design and optimization to increase the average torque of the motor, reduce core material consumption, and decrease the torque ripples. This work starts with the review and assessment of the optimization environment elements such as models, methods, and algorithms to gain a deeper understanding of optimization principles. Prior to the optimization, this study designs an SRM utilizing the classic SRM design method. Then, a new multi-level optimization methodology is proposed based on a promising optimization method – topology optimization (TO). TO is known to impose a high burden on computational resources [10]. To reduce the computational complexity of TO, the design space is compacted using initial parameter optimization and sensitivity analysis of advanced optimization parameters. Thanks to implementing such an approach, the design space of the whole SRM can be minimized to a very essential and prompting area. High-performance improvement can be noticed after the SRM optimization. Additionally, this work makes

a deep overview of the AM and highlights the AM prospects for the optimization of EMs, in particular, SRMs. Lastly, initial and optimal designs of the SRM are produced employing AM techniques.

The objectives of the study can be summarised as follows:

- Increase the average torque, reduce the torque ripple, and decrease the core material consumption of an SRM using optimization techniques.
- Select an optimization environment suitable for additively manufactured SRM.
- Propose an optimization methodology with reduced computational complexity.
- Design an SRM taking into account AM possibilities.
- Acquire an optimal design of an SRM through the worked-out optimization methodology.
- Verifying results through modeling and prototyping using AM techniques.

1.3 The Novelty of the Study

One of the key elements of the motor optimization process is motor modelling. Motor modeling method plays an important role in defining the quality of the optimization results and time consumption [3]. In this thesis, SRM modeling methods are carefully studied and the classification of the methods is created. Based on the major characteristics such as accuracy, flexibility, rapidity, and simplicity, the SRM modeling methods are compared.

Through a wide literature review, major optimization models, methods, and algorithms of SRM optimization are defined and studied in detail. The importance of the correct selection of these key elements of the optimization can not be overlooked, since it plays the biggest role in the result of the optimization [11]. The models, methods, and algorithms are carefully compared in the scope of the SRM optimization.

In this thesis, the optimization approaches are scrutinized and assessed in detail. The TO approach is found to be promising and beneficial for SRM design, yet it yields extremely high computational costs [4], [12]. To overcome the issue of high computing effort, a novel optimization approach is designed. This approach considerably shrinks out the design space of the TO by carrying out two pre-optimizations: initial design optimization, and sensitivity analysis. The initial design optimization helps to optimize global design parameters such as the diameters of the rotor and stator, and teeth openings. Then, sensitivity analysis explores the influence of the shape of the rotor and stator on the motor performance and helps to define the most crucial areas. These vital areas of the motor geometry are then selected as search spaces of the TO. Thanks to this approach, the search space and, consequently, the time consumption of the TO can be reduced by more than 70%.

As a part of the optimization, sensitivity analysis provides valuable information about the influence of motor design parameters on the average torque and torque ripple of the SRM. This works presents the dependence of the torque characteristic on the tooth angle of the rotor and stator both at the air gap and at the core, eccentric air gap, and additional tooth implementation.

The outcomes of the SRM optimization are the initial optimal design, sensitivity analysis optimal design, and TO optimal design. These three designs not only present a

significant improvement of the SRM's torque characteristics but also contrast different optimization methods revealing their opportunities and challenges.

As a part of this thesis, the initial and optimal designs were produced using AM techniques.

The novelties of the study can be summarised as follows:

- SRM modelling methods are classified. Based on the major characteristics such as accuracy, flexibility, rapidity, and simplicity, the SRM modelling methods are compared.
- Various methods and algorithms are carefully compared in the scope of the SRM optimization.
- A novel optimization approach is designed. This approach considerably shrinks out the design space of the TO by carrying out two pre-optimizations: initial design optimization, and sensitivity analysis.
- As a part of the optimization, sensitivity analysis provides valuable information about the influence of motor design parameters on the average torque and torque ripple of the SRM.
- The outcomes of the SRM optimization are the initial optimal design, sensitivity analysis optimal design, and TO optimal design.
- As a part of this thesis, the initial and optimal designs were produced by means of AM techniques.

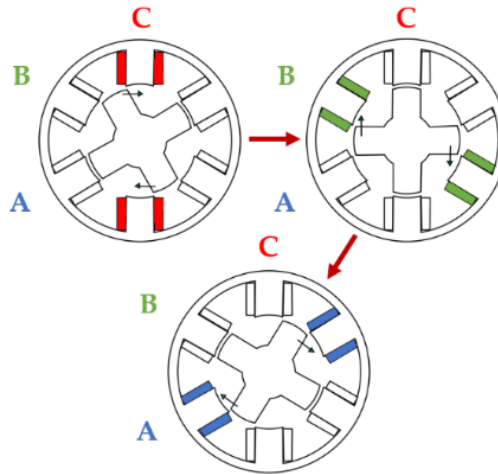


Figure 2-2: Rotation principle of SRM [8].

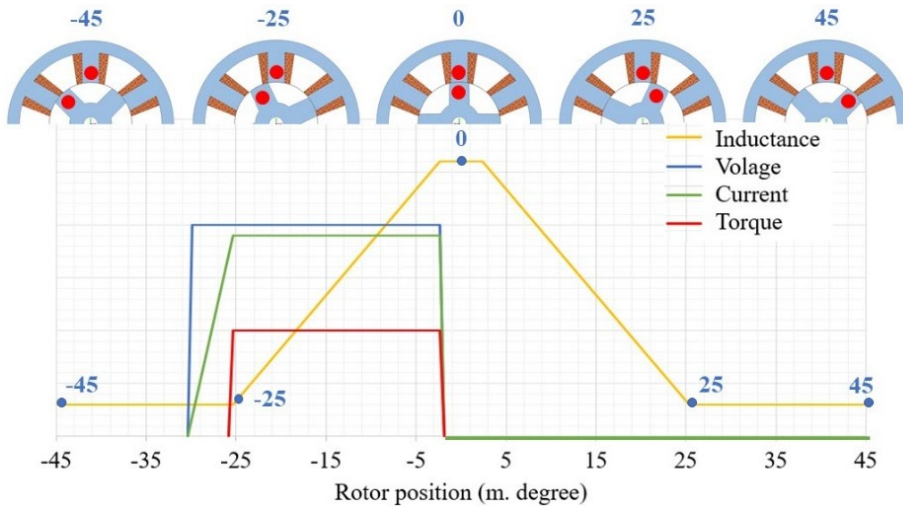
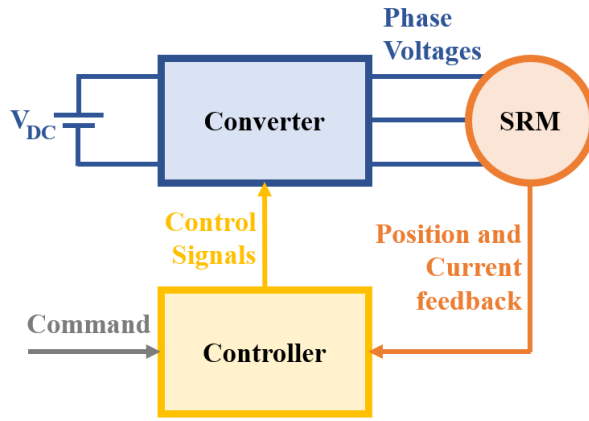


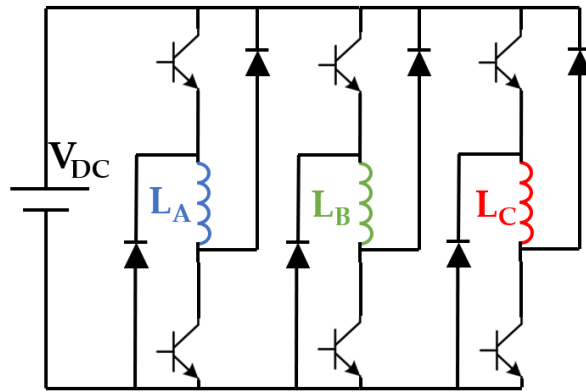
Figure 2-3: Ideal inductance profile of SRM's one phase [8].

A classic drive concept and control scheme of a three-phase SRM is presented in Figure 2-4. It can be seen from the Figure 2-4 (b) that each phase of the motor is controlled autonomously. The SRM control requires two switches per phase, which are controlled by the rotor position and current. The rotor position control is necessary in order to switch the driving phases at the right moments, and the current control is required to regulate the defined reference current value.

Frequently, the phase inductance profile of SRM defines the commutation pattern of the drive. For the three-phase SRM, the duration of the inductance growing phase is 30 mech. deg. Consequently, each of the phases should be turned on for 30 mech. deg with a step of 90 mech. deg. Yet, there are drive circuits that involve the overlapping of two phases with each other (see Figure 2-5).

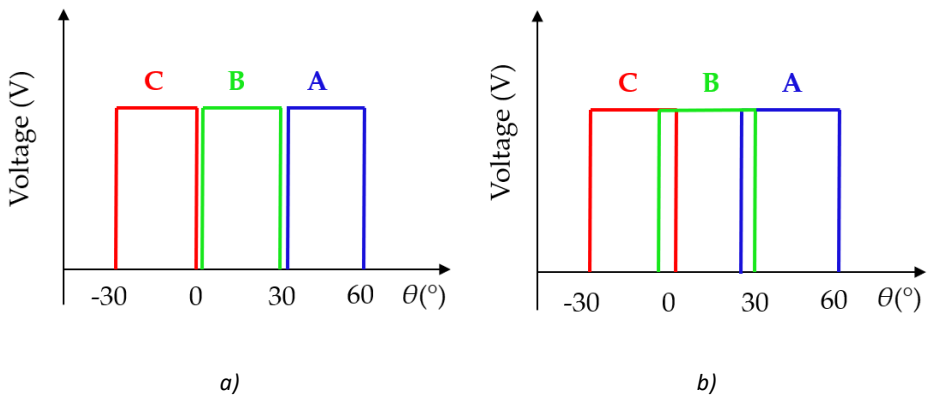


a)



b)

Figure 2-4: SRM drive: (a) SRM drive concept; (b) Asymmetric bridge converter [8].



a)

b)

Figure 2-5: Commutation pattern of three-phase SRM drive [8].

2.1.2 Challenges of Switched Reluctance Motors Application

A key challenge of the SRM application is closely related to the inductance profile of the motor phases. The inductance profile presented in the Chapter 2.1.1 is called the “ideal inductance profile”. It can be used for simplified estimation of the motor behavior. In reality, the inductance profile of the SRM is non-linear and called the “real inductance profile” (see Figure 2-6). Due to the salient nature of the SRM, its phase inductance is growing non-linearly due to the appearance of the fringing flux at the beginning of the rotor and stator teeth overlap (see Figure 2-7). The nonlinearity of the inductance leads to the nonlinear growth of the current and torque. Therefore, the SRM is characterized by high torque ripple and, thus, high vibration and noise levels while operating.

To overcome the issue of the torque ripple, the researchers have defined two solid approaches. One approach is related to the control of the motor. It has been shown, that the correct definition of the commutation parameters and currents can considerably improve the torque characteristics of SRMs. Another approach is focused on motor design and optimization. The literature presents many examples of torque improvement thanks to the introduction of certain teeth shapes of both stator and rotor.

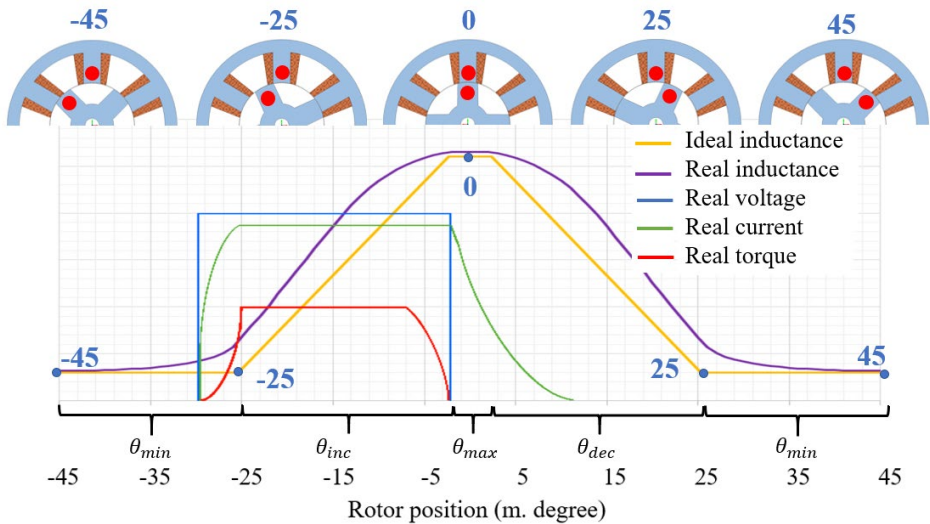


Figure 2-6: Ideal and real phase inductance comparison [8].

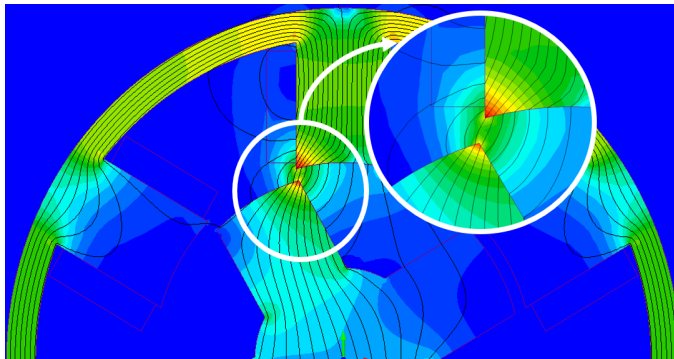


Figure 2-7: Fringing flux at the beginning of overlap [8].

2.2 Optimization Environment

Recent literature shows, that optimization is an effective tool that is used to improve the performance of EMs. For the EMs, optimization is a process of finding a set of design or control parameters that leads to the best (targeted) performance characteristics of the motor. The key elements of an optimization are the optimization model, optimization method, and optimization algorithm.

2.2.1 Optimization Models

An optimization model can be defined as a mathematical or numerical formulation of an optimization task. Usually, an optimization model includes:

1. The objective function, defines the aims of optimization such as maximization of average torque, maximization of torque density, minimization of torque ripple, minimization of mass, etc;
2. Constraints, define certain limits necessary for the optimal result such as iron losses less than 10 W, average torque more than 100 N, iron volume less than 10 l, etc. The objective function and constraints are sometimes interchangeable depending on their formulation and importance for the targeted designs;
3. Optimization parameters, which define the geometrical or control parameters of the motor. By varying the optimization parameters, an optimal set of them can be found that leads to the best-targeted performance of the motor.

The optimization model is responsible for forecasting the objectives and constraints for a particular set of optimization parameters. The optimization model can be defined as an analytical, numerical, or magnetic circuit (MEC) model. Basically, an optimization model is a design model which has the freedom to change design/control parameters in order to search for their optimal set.

In general, the design of an SRM involves several stages such as electromagnetic analysis, structural analysis, and thermal analysis. Usually, for each of these stages, a model should be created. In this thesis, only the electromagnetic basis of the optimization will be covered. Therefore, this section will be focused on the electromagnetic modeling of SRMs. Yet, some overview is given for thermal and structural analysis.

The main task of the electromagnetic modeling of an SRM is to find out the relation of the flux linkage ψ , phase voltage V , phase current i , and phase resistance R . Then, the key performance characteristics can be defined such as torque, losses, and efficiency.

$$\frac{d\psi}{dt} = V - Ri \quad 2.2$$

As it was mentioned in Chapter 2.1.2, the great challenge of the SRM design is the nonlinearity of the inductance of the SRM. Together with the operation under high saturation, these two specialties of SRMs bring a great challenge to the simulation of the motor.

This section gives a deep overview of the SRM modeling methods such as analytical methods, numerical methods, and the magnetic equivalent circuit (MEC) approach [13].

2.2.1.1 Magnetic circuit approach

The MEC method has been extensively used for modeling EMs owing to its simplicity and fast results prediction [14]–[21]. Yet, the accuracy of this method is quite low since it often can not take into account such processes as fringing flux or high saturation of SRMs (see Figure 2-8). The working principle of the MIC is illustrated in Figure 2-9. As can be seen from the figure, each core element of the SRM is represented by a gray rectangle or permeance. Then, each winding is illustrated as a circle. Lastly, the dashed line represents the airgap permeances [14]. Using the scheme presented in Figure 2-9, a system of equations is built and solved based on the circuit laws.

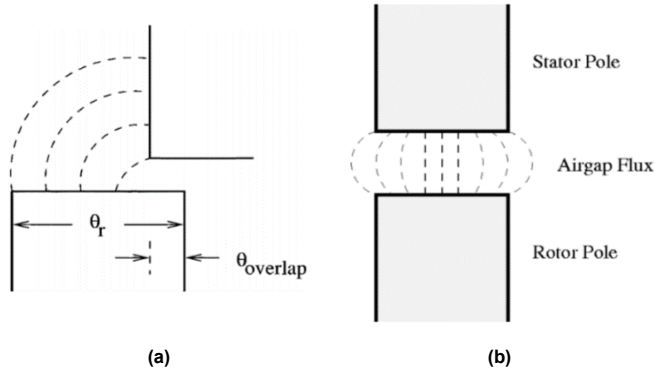


Figure 2-8: (a) Fringing effect in partial overlap position; (b) Fringing effect in complete overlap position [2].

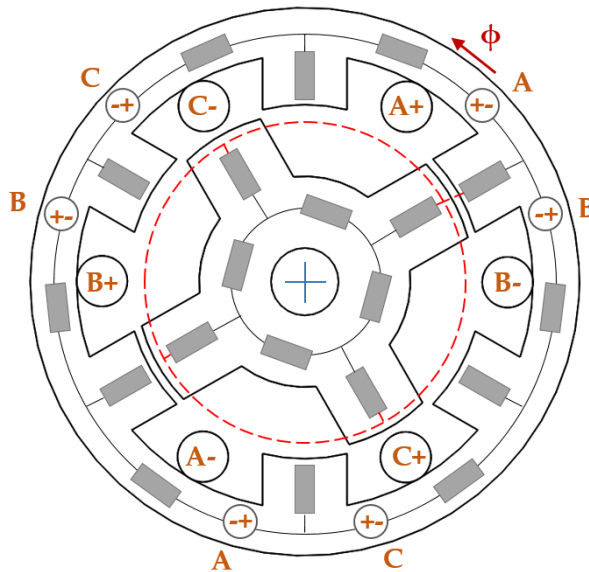


Figure 2-9: Magnetic circuit model of SRM [2].

To overcome the issue of lower accuracy, researchers attempted to take into account the high saturation of the rotor and stator pole tips by dividing the teeth into areas with different permeabilities [14]. Moreover, recent literature shows that the fringing effect

of the stator and rotor poles can be taken into account by appending the fringing air-gap permeance into MIC [19], [20]. For certain rotor positions, these MEC improvements lead to an accuracy comparable with the FE method while keeping the computation efforts low. Additionally, the MEC approach can be applied with the support of the FE method analysis [16]–[18]. The literature review showed, a 3D MEC method successfully combined with the FE-calculated fringing effect parameters [18]. This united technique has been validated by experimental results with high accuracy (see Figure 2-10).

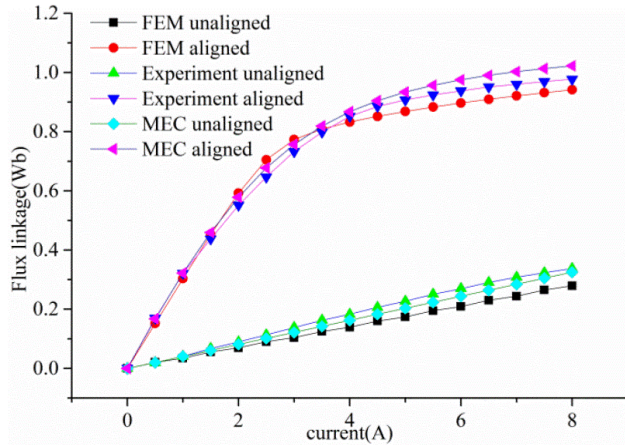


Figure 2-10: Comparison of flux linkage curves obtained by FEM, MEC, and experiment [6].

To the author’s knowledge, no literature presented the implementation of the MEC approach or MEC approach assistant by the FE method toward the optimization of SRM. A possible reason can be that there are limited possibilities to comprehensively parametrize the SRM within the MEC method. Basically, the freedom of the motor geometry modeled with MEC is relatively low, so the results of the optimization can hardly be significant.

2.2.1.2 Analytical approaches

For many years, analytical approaches have been broadly used for SRMs modeling. The analytical methods can be classified as follows:

- 1) Maxwell’s equation-based method
- 2) Interpolation methods
 - a) Lookup table-based interpolation method [22], [23]
 - b) Artificial neural network (ANN) based interpolation method [24]–[27]
 - c) Fourier-series-based interpolation method [28]–[31]

Maxwell’s equation-based method utilizes the magnetic potential \mathbf{A} together with Maxwell’s equations for solving 2D or 3D magnetic problems.

$$\nabla \times \mathbf{A} = \mathbf{B}, \nabla \cdot \mathbf{A} = 0 \quad 2.3$$

where \mathbf{B} is the magnetic field density. Together with Maxwell’s equation, equation 2.3 becomes:

$$\nabla^2 \mathbf{A} = -\mu \mathbf{J} \quad 2.4$$

where \mathbf{J} implies the current density and μ presents the magnetic permeability.

Maxwell’s method presents good accuracy and reliability, yet high computational complexity. Much research has been done on Maxwell’s method applied to SRM simulation [32]–[34].

To obtain the phase inductances of the SRM at arbitrary rotor positions, Sufei Li et al. devised a method employing Maxwell’s equation and conformal mapping technique. As it is shown in Figure 2-11, the proposed technique has a decent agreement with the FEA [33]. The alternative method offered in [34], simulates the magnetic field of the SRM operating under high saturation. The presented nonlinear analytical model has shown a positive correlation with FEM unlike the linear one (see Figure 2-12).

The MEC method, Maxwell’s equation-based approaches, and FEA require separate consideration of each operating condition of the machine. By contrast, the interpolation techniques propose models that can predict the performance of the machine based on a limited number of simulations or experimental tests. Therefore, a common feature of interpolation techniques is time efficiency.

A good example of an intuitive interpolation technique is presented in [23]. The authors utilized FEM analysis to construct a lookup table of the inductance characteristic depending on the rotor position and excitation. Using the lookup table along with a MEC, the dynamic characterization of the SRM was obtained. The benefit of this approach is that it is quite clear and smooth; however, its accuracy is not reasonable for some applications [29].

Nowadays, artificial neural networks (ANNs) based techniques are one of the most well-known tools for the interpolation of experimental or simulation data. ANNs have been extensively employed in numerous applications from forecasting and trends to signal processing and design optimization.

ANNs are essentially computing systems, which concept is inspired by the biological neural networks of human brains. Figure 2-13 illustrates the ANN working principle.

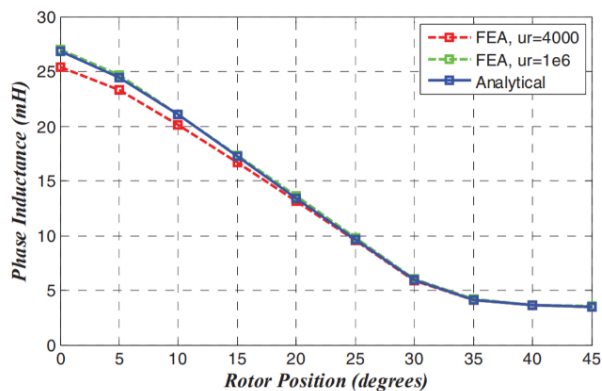


Figure 2-11: Comparison of the proposed analytical approach with FEA.

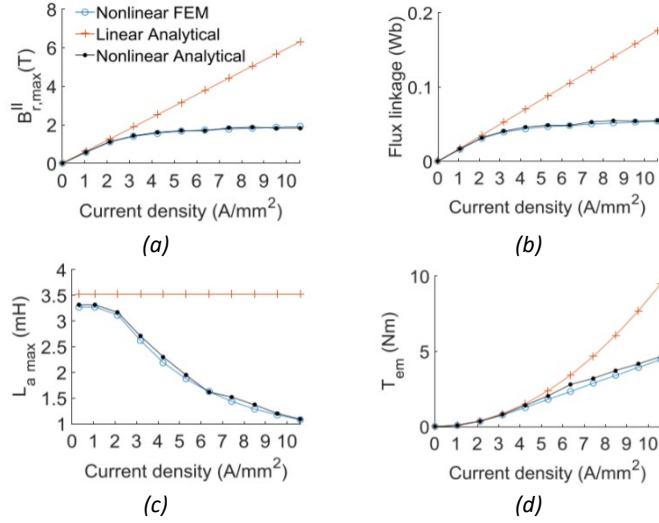


Figure 2-12: Performances versus current density with excitation in one phase. (a) Radial peak flux density values. (b) Flux linkage. (c) Maximum self-inductance. (d) Electromagnetic torque [22].

The neurons, which are the main components of a neural network (NN), accept inputs X_i , $i=1..n$. Then, the inputs together with the bias θ are multiplied by corresponding weight parameters. After that, the weighted inputs can be summed up to a set called net and then send to an activation function. Another way is to use a separate activation function for each weighted input and then, adding the bias, sum them up. The calculated result proceeds to the output. Additionally, Equation 3 illustrates the working principle of NN mathematically [35].

$$S = \sum_{i=1}^n w_i \cdot X_i + w_0 \cdot \theta,$$

$$\Omega_1 = f(S), \quad 2.5$$

$$\Omega_2 = \sum_{i=1}^n f_1(w_i \cdot X_i) + w_0 \cdot \theta,$$

where S introduces the set of the weighted inputs or net, while Ω demonstrates the set of outputs. Particularly, Ω_1 illustrates the case when the activation function is applied to the net S and Ω_2 illustrates the case when the activation function is applied to each weighted input.

Parameters of a NN such as weights and threshold of the inputs are defined through training a NN model. The activation functions are chosen by a user through experiments.

The ANN techniques have demonstrated several remarkable features, which are particularly useful in SRM design and simulation. For example, one of the unique qualities of ANNs is the ability to interpolate highly nonlinear systems. This quality is exceptionally valuable for modeling the nonlinear electromagnetic characteristics of the SRM. Moreover, previous research has demonstrated another advantage of the ANNs – the high accuracy of the interpolation models. On the other hand, the model's accuracy is greatly dependent on the training process and the provided training data.

An early example of the ANN application in the SRM design is presented in [26].

The research proposed a discrete-time model, which could simulate a faulty and fault-free SRM. The authors constructed a reliable ANN architecture with the support of the evolutionary algorithm (EA).

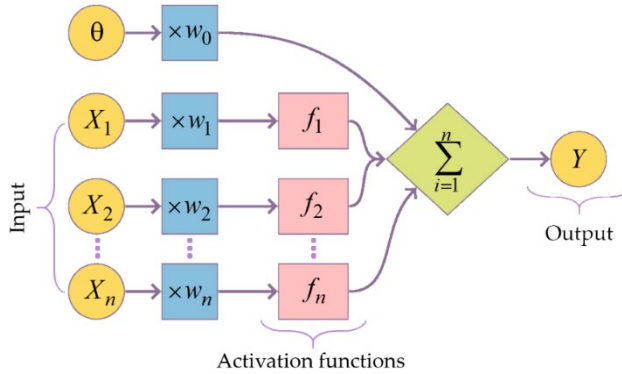


Figure 2-13: ANN working principle.

In a study conducted by W. Ding et al., the adaptive neural fuzzy inference system (ANFIS) techniques were used for modeling the SRM [36]. The researchers have been able to form an accurate and comprehensive SRM model verified by experimental data. Relatively recent research successfully utilized B-Spline NNs for online modeling of the SRM [37]. The online training of the B-Spline NN provided the obtained model with high robustness and accuracy.

To date, researchers have developed a list of effective methods based on the Fourier series for the SRM simulation. The following equation represents the considered Fourier series:

$$\lambda(i, \theta) = \sum_{k=0}^2 f_k(\theta) \cos(k\theta), \quad 2.6$$

where λ is the phase flux linkage, $f_k(\theta)$ are the series coefficients, i and θ are the phase current and the electric angle of the rotor, respectively.

Thanks to the possibility to change the number of Fourier terms used for interpolation, this approach proposes high flexibility of accuracy. Another advantage of this method is that the amount of data required for approximation is considerably lower than for the ANN interpolation method or FEM. Using a second-order Fourier series, S. Song et al. proposed a way to approximate the flux linkage of the SRM. Working just with 21 data points for determining the series coefficients, this method could demonstrate a good agreement with the test results (see Figure 2-14) [38]. A simple and reliable model of the SRM for real-time controller implementation was introduced in [30]. Additional consideration of the machine's geometry and materials makes this approach suitable within the design stage. Another good example of Fourier series usage for SRM modeling was presented in [39]. The researchers could successfully estimate the flux linkage profile without using complex and costly clamping devices and position sensors.

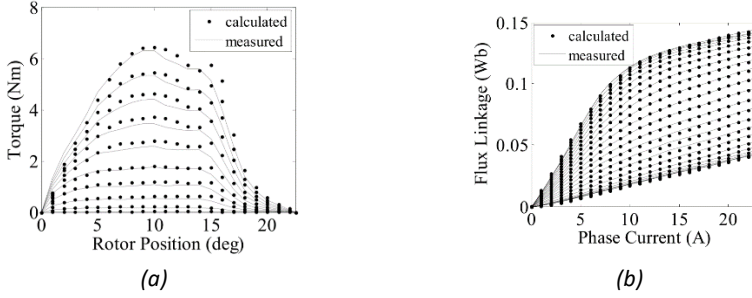


Figure 2-14: Calculated and measured SRM magnetic and torque characteristics [38].

There are not many papers, which show the implementation of the analytical methods within SRMs optimization. Yet, a new method called multiphase excitation used for the calculation of static torque taking into account the cross-coupling and magnetic saturation is introduced and utilized within the parameter optimization [40].

Another model widely utilized within the SRM optimization is a surrogate model. A surrogate model was initially developed for reducing the computational complexity of the optimization compared to FEM and obtain more precise results than through analytical methods. Basically, a surrogate model is a set of mathematical expressions which replace the FEM constructed using the design of experiment or ANN techniques. An example of the surrogate model utilization within the SRM optimization is presented in [41], where the flux linkage and torque characteristics are represented by the approximate models which are based on the data gained from the FEM.

2.2.1.3 Numerical Approaches

Simulating the SRM nonlinear behavior with good accuracy is a great challenge for researchers. Despite the merits of the MEC approach or analytical methods, the finite element method (FEM) is the most widely used way to model the SRM.

Principally, a FE model of an electromagnetic device is made up of finite elements, which carry the following information: geometry, materials, excitations, and constraints. A simple variation of the electric and/or magnetic potential exists within each finite element. Based on that, FE computing solves all the unknown electric and magnetic potentials and the associated fields. The classic formulation of the electromagnetic problem in FEA is A- ϕ (magnetic vector potential – electric scalar potential) formulation:

$$\begin{cases} \mathbf{B} = \nabla \times \mathbf{A} \\ \mathbf{E} = -\nabla\psi - \dot{\mathbf{A}}, \dot{\psi} = \varphi \end{cases} \quad 2.7$$

where B and E illustrate the magnetic and electric fields, respectively. Then, the final mathematical expression of a FE problem is the following:

$$[\mathbf{M}] \begin{Bmatrix} \dot{\mathbf{A}} \\ \dot{\psi} \end{Bmatrix} + [\mathbf{B}] \begin{Bmatrix} \mathbf{A} \\ \psi \end{Bmatrix} + [\mathbf{K}] = \{F_1(t)\} + \{F_2(t)\} \quad 2.8$$

where the A-partition of the equation illustrates Ampere's law, including induction and displacement currents, while the ψ -partition represents the charge continuity condition. Matrixes M, B, K are finite element matrices representing dielectric, conductivity, and reluctivity properties. The two load vectors F1 and F2 represent volume current loads and surface loads.

One of the primary benefits of the FEM is the ability to find an accurate solution for a

machine with complex, intricate geometry. Furthermore, this method can easily deal with anisotropic materials with nonlinear permeability. All these advantages make it particularly valuable in the SRM design.

There exists a considerable body of literature on the SRM simulation using the FEM [42]–[45]. To reduce the torque ripple of an SRM, an optimum rotor design has been found in [42] using the 2D FEM. Later, K. Kiyota et al. researched an SRM, where 2D and 3D-FEM analysis results were carefully compared with the tests (see Figure 2-15). It has been shown that the 3D-FEM analysis was capable of providing an accurate solution for an SRM design with an error of less than 5% [43].

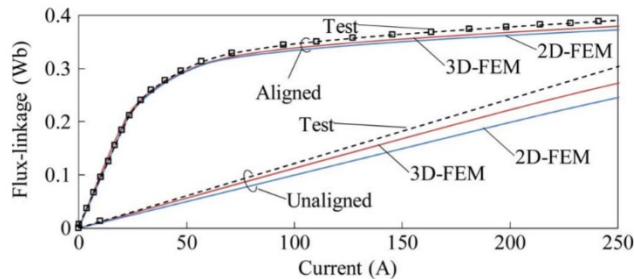


Figure 2-15: Flux linkage curve of the SRM [43].

Unfortunately, the 3D-FEM approach results in problems related to the model’s meshing. The mesh in a 3D-FEM model should have a high number of finite elements to achieve good accuracy. This makes up for the problem of high computational complexity and long execution time. This turns out to be even more problematic within an optimization, where thousands of machine designs should be analyzed. Certainly, the 2D-FEA can obtain simulation results much quicker compared to the 3D-FEA. However, the following limitations do not allow it to replace the comprehensive 3D-FEA:

- Alteration of material properties along the axial direction cannot be taken into account;
- Consideration of the machines with axial-field topologies is not possible;
- The flux linkage in the end-winding region is neglected;
- Eddy current losses related to steel lamination are not considered;
- Design features along the axial direction cannot be taken into account.

Despite the challenges of the FE implementation, many researchers have been intensively working toward 3D-FEA optimization. Several techniques have been proposed to improve the efficiency of 3D-FEA, some focusing on T- Ω (electric vector potential – magnetic scalar potential) problem formulation [46]–[48], others on the domain [49] or time decomposition [50]. These methods help to achieve a considerable reduction in the simulation time.

A huge amount of literature focuses on SRM optimization using FEA. For example, an SRM utilized in low-speed electric vehicles is multi-objectively optimized base on a FEM and the vehicle balance equations in [51]. In another paper, an SRM for high-volume traction applications is optimized by taking into account the control algorithm using FEA [52]. For SRM optimization, FEM proposes a great opportunity to create complex intricate geometries that is hardly possible using MEC or analytical techniques.

2.2.1.4 Modeling approaches comparison

To summarize the strengths and weaknesses of the modeling methods discussed in this section, Figure 2-16 is provided. In the figure, orange bubbles show the main groups of the electromagnetic design methods, and cyan bubbles illustrate a particular method. The methods are assessed in terms of accuracy, rapidity, flexibility, and simplicity. Each of these specifications has a particular color, which is assigned or not to a particular method. For instance, the highlighted attributes of the methods based on ANN are high accuracy and flexibility.

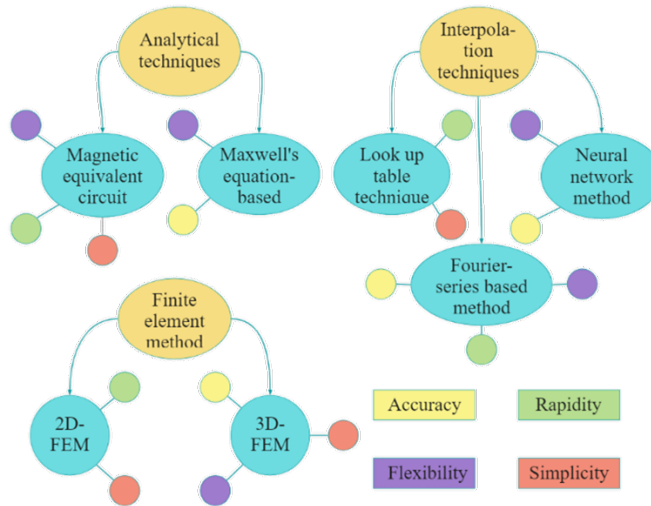


Figure 2-16: Comparison of electromagnetic analysis methods of SRM.

2.2.1.5 Structural and Thermal Analysis

Structural and thermal analysis are the important stages of motor development and optimization. Sometimes, due to the optimization, structural characteristics such as mechanical strength or manufacturability can be reduced. Therefore, for certain optimization problems, it is worth carrying out mechanical analysis after or during optimization. The key aspects of structural analysis are the following [53]:

- Mechanical stress/strain analysis
- Buckling analysis
- Vibration and noise analysis

Specifically, the mechanical stress/strain analysis is associated with a test of strength and aims to reveal whether the machine's structure and its components are able to bear the intended load without failure. By means of the buckling test, a designer ascertains that the machine and its components will not lose their stability. Finally, the vibration and noise analysis not only ensures that the machine's operation is stable but also guarantees that the noise produced by the machine is acceptable for the work environment.

Another key thing to remember within the structural analysis is an assessment of manufacturability. This process involves a determination of geometric dimensions and tolerances, setting up an appropriate fitness between mechanically mating parts of the machine.

It is known that one of the primary issues of SRM is the torque ripple and, consequently, the vibration and acoustic noise. The vibration and noise not only adversely affect the performance of the machine and its safety but also can be harmful to a human being. Moreover, the undesired vibration can easily damage the SRM parts such as stator windings, and rotor bearings, and even lead to failure. The vibration problem can be solved by approaching it through electromagnetic analysis and reducing the torque ripple. Additionally, the electromagnetic problem can be transferred to the mechanical analysis software and the vibration characteristics can be assessed directly [54]–[58].

Thermal analysis plays an important role in SRM design and optimization. The temperature of the machine strongly affects its performance, insulation life, mechanical strength, reliability, etc. Therefore, it is often important to check the thermal stability of a final optimization design or include the thermal characteristics in the optimization of SRM. The recent literature on EM design and analysis shows two major approaches used to carry out a thermal analysis. The first one is based on the equivalent heat circuit (EHC) [59], while the second employs numerical techniques such as computational fluid dynamics (CFD) and FEM [55], [60], [61], [62].

2.2.2 Optimization Algorithms

Using the optimization model, an optimization algorithm is aimed to find optimal designs, so-called sets of design parameters. An optimization algorithm is a set of mathematical operations which search for the best available alternative taking into account given constraints. So far, many optimization algorithms have been developed. Within the optimization of electrical machines, evolutionary algorithms, and particle swarm optimization algorithms appear to be the most prevalent.

The group of evolutionary algorithms (EAs) includes single- and multi-objective genetic algorithms, evolution programming, and evaluation strategy. All of these are inspired by biological evolution and use the knowledge of evolution's mechanisms such as reproduction, recombination, selection, and mutation. An overview of the EAs' terms and operations can be found in [63].

The evolutionary algorithms are widely applied in EM and electromagnetic device optimization. An example of an optimization of geometrical and control parameters of SRM using a non-sorting genetic algorithm II (NSGA-II) is presented in [52]. In another paper, the authors propose a new design optimization outline utilizing a fast-current profile estimation method and multi-objective differential evolution algorithm (DE).

As it is shown in the literature, the EAs have exceptional qualities. High algorithm flexibility, fast search space narrowing, and the capacity to find a global minimum are the main advantages to name. Yet, the optimization of the SRM using EAs can be computationally expensive.

The particle swarm optimization algorithm (PSO) is based on the birds' flock movement and was initially designed to simulate social behavior. This method defines a candidate solution and using a sequence of iterations tries to improve it. A comprehensive description of the algorithm theory and implementation can be found in [64]. There are many examples of PSO implementation for EM optimization. However, rarely it is used for SRM. One article presents a surrogate model coupled with the PSO algorithm for the multi-objective optimization of an SRM [64].

2.2.3 Optimization Methods

An optimization method is basically a procedure that solves the optimization problem using the optimization model and algorithm. There are three main groups of optimization methods used within the SRM design optimization: direct, indirect, and statistical optimization methods. The direct optimization method is a method that involves the direct interconnection of an analytical or FE model with an optimization algorithm. The indirect optimization method is one that uses a surrogate model for solving the optimization problem. And statistical optimization method involves a robust optimization model. As can be noticed, the key element that defines the optimization method is the optimization model.

2.2.4 Optimization Types and Model/Algorithm Selection

The selection of the modeling methodology and optimization algorithm strongly depends on the type of optimization and computational resources available. There are three types of SRM optimization:

- Parameter optimization [10]
- Shape optimization [63], [65]
- Topology optimization [10], [12]

Parameter optimization is an optimization where the geometry is controlled by linear and angular dimensions. Within the parameter optimization, the geometry always remains conventional. Therefore, the analytical modeling resources or FEA can be used for direct parameter optimization.

Shape optimization is an optimization where the geometry is controlled by surface lines, defining the shape of the motor. And topology optimization is an optimization where the geometry is defined by material distribution, sometimes, over the whole body of the motor. In the case of shape and topology optimizations, it is hardly possible to use analytical methods alone, due to the intricate shapes (or topologies) of the motor geometry. Moreover, there is no solid knowledge regarding the influence of various geometries of the motor on its performance. Therefore, the possible methods to be applied within the shape and topology optimization are the numerical method – FEM and partially numerical, partially analytical – surrogate modeling.

One of the promising but not yet widely applied optimization models within the SRM optimization is a robust optimization model. The key feature of a robust optimization model is that takes into account the manufacturing tolerances of a particular design and uses them while determining an optimal solution. In contrast with other optimization models where the aim is to define a global optimum, the robust optimization searches for a robust minimum which has a lower sensitivity to parameter variations. The optimization methods and algorithms associated with the robust optimization model are usually statistical and refer to the design of experiment (DoE) and Taguchi methods. An example of a robust optimization of an SRM is presented in [66], where the manufacturing tolerances are taken into account to ensure the robustness of the optimal solution.

Figure 2-17 compares the optimization models, methods, and algorithms discussed in this section.

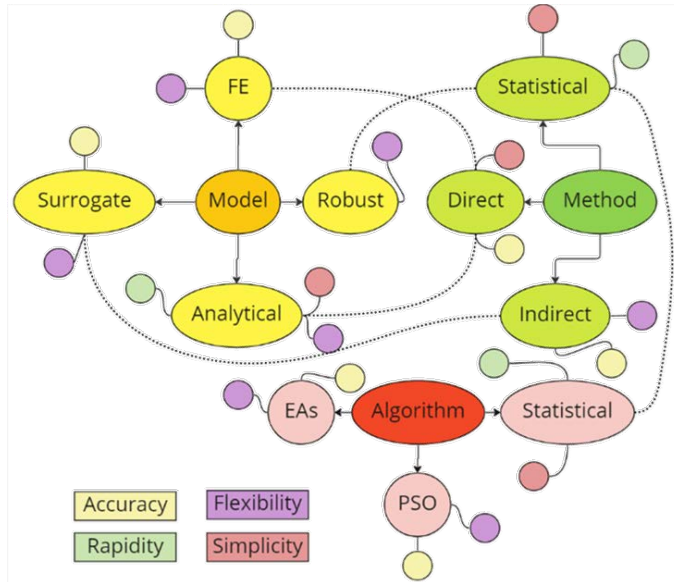


Figure 2-17: Comparison of methods, models, and algorithms for SRM optimization.

2.3 Additive Manufacturing of Switched Reluctance Motor

Up to now, the key considerations that an engineer should have been taking into account are the manufacturability of a machine element and the possibility to assemble elements of a machine together. The restrictions of shapes and topologies have been always accompanying the EM design. Nowadays, additive manufacturing is a promising way of EM production thanks to the geometry freedom it proposes. AM is a great chance to produce various shape and topology optimization solutions with enhanced performance, which is hardly possible with conventional manufacturing techniques. An example of topology optimization and its initial results can be found in [10].

Previous research has shown several examples of additively manufactured electromagnetic materials and EM. The soft magnetic material properties were explored in [67], where the rotor of an SRM was printed together with a conventional stator, and the performance of the SRM was assessed. Figure 2-18 presents the segments of a 3D-printed SRM rotor. The methodology of soft magnetic core manufacturing using 3D printing was presented in [68]. Moreover, the author showed the implementation of the developed methodology for printing an induction motor (IM) and conducted a comparative analysis with a conventional counterpart. The 3D-printed IM and the model of its inner structure are presented in Figure 2-19.

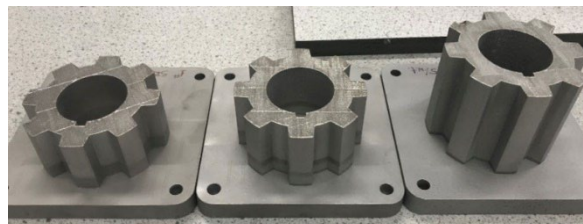


Figure 2-18: Segments of a 3D-printed SRM [67].

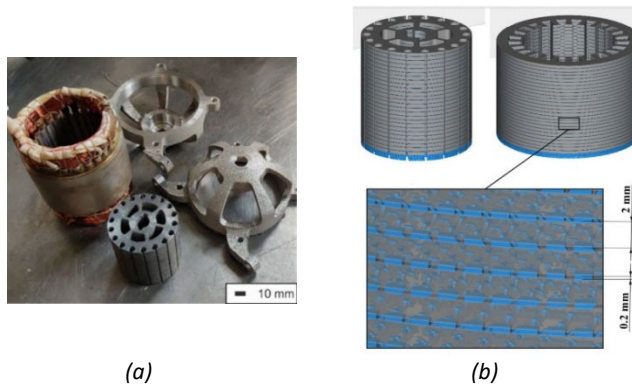


Figure 2-19: (a) 3D-printed IM; (b) rotor and stator core design [67].

Through the literature review, several challenges that AM development faces were revealed. It is well known that using conventional manufacturing techniques, the price of a single product decreases with the growth of the number of parts produced. In contrast with conventional manufacturing, AM does not allow the price of a part in mass production to decrease compared to a price of an individually produced part. In other words, an additively manufactured part will be the same expensive in mass production as in prototyping, because the amount of time and energy required to produce a part is the same [69]. Another challenge more related to EM basic characteristics is the eddy current which appears in a printed core of an EM. Due to the solid structure of the printed core and absence of laminations, EM experiences very high eddy current which can lead to poor performance and high core losses. Yet, there are promising possibilities of using lattice structures or lamination-like structures to reduce the eddy currents and achieve the performance presented by conventional EM as is presented in Figure 2-19 (b) [68], [70], [71]. Nowadays, AM has a limitation of using only one powder material for part production. Yet, for manufacturing automation and meeting the tolerances, it is necessary to use several materials how, for example, in coil manufacturing [72], [73].

Nevertheless, AM is a promising manufacturing possibility that is beneficial for the production of topologically optimized designs. Yet, the challenges presented in the previous paragraph should be addressed in the future.

3 Optimization and Additive Manufacturing of Switched Reluctance Motor

3.1 Design of Switched Reluctance Motor

Creating an initial design of an SRM has a quite well-established way. Usually, the key geometrical parameters such as bore diameter (D_r), and stuck length (L_c), have a direct relation to the output of the SRM.

$$T_e = K \cdot D_r^2 \cdot L_c \quad 3.1$$

where T_e is the output torque and K implies the output coefficient which is related to the electromagnetic loadings of the motor. The values of the output coefficient vary between 10 to 35 kN/m².

The next important step in creating the SRM design is to select the air gap length. Obviously, a smaller air gap in an SRM provides a higher inductance ratio and higher torque density. In this thesis, the air gap was set to the minimum possible to achieve according to the available tolerance limits of the manufacturing and was equal to 0.3 mm.

After defining the air gap, the stator inside diameter D_{si} and outside diameter D_{so} can be defined.

$$D_{si} = D_r + 2g, \quad D_{so} = (1.5 - 1.8)D_{si} \quad 3.2$$

where g is the air-gap length. The coefficient in front of D_{si} strongly depends on the number of stator poles. In this thesis, three phases 6 stator pole and 4 rotor pole SRM was considered. Therefore, a bigger coefficient was selected. Due to the size limitation of the 3D-printing machine to 80 mm, D_{so} was set to 80 mm. Other dimensions such as D_{si} , D_r were derived using equations (3.2) and were equal to 45 mm and 44.4 mm, respectively.

The stuck length of the motor is simply calculated using equation 3.3.

$$L_c = k \cdot D_r \quad 3.3$$

where k implies the length to bore coefficient and varies from 0.25 to 0.70 for non-servo and 1 to 3 for servo applications. In this thesis, the k was set to 1 and led to $L_c = 44.4$ mm.

Another important step of the SRM design is to define the configuration of the coil. Due to the decision not to use any cooling elements such as fans, etc., the current density was restricted to 5 A/mm². For a given current of $i=4$ A, the strand area of a wire was selected as 0.823 mm². The number of turns was selected such that the available winding space will be filled and was equal to 58 turns per coil.

Last but not least, the stator and rotor pole arcs are selected. Usually, to minimize the inductance at the unaligned rotor position, the total arc length of the rotor and stator poles should be shorter than the rotor pole pitch.

$$\beta_s + \beta_r < \frac{2\pi}{N_r} \quad 3.4$$

where N_r is the number of rotor poles. Classic stator and rotor pole values were used in this thesis and were equal to 30 mech deg.

The FE model of the described design was created using Simcenter MagNet software. The geometry of the initial design is illustrated in Figure 3-1. Additionally, the inductance profiles, static and transient torque are presented in Figure 3-2.

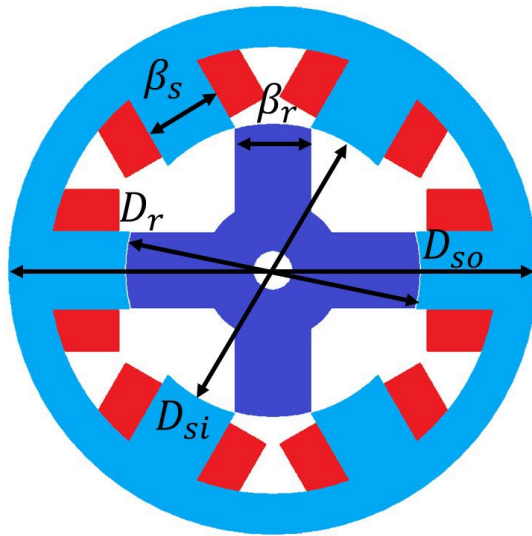
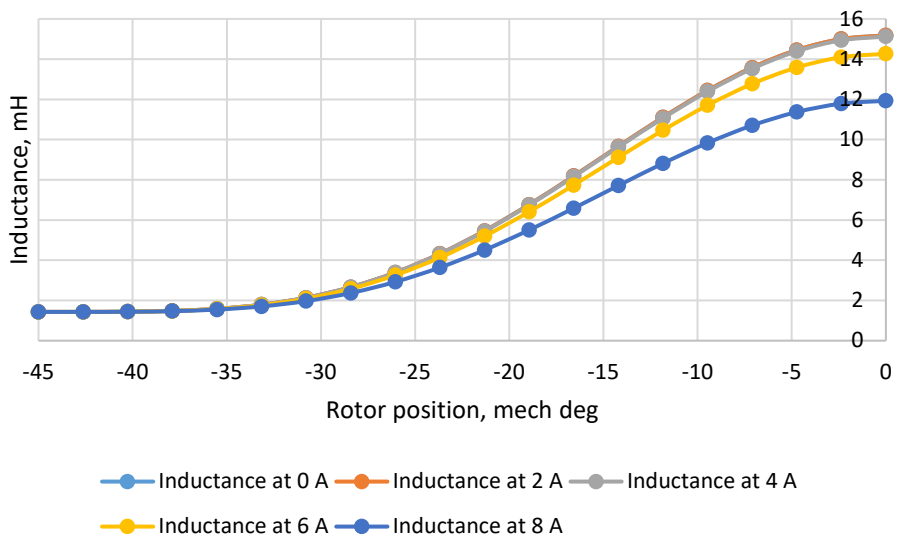
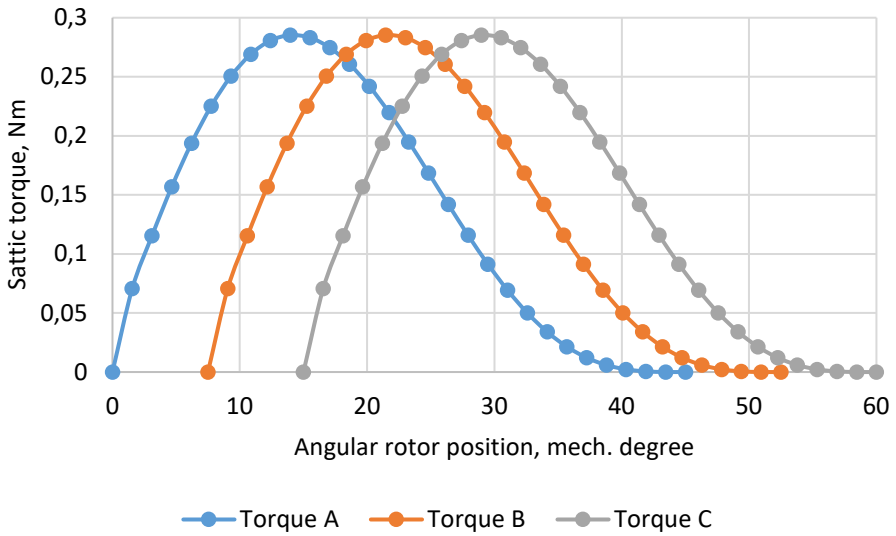


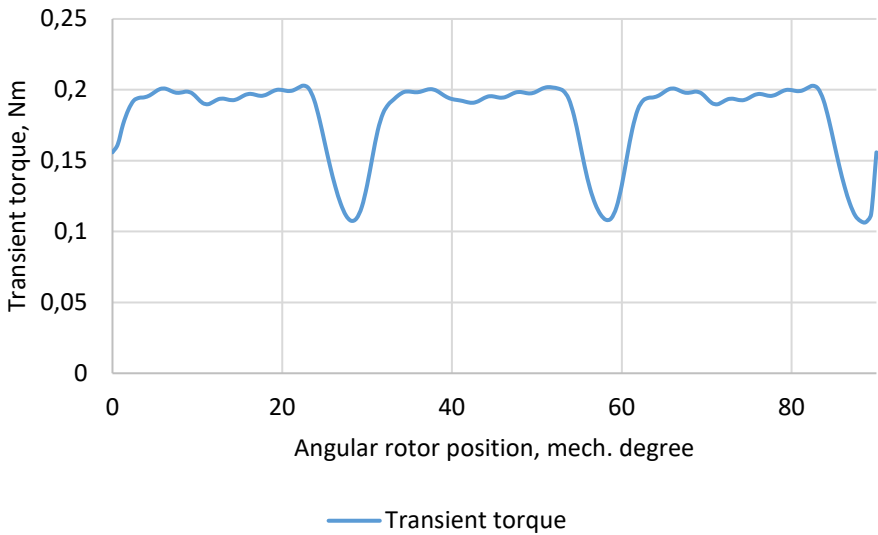
Figure 3-1: Initial design of SRM.



(a)



(b)



(c)

Figure 3-2: Initial design of SRM performance characteristics: (a) real inductance profiles, (b) static phase torques, and (c) transient torque.

3.2 Proposed optimization method

The TO is fast becoming a key instrument in EM optimization. Compared to the other optimization types such as parameter optimization and shape optimization, the TO proposes a vast variety of possible designs with the freedom to change not only the design parameters of SRM or motor shapes, but also the distribution of the material within a whole motor. The TO can play an especially important role in addressing the issue of SRM torque ripple, as geometrically very sensitive performance characteristics of SRM. As it will be shown in this section, design parameters, shapes, and material distribution within an SRM can significantly influence its performance.

In this thesis, turn-on/off topology optimization is considered. Essentially, the turn-on/off TO technique helps to optimize the layout of material in a given design space and includes the following steps: selection of design space, parametrization of the selected design space, and optimization.

The selection of design space for optimization is an important stage that has the biggest influence on the computational complexity and quality of optimization. The bigger the design space, the higher number of parameters needs to be used, consequently, the higher the computational burden is. It is essential to define the design space with optimal size and optimal location within a motor geometry. Depending on the objective of the optimization, the most influencing areas of an SRM need to be included in the design space. In this thesis, with the aim of reducing the computational complexity of TO, the design space was compacted using initial parameter optimization and sensitivity analysis of advanced optimization parameters. Thanks to implementing such an approach, the design space of the whole SRM can be shrinkaged to a very essential and prompting area of the SRM.

Parametrization of the design space essentially means that the design space is being divided into material cells, that can be filled in with material or with air. The number of parameters, their size, and shape can strongly influence the accuracy and the speed of the optimization. The parameterization of the considered SRM will be explained in detail in the following sections.

The optimization method is summarized in a flowchart (see Figure 3-3). Each of the milestones of the optimization is reflected in this flowchart and described in the following sections. Section 3.2.1 is dedicated to optimization model creation and initial optimization. Then, the sensitivity analysis procedure is described in Section 3.2.2 and the results are presented and discussed. Lastly, parametrization of the TO design space and TO optimization of the SRM is discussed in Section 3.2.3. Additionally, Section 3.2.4 summarizes key steps of the optimization integration using Matlab – MagNET software packages.

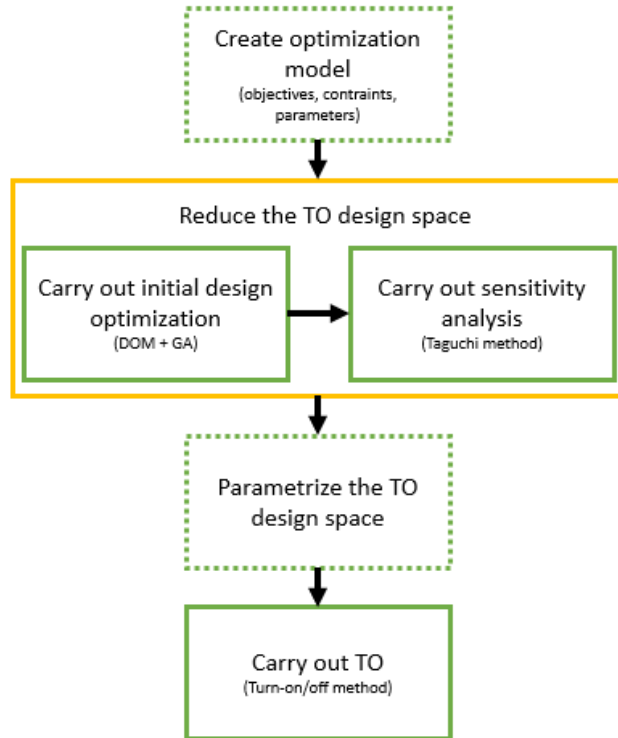


Figure 3-3: SRM optimization flowcharts.

3.2.1 Initial Design Optimization

As it is mentioned in earlier chapters, the main challenge of the SRM implementation is the torque ripples during the operation. It is well known that the reduction of the torque ripple often leads to the reduction of the average torque. Therefore, for the initial design optimization, it is worth finding an optimal design that can propose a good average torque while reducing the material volume of the core. Here, the reduction of the core volume directly affects the aim of the TO design space reduction.

3.2.1.1 Optimization model and method

The second step of the initial design optimization is to carry out the parametrization of the SRM. Six main geometrical parameters which are presented in Table 1 and Figure 3-4 were utilized for the optimization. Then, the optimization model can be mathematically formulated as follows.

$$\min f(D_{so}, D_{si}, D_{st}, D_{ri}, \beta_s, \beta_r) = [T_{peak}, V]^T \quad 3.5$$

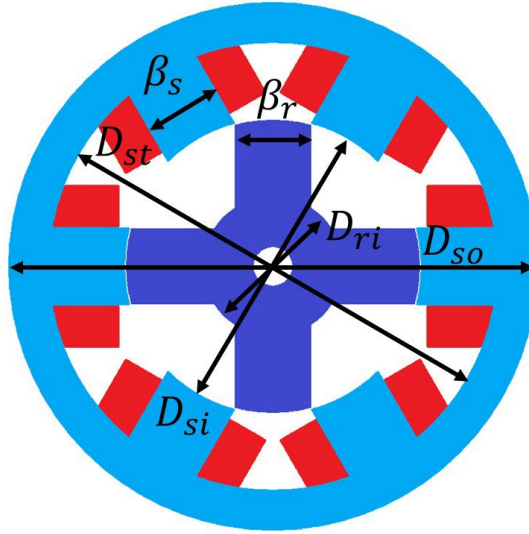


Figure 3-4: SRM initial optimization parametrization.

Table 3-1: SRM initial optimization parametrization

| Parameter | Notation | Range |
|----------------------------|-----------|--------|
| Stator outer diameter (mm) | D_{so} | 70..80 |
| Stator inner diameter (mm) | D_{si} | 40..50 |
| Stator teeth diameter (mm) | D_{st} | 60..70 |
| Rotor inner diameter (mm) | D_{ri} | 10..15 |
| Stator pole angle (°) | β_s | 25..35 |
| Rotor pole angle (°) | β_r | 25..35 |

The initial design optimization was carried out using DOM, where a FE model of the SRM is optimized by an optimization algorithm. The flowchart of the initial design optimization is presented in Figure 3-5. In this thesis non-dominated Sorting Genetic Algorithm - II (NSGA-II) was applied within Matlab software package. To evaluate the torque of the SRM, a 2D FE adaptive model was constructed in Simscenter MagNET software [74]. More details on creating an adaptive parametrized model within Matlab – MagNET environment are presented in Section 3.2.4. Additionally, the windings of the motor were simulated in 3D, and additional resistance and inductance due to the end-windings were added into the 2D model. With the aim to reduce the computational complexity only one phase of the motor was simulated (see Figure 3-6). Furthermore, to achieve precise analysis results, the material of the core was created within MagNET software with the additively manufactured silicon steel characteristics presented in Figure 3-7.

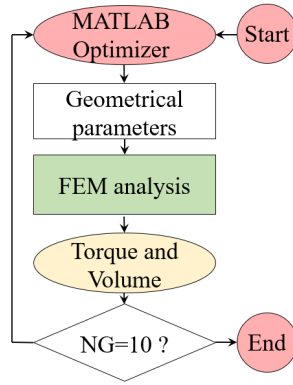


Figure 3-5: Initial optimization flowchart.

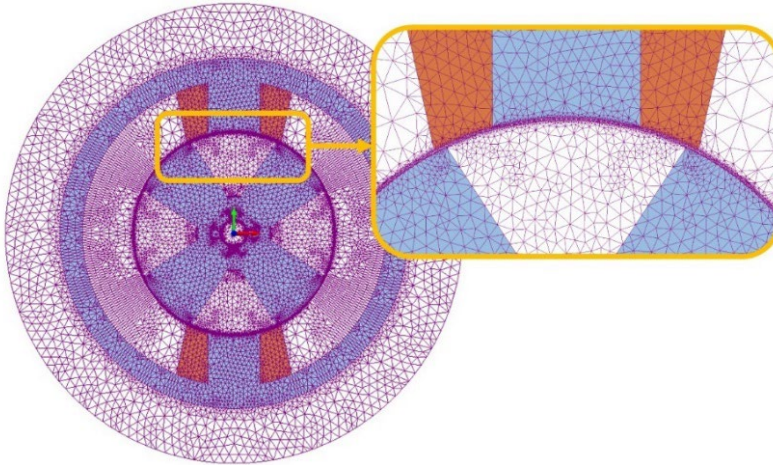


Figure3-6: SRM's 2D FE model for one phase [8].

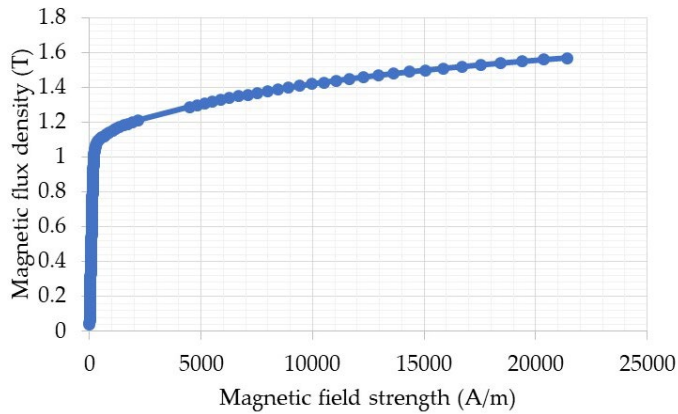


Figure 3-7: B-H curve of printed steel [63], [75].

3.2.1.2 Optimization algorithm

Lately, NSGA-II has been widely utilized for EM optimization due to its unique features such as the ability to find a global minimum of an optimization problem, handle problems in non-analytical form, and high flexibility. NSGA belongs to the group of evolutionary algorithms (EA) and multi-objective GA (MOGA) which defines its functional basis. Basically, NSGA-II is a method of solving constrained and non-constrained optimization problems using the principles of natural selection in biological evolution. A detailed explanation of the MOGA working principle is presented in [63].

The flexibility of NSGA-II is defined by the possibility of easily controlling the following parameters:

- Population size
- Number of generations
- Settings of the selection operator
- Settings of the crossover operator
- Settings of the mutation operator
- Stop criteria

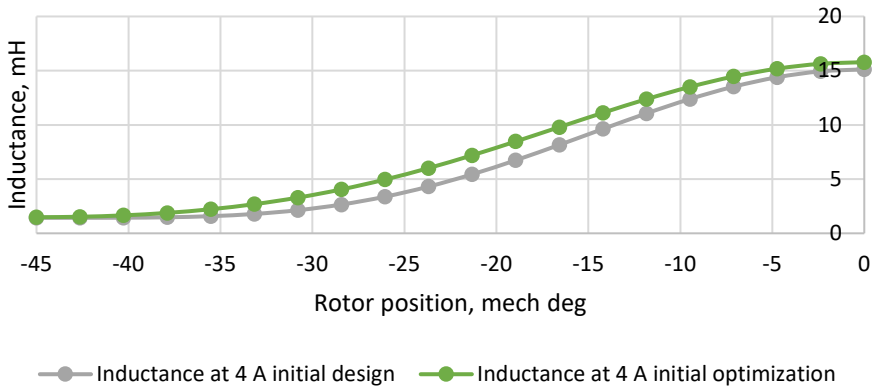
In this thesis, the optimization was carried out with 10 generations and a population size 100. The stop criteria were set as the competence of all 10 generations.

3.2.1.3 Optimization Results

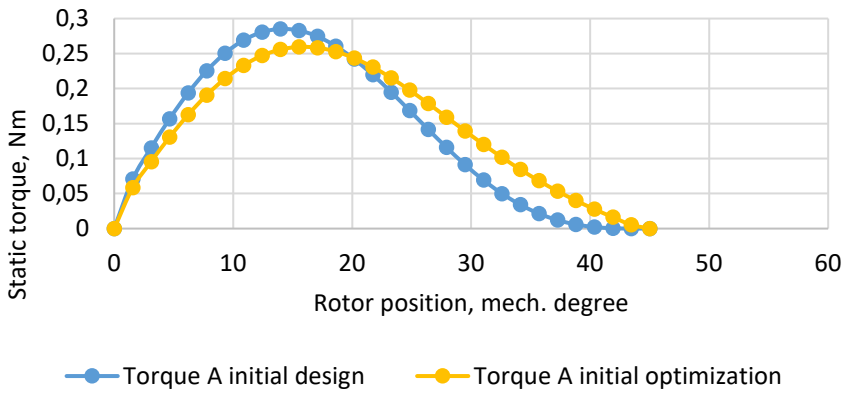
The optimization was successfully carried out within MagNET – Matlab environment. The comparison of the initial and optimal design is presented in Table 3-2 in numbers and in Figures 3-8 in the graphs listing the main performance characteristics of SRM such as inductance, static, and transient torque.

Table 3-2: SRM initial and optimal design dimensions

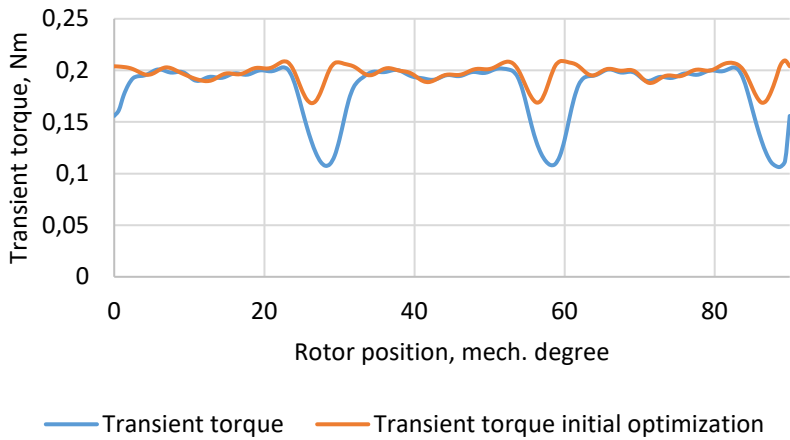
| Parameter | Notation | Initial | Optimal |
|----------------------------|-----------|---------|---------|
| Stator outer diameter (mm) | D_{so} | 80 | 80 |
| Stator inner diameter (mm) | D_{si} | 45 | 46.6 |
| Stator teeth diameter (mm) | D_{st} | 68 | 69.6 |
| Rotor inner diameter (mm) | D_{ri} | 21.2 | 17.1 |
| Stator pole angle (°) | β_s | 30 | 28.5 |
| Rotor pole angle (°) | β_r | 30 | 35 |
| Volume (mm ³) | V | 136575 | 137384 |



(a)



(b)



(c)

Figure 3-3: Comparison of the initial and optimal designs of SRM in terms of: (a) real inductance profiles, (b) static phase torques, and (c) transient torque.

What stands out from the presented figures is that the static torque improved its average value after the optimization: the initial average static torque was 0.13 Nm while the optimal was 0.14 Nm. Transient torque saw a considerable improvement as well: the initial average transient torque was equal to 0.181 Nm while the optimal was equal to 0.197 Nm. Moreover, with the new design, the torque ripple was significantly reduced from 0.53 to 0.21. Volume reduction was not noticed in the results due to the initially compact design of the motor. Yet, although the increase of the rotor pole angle was considerable, the optimization algorithm could keep the volume literally constant. The increase in average torque led to a 10% increase in the torque density from 1318 N/m³ to 1456 N/m³. The optimal geometry of the motor is presented in Figure 3-4.

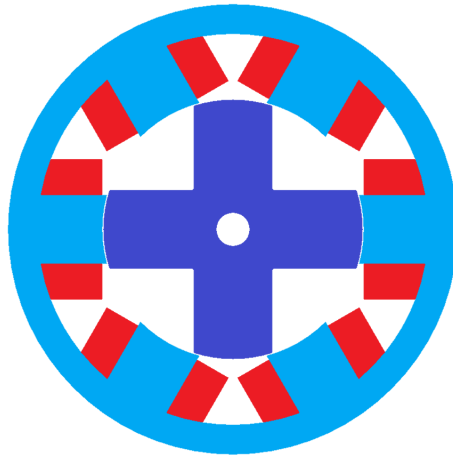


Figure 3-4: Initial optimal design of SRM.

3.2.2 Sensitivity Analysis

The aim of the sensitivity analysis in this thesis is mainly to reduce the computational complexity of the future TO by identifying the most crucial areas and parameters of the SRM design for torque ripple reduction and average torque increase. Taguchi's design of experiment (DoE) was used to carry out the sensitivity analysis due to its simplicity, rapidness, and reliability. A detailed description of the Taguchi DoE method is presented in [63].

3.2.2.1 Sensitivity analysis model and method

Through the extended literature review, a list of geometrical parameters was created for in-depth analysis of the SRM geometry. Figure 3-5 presents the parameters considered in this thesis: rotor pole angle, rotor pole angle at the core, stator pole angle, stator pole angle at the core, airgap shift, and additional tooth angle on the rotor. Rotor and stator pole angles are known to expressively affect the performance of SRM due to their direct influence on the inductance profile and duration of the minimum, maximum inductance, and duration of the growing and decreasing phases. On the other hand, angles at the core of both the stator and rotor were noticed in the torque ripple minimization. At the same time, an additional tooth angle at the core can propose a solution similar to the angles at the rotor and stator core. Last but not least, the airgap shift has shown an enormous influence on the torque ripple reduction. An in-depth description of the mentioned geometrical parameters is presented in [8].

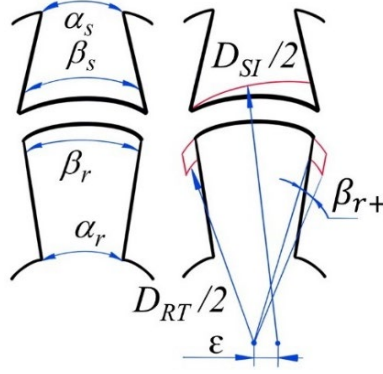


Figure 3-5: Sensitivity analysis parameters [8].

In this thesis, the parameters with the following constraints we assessed:

$$\mathcal{F}_{\Delta} = \begin{cases} 25^{\circ} \leq \beta_s \leq 40^{\circ} \\ \beta_s - 5^{\circ} \leq \alpha_s \leq \beta_s - 15^{\circ} \\ 25^{\circ} \leq \beta_r \leq 40^{\circ} \\ \beta_r + 25^{\circ} \leq \alpha_r \leq \beta_r + 50^{\circ} \\ 0 \text{ mm} \leq \varepsilon \leq 1 \text{ mm} \\ 0^{\circ} \leq 2 \cdot \beta_{r+} \leq 15^{\circ} \end{cases} \quad 3.6$$

Using the Taguchi method, the orthogonal array with the minimum necessary parameters combinations was constructed and consisted only of 25 designs. Thanks to the Taguchi method, the number of designs exploring six parameters with five levels each (see Table 3-3) could be considerably minimized compared to the full factorial experiment that would include more than 7000 designs.

Table 3-3: Design parameters' sampling.

| Design Parameter / Control Factor | Symbol | Factor | Level | | | | |
|-----------------------------------|----------------------------|--------|-------|-------|------|-------|----|
| | | | 1 | 2 | 3 | 4 | 5 |
| Stator pole angle (°) | $\beta_s = X_1$ | X_1 | 25 | 28.75 | 32.5 | 36.25 | 40 |
| Stator pole angle at core (°) | $\alpha_s = \beta_s - X_2$ | X_2 | 5 | 7.50 | 10 | 12.50 | 15 |
| Rotor pole angle (°) | $\beta_r = X_3$ | X_3 | 25 | 28.75 | 32.5 | 36.25 | 40 |
| Rotor pole angle at core (°) | $\alpha_r = \beta_r + X_4$ | X_4 | 25 | 31.25 | 37.5 | 43.75 | 50 |
| Airgap shift | $\varepsilon = X_5$ | X_5 | 0 | 0.25 | 0.50 | 0.75 | 1 |
| Additional tooth angle (°) | $\beta_{r+} = X_6/2$ | X_6 | 0 | 3.75 | 7.50 | 11.25 | 15 |

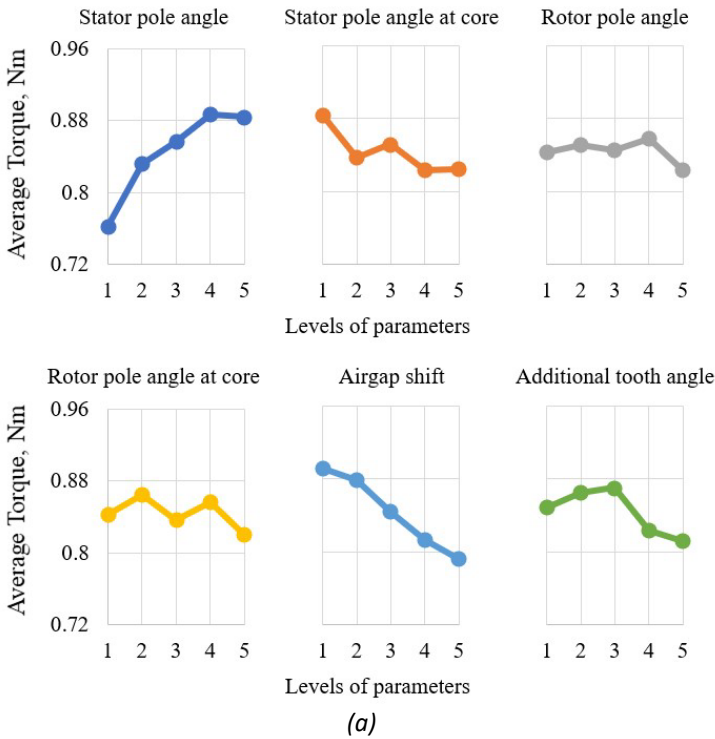
After all the designs were calculated and the objectives (the average torque, torque ripple) were assessed, their peak-to-peak values and a sum of squares were estimated for each parameter and level.

3.2.2.2 Sensitivity analysis results

The results of the sensitivity analysis are shown in Figure 3-6. It is worth mentioning, that these results should be considered as an example, illustrating the influence of various parameters on the torque characteristics. The presented figures were built for an SRM with slightly different dimensions, presented in [8].

According to the presented graphs, stator pole angle and air gap shift have the key influence on the average torque value. With the increase of stator pole angle, the average torque increases, while with the increase of the air gap, the average torque decreases. On the other hand, the enhancement of the air gap shift significantly reduces the torque ripple, while an increase in the rotor pole angle and the introduction of the additional tooth angle increases the torque ripple. The influences of the airgap shift and stator pole angle can be confirmed by the literature [76]. However, the negative influence of the rotor pole angle needed to be reassessed.

Figure 3-7 presents the results of the cross-check analysis of the transient torque for different rotor pole angles with the rest geometry of the motor fixed. It can be clearly seen that with the increase of the rotor pole angle, the average torque slightly increases. At the same time, the torque ripple gets impressively reduced until the rotor pole angle reaches 40°. The values of the average torque and torque ripple can be seen in Table 3-4. One of the reasons for the opposite result in Figure 3-6 (b) can be that the initial assessment was made with the static torque.



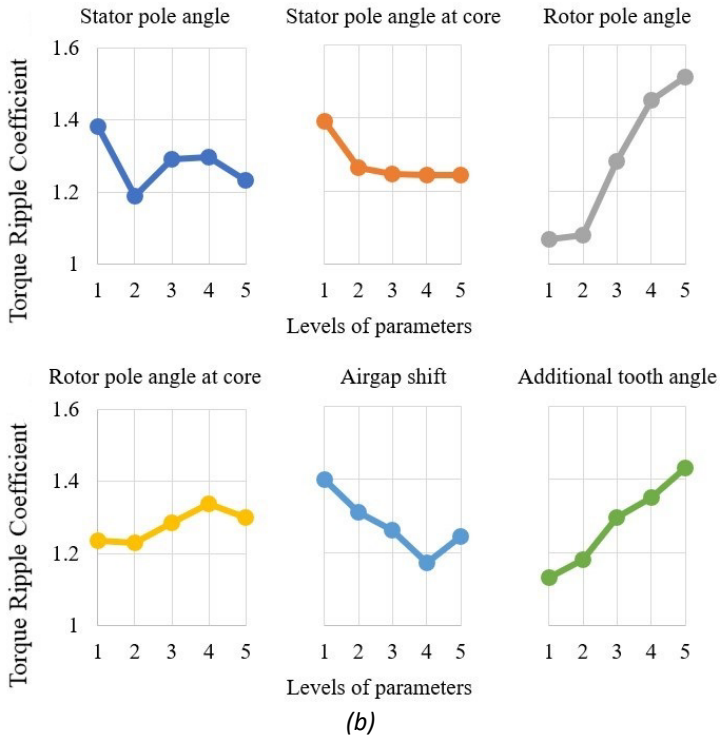


Figure 3-6: Peak-to-peak values of (a) average torque; (b) torque ripple [8].

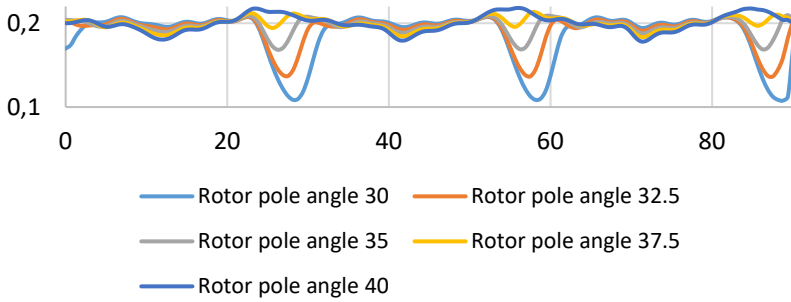


Figure 3-7: Rotor pole angle variation results.

Table 3-5: Rotor pole angle variation results.

| Characteristic | Angle | | | | |
|--------------------|-------|-------|-------|-------|-------|
| | 30 | 32.5 | 35 | 37.5 | 40 |
| Average torque, Nm | 0.186 | 0.192 | 0.197 | 0.199 | 0.200 |
| Torque ripple | 0.537 | 0.371 | 0.210 | 0.148 | 0.199 |

Due to the high influence of the airgap shift on both average torque and torque ripple, it was highly beneficial to explore its influence in more detail. Within another case study, additional designs were explored, which can be defined by Figure 3-7 and Table 3-6. Figure 3-7 presents a slightly different but analogous definition of the air gap through the stator inner diameter shift and Table 3-6 maps this shift. Figure 3-8 presents interesting results obtained from this experiment. Using the airgap shift, the shape of the static torque can be visibly controlled. For instance, with the increase of the airgap shift, the torque becomes wider which is exactly helpful for the reduction of the torque ripple. At the same time, an increase in the airgap shift makes the torque reduce at the beginning and increase at the end of the torque production cycle. This way, torque can be forced to be more constant using an appropriate airgap shift. On the other hand, the average torque is obviously reducing with the increase of the airgap shift, which was also shown by the Taguchi sensitivity analysis.

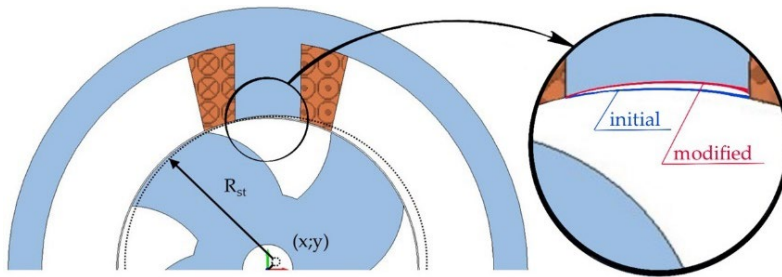


Figure 3-7: Schematic illustration of the second group of design modifications of the SRM.

Table 3-6: Design modifications parameters.

| Design | Coordinates (x; y), mm |
|-------------------------|------------------------|
| 1st design modification | 1; 0.30 |
| 2nd design modification | 0.50; 0.15 |
| 3rd design modification | 0.25; 0.07 |
| 4th design modification | 0.125; 0.035 |

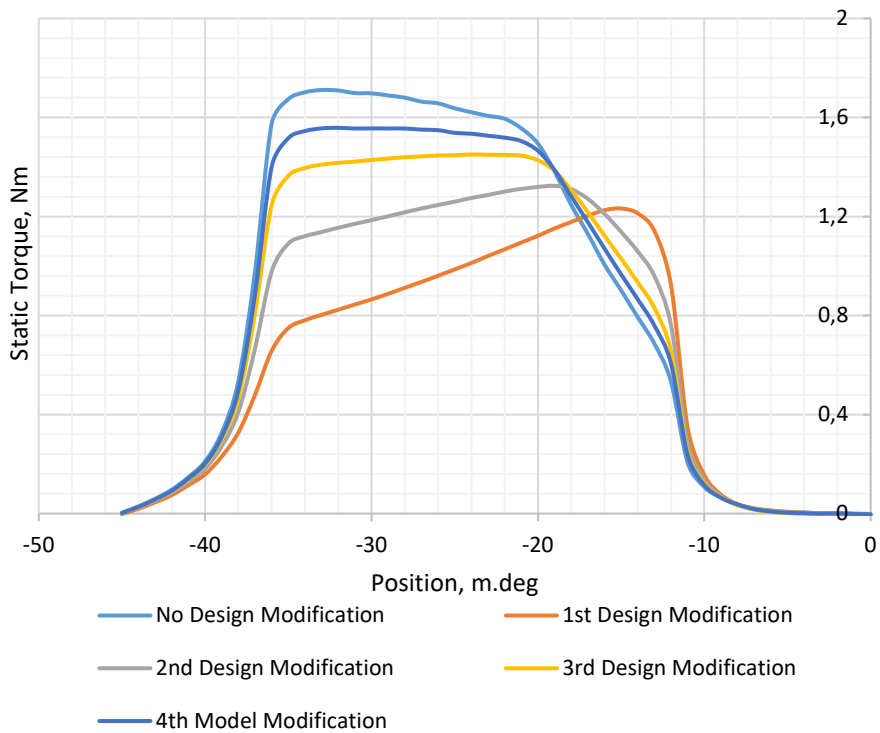


Figure 3-8: Airgap shift variation of the SRM.

The results of the sensitivity analyses indicated the most influencing areas of the SRM design. It was revealed that airgap shift variation, rotor and stator pole angles, and additional tooth angle of the rotor have a major impact on the average torque and torque ripple. To reduce the computational complexity, the following areas of the SRM were considered within the following TO (see Figure 3-9). Moreover, to speed up the calculations and future preparation of the prototype, only the rotor was topologically optimized in this thesis. Additionally, through the sensitivity analysis, an update of the rotor geometrical parameters was done with the aim to reduce the torque ripple and increase the average torque. A comparison of the initial design, initially optimized design, and design selected by the SA is presented in Figure 3-10. As can be noticed, transient torque shows a slight increase in the average torque to 0.199 N/m and a reduction of the torque ripple to 0.152. Moreover, Figure 3-9 shows not only the area of interest for future TO but also reflects the geometry of the new design. It is important to notice, that the results of the sensitivity analysis such as updates in the geometry and selection of the crucial areas for the TO, lead to a more than 70% decrease of the future TO design space.

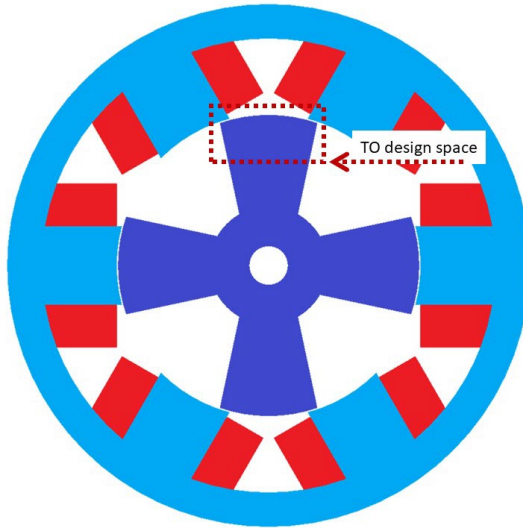
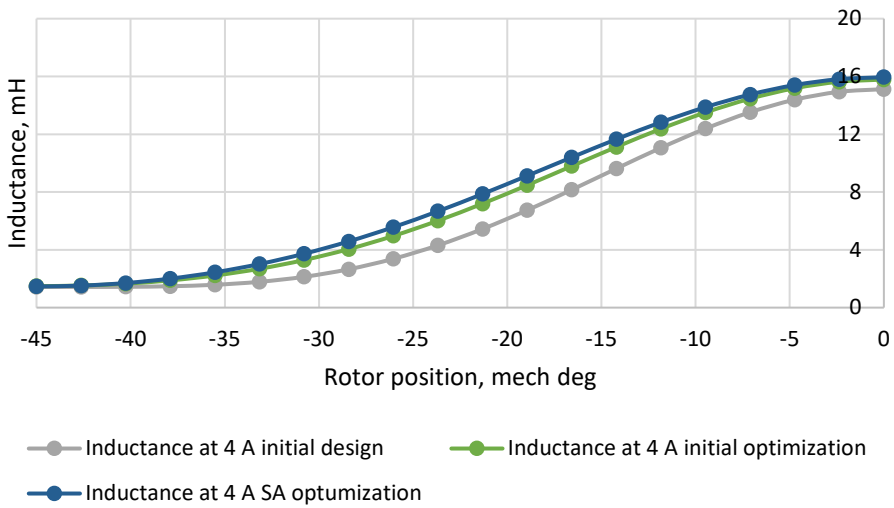
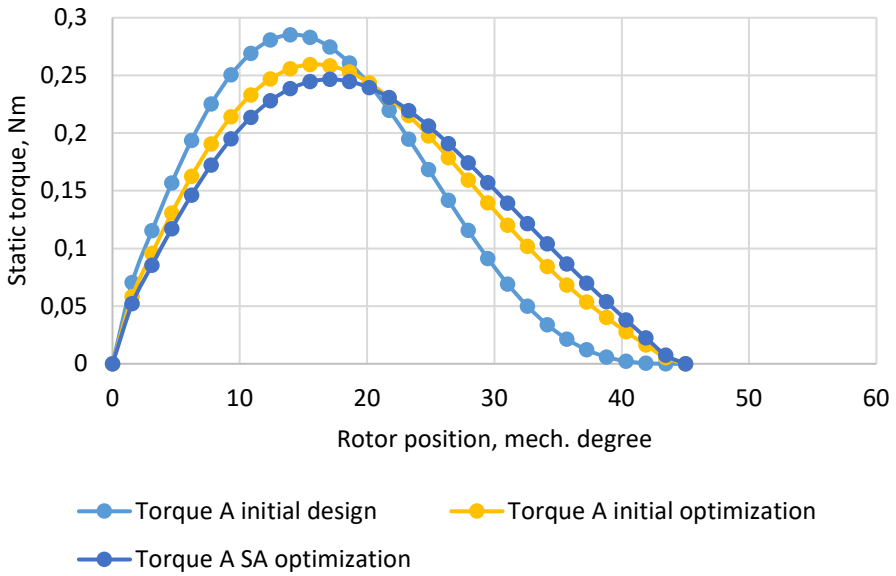


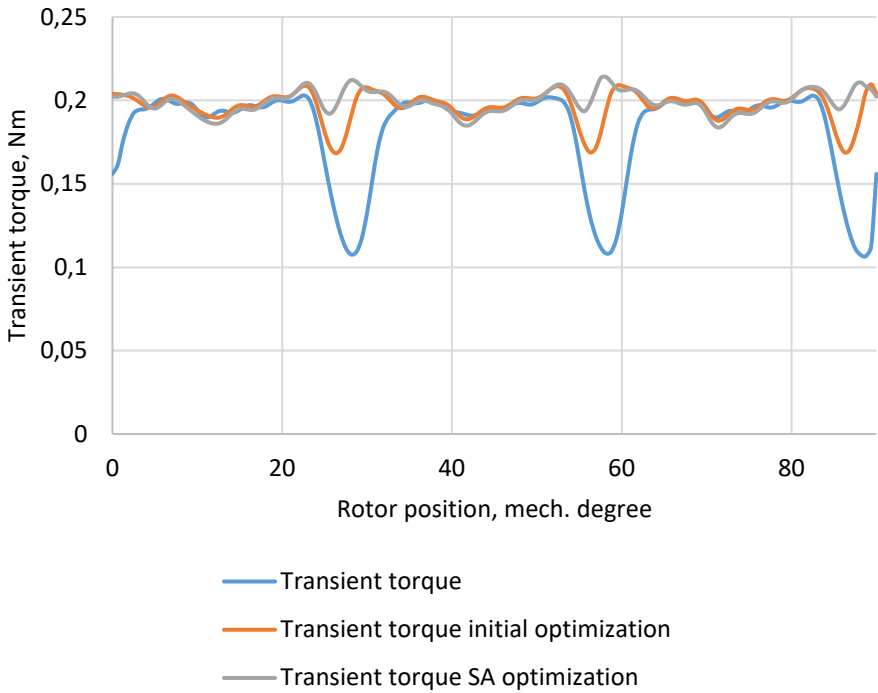
Figure 3-9: TO design space with SA optimal design.



(a)



(b)



(c)

Figure 3-10: Comparison of the initial, initial optimal, and SA optimal designs of SRM in terms of: (a) real inductance profiles, (b) static phase torques, and (c) transient torque.

3.2.3 Topology optimization

TO is known to be a powerful tool used for motor optimization. Very well established in mechanical design, the TO method starts opening new ground in electromagnetics as well [77]. Several studies have shown that TO can considerably reduce the torque ripple in reluctance motors [12], [78].

Several types of TO exist, one of the most widely applied is the On/Off TO method. As it was mentioned before, the On/Off optimization method uses the material distribution over the design space as optimization parameters. The design space parametrization which was applied within this thesis is presented in Figure 3-11. As can be seen, the design space is divided into many sections, in our case 150, which are considered optimization parameters. To reduce the number of parameters and prevent a chess board-like structure, parameters were grouped between each other in shapes “L” or rotated “L”. This way, only 50 parameters were participating in the TO.

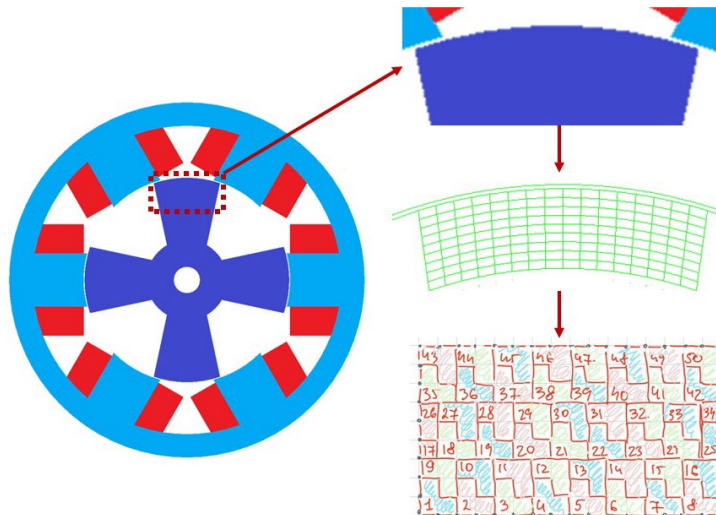


Figure 3-11: TO design space parametrization.

A single-objective optimization was performed with the aim to minimize the torque ripple. Due to the restrictions of the optimization algorithm of Matlab software associated with the TO discrete nature of the parameters, only one objective could be targeted. As in the initial optimization, NSGA-II was utilized along with a transient model of the SRM.

The resulting geometry is presented in Figure 3-12 as well as the main electromagnetic characteristics are shown in Figure 3-13. As can be seen on the transient curve graph, the average torque slightly increased to 0.201 N/m, while the torque ripple decreased to 0.123. The inductance curve and static torque did not experience many changes. The obtained shape has formed two distinguishing islands. Gained asymmetry of the rotor teeth can be described by the clock-overwise rotation of the rotor during the simulation.

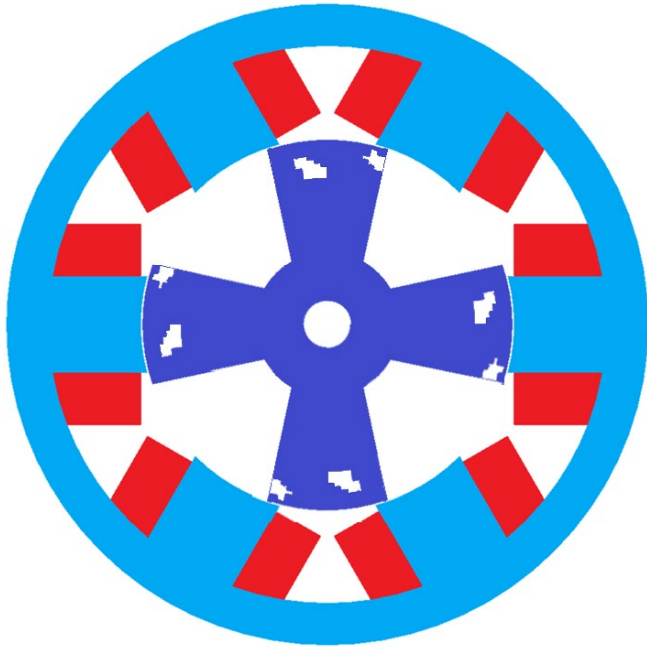
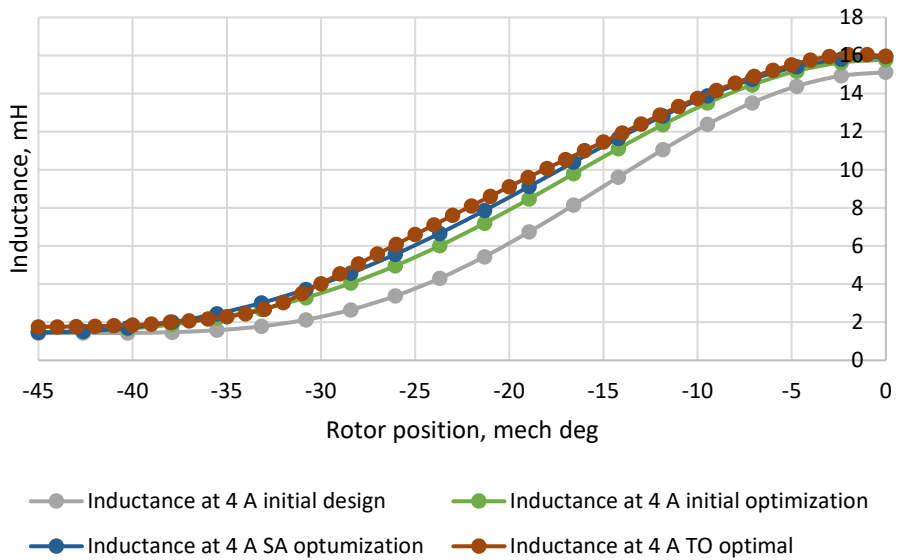
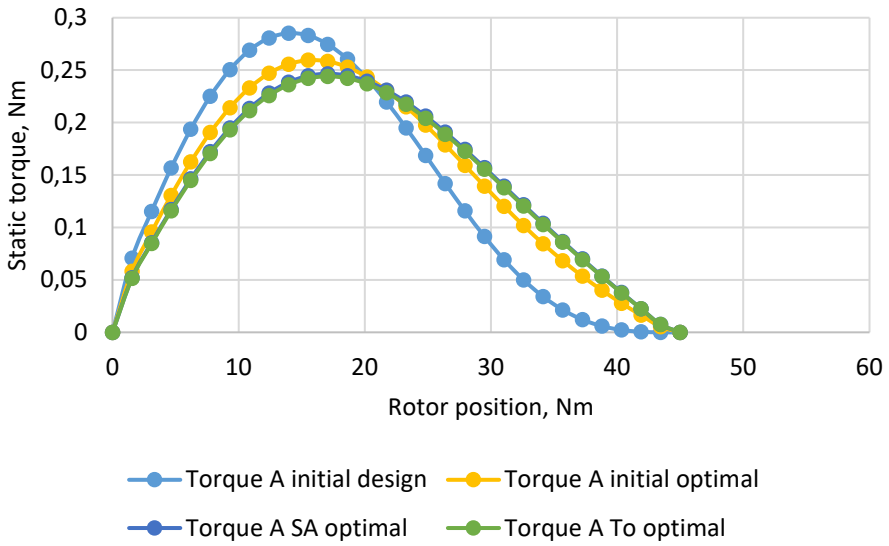


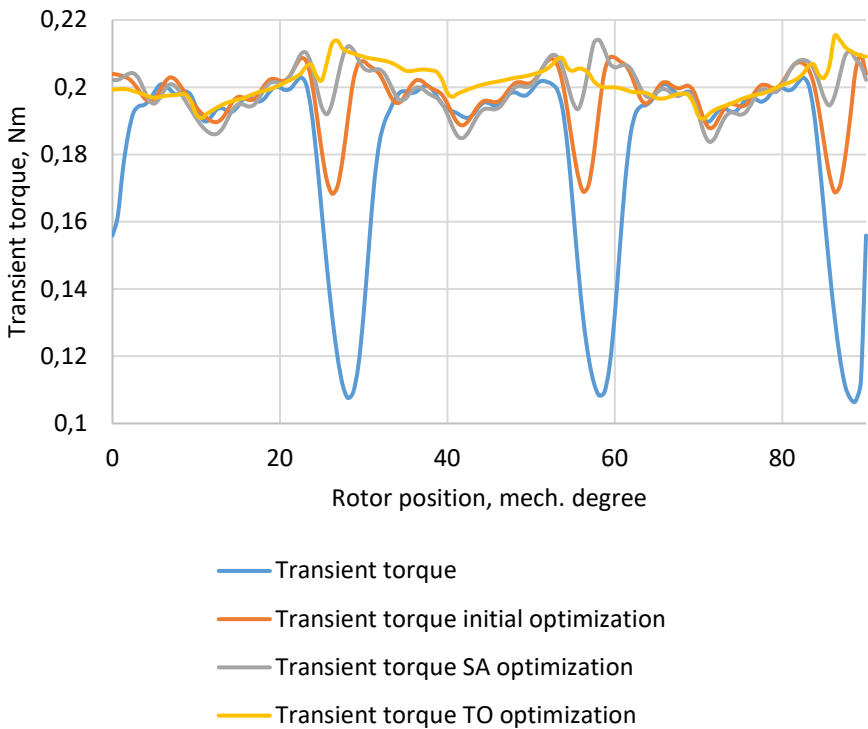
Figure 3-9: TO optimal design of SRM.



(a)



(b)



(c)

Figure 3-13: Comparison of the initial, initial optimal, SA optimal, and TO optimal designs of SRM in terms of: (a) real inductance profiles, (b) static phase torques, and (c) transient torque.

Table 3-7 summarizes in numbers all the results obtained during design, initial optimization, sensitivity analysis, and topology optimization. It can be obviously seen that the improvement of the SRM is significant. Compared to the initial design, the latest optimal solution helped to reduce the torque ripple by 77% while increasing the average torque by 10%.

Table 3-7: Optimization flow results.

| Characteristic | Design | | | |
|--------------------|---------|-----------------|------------------------------|-------------------------------|
| | Initial | Initial optimal | Sensitivity analysis optimal | Topology optimization optimal |
| Average torque, Nm | 0.181 | 0.197 | 0.199 | 0.201 |
| Torque ripple | 0.531 | 0.210 | 0.152 | 0.123 |

This section designed and optimized SRM. Additionally, this this section simulated the SRM, and explored various geometrical parameters and their effect on the average torque and torque ripple. Moreover, a novel optimization method was proposed which reduced the computational complexity of the TO. At first, the motor was designed using a classic design approach. Then, the main dimensions of the motor were optimized using the DOM along with the GA. A considerable improvement of the average torque and torque ripple were achieved. Particularly, the increase of the average torque 9% and reduction of torque ripple by 60% were noticed. Another step of the optimization was dedicated to the SA through which the average torque was upgraded by 10% and torque ripple condensed by 71% comparing to the initial design. As the last step, the TO cut out the torque ripple by 77%. It can be noticed that the main improvement of the torque quality was completed by the initial design optimization. Not surprisingly, the global parameters of the SRM geometry shape the performance the most. Such key dimensions as rotor diameters, stator and rotor poles angles have a huge impact on the SRM performance. Yet, through the application of the SA and usage of a new parameter such as the rotor pole angle at the core, additional 11% could be gained in the reduction of the torque ripple. Lastly, it can be seen that the TO optimization diminished the torque ripple by additional 6%. A potential of the TO could be open more in case of 3D TO and improvement of the additively manufactured motor characteristics considering inner structure of the motor and its influence not only on the torque ripple, but also on the core losses and thermal condition.

4 Conclusion

The purpose of the current thesis was to investigate the opportunities for SRM design, shape, and topology optimization. Moreover, this research was undertaken to explore the prospects that additive manufacturing provides for EMs optimization. Another aim of this study was to design and optimize a SRM, while presenting various methods of EMs optimization.

This thesis has reviewed extensive literature to show various optimization modeling techniques, methodologies, and algorithms. One of the most important conclusions of the introductory part of the thesis was a comprehensive comparison of various modeling techniques and methodologies in terms of accuracy, rapidity, simplicity, and flexibility. These conclusions provide insights into design optimization opportunities and open up the advantages and disadvantages of various optimization methodologies.

This research has also shown the opportunities opened up by rapidly developing additive manufacturing techniques. The possibilities of EMs additive manufacturing have been reviewed and presented in this thesis. This finding will be of interest to motor design and optimization researchers.

Another chapter of this thesis was dedicated to the design and optimization of the SRM with the aim to increase the average torque, decrease the core volume, and reduce the torque ripple. One of the most significant results of this study is the creation of a new multi-level optimization method. Initially, TO was selected as a promising approach toward SRM optimization. However, high computational complexity posed a challenge that could not be neglected. To overcome the issue of TO high time consumption, a novel method has been proposed. The proposed approach aimed to reduce the design space of the TO by applying initial optimization techniques and sensitivity analysis. The first step involved initial parameter optimization, where main geometrical parameters such as the diameters of the stator and rotor, pole angles, etc. were optimized using the direct optimization method. The result of this optimization was an optimized structure of the motor which could limit TO design space. Another step of the proposed approach was SA, which could identify the most vital areas of the SRM design for the average torque increase and reduction of the torque ripple. One of the most significant findings to emerge from the SA was limited design space that was taking less than 30% of the initial design space of the SRM. And final step of the optimization was TO in the selected area of the SRM. A significant increase in the average torque by 10% and a major reduction of the torque ripple by 70% were the results of the SRM optimization. This thesis has provided a deep insight into SRM optimization, covering in detail the design of the motor, selection, and setup of the optimization. These results add to the rapidly expanding field of EMs optimization and open up a new ground for SRM development.

5 Future studies

To benefit the highest performance of additively manufactured SRM, the 3D topology optimization (3D TO) should come into a greater focus. The 3D TO can open up a new ground of opportunities for the improvement of the SRM performance characteristics. It has been shown in this thesis, that 2D geometry of the SRM significantly influences the torque curve. On the other hand, recent literature presents the 3D modification possibilities such as rotor skewing for SRM torque ripple reduction. Another motor characteristic which could benefit from 3D TO is the thermal condition of the motor. Using 3D TO, novel heat transfer ways and geometries can be found. Last but not least, 3D TO can be of a good use for reducing the core losses of additively manufactured EM. A search for new lattice structures can be carried out by 3D TO. Taking into account the mentioned promising benefits of 3D TO, a further study should properly assess and carry out 3D TO.

More broadly, research into the control of SRM drive is also needed to fully alter the motor performance. It has been shown in this thesis, that control of SRM is very adaptive and flexible. Moreover, it has been observed, that the influence of the commutation parameters of the SRM control, visibly affects the torque of the motor. Therefore, commutation pattern parameters are suggested to be the elements of the future optimization.

References

- [1] P. Waide and C. U. Brunner, "Energy-Efficiency Policy Opportunities for Electric Motor-Driven Systems," *Int. energy agency*, vol. na, no. na, 2011.
- [2] C. U. Brunner, P. Waide, and M. Jakob, "Harmonized Standards for Motors and Systems Global progress report and outlook," 2011.
- [3] Y. Duan and D. M. Ionel, "A review of recent developments in electrical machine design optimization methods with a permanent magnet synchronous motor benchmark study," in *IEEE Energy Conversion Congress and Exposition: Energy Conversion Innovation for a Clean Energy Future, ECCE 2011, Proceedings*, 2011, pp. 3694–3701, doi: 10.1109/ECCE.2011.6064270.
- [4] S. Sato, T. Sato, and H. Igarashi, "Topology optimization of synchronous reluctance motor using normalized gaussian network," *IEEE Trans. Magn.*, vol. 51, no. 3, Mar. 2015, doi: 10.1109/TMAG.2014.2359679.
- [5] Maciej Serda *et al.*, "Manufacturing of topology optimized soft magnetic core through 3D printing," *Uniw. śląski*, vol. 7, no. 1, pp. 343–354, 2016, doi: 10.2/JQUERY.MIN.JS.
- [6] J. Dang, J. R. Mayor, S. A. Semidey, R. Harley, T. Habetler, and J. Restrepo, "Practical considerations for the design and construction of a high speed SRM with a flux-bridge rotor," in *2014 IEEE Energy Conversion Congress and Exposition, ECCE 2014*, Nov. 2014, pp. 3842–3849, doi: 10.1109/ECCE.2014.6953923.
- [7] W. Xu, J. Zhu, Y. Guo, S. Wang, Y. Wang, and Z. Shi, "Survey on electrical machines in electrical vehicles," *2009 Int. Conf. Appl. Supercond. Electromagn. Devices, ASEMD 2009*, no. c, pp. 167–170, 2009, doi: 10.1109/ASEMD.2009.5306667.
- [8] E. Andriushchenko *et al.*, "Sensitivity Analysis for Multi-Objective Optimization of Switched Reluctance Motors," *Mach. 2022, Vol. 10, Page 559*, vol. 10, no. 7, p. 559, Jul. 2022, doi: 10.3390/MACHINES10070559.
- [9] Y. Tang, G. Dong, Q. Zhou, and Y. F. Zhao, "Lattice Structure Design and Optimization with Additive Manufacturing Constraints," *IEEE Trans. Autom. Sci. Eng.*, vol. 15, no. 4, pp. 1546–1562, Oct. 2018, doi: 10.1109/TASE.2017.2685643.
- [10] E. Andriushchenko, M. H. Mohammadi, D. A. Lowther, H. Heidari, A. Kallaste, and A. Khan, "Topology Optimization of a 3D-Printed Switched Reluctance Motor," *2022 Int. Conf. Electr. Mach.*, pp. 1976–1980, Sep. 2022, doi: 10.1109/ICEM51905.2022.9910829.
- [11] G. Lei, J. Zhu, Y. Guo, C. Liu, and B. Ma, "A review of design optimization methods for electrical machines," *Energies*, vol. 10, no. 12, 2017, doi: 10.3390/en10121962.
- [12] H. Zhang and S. Wang, "Topology Optimization of Rotor Pole in Switched Reluctance Motor for Minimum Torque Ripple," <http://dx.doi.org/10.1080/15325008.2017.1310769>, vol. 45, no. 8, pp. 905–911, May 2017, doi: 10.1080/15325008.2017.1310769.
- [13] M. ROSU *et al.*, *MULTIPHYSICS SIMULATION BY DESIGN FOR ELECTRICAL MACHINES, POWER ELECTRONICS, AND DRIVES*. 2018.
- [14] J. M. Kokernak and D. A. Torrey, "Magnetic circuit model for the mutually coupled switched-reluctance machine," *IEEE Trans. Magn.*, vol. 36, no. 2, pp. 500–507, 2000, doi: 10.1109/20.825824.

- [15] W. Sun, Q. Li, L. Sun, L. Zhu, and L. Li, "Electromagnetic analysis on novel rotor-segmented axial-field srm based on dynamic magnetic equivalent circuit," *IEEE Trans. Magn.*, vol. 55, no. 6, Jun. 2019, doi: 10.1109/TMAG.2019.2901002.
- [16] N. Sadowski, "Finite elements coupled to electrical circuit equations in the simulation of switched reluctance drives: attention to mechanical behaviour," *IEEE Trans. Magn.*, vol. 32, no. 3 PART 2, pp. 1086–1089, 1996, doi: 10.1109/20.497430.
- [17] H. Chen, W. Yan, and Q. Wang, "Electromagnetic Analysis of Flux Characteristics of Double-Sided Switched Reluctance Linear Machine," *IEEE Trans. Appl. Supercond.*, vol. 26, no. 4, Jun. 2016, doi: 10.1109/TASC.2016.2539215.
- [18] H. Chen, X. Liu, and W. Yan, "Three-Dimensional Magnetic Equivalent Circuit Research of Double-Sided Switched Reluctance Linear Machine," *IEEE Trans. Appl. Supercond.*, vol. 30, no. 4, Jun. 2020, doi: 10.1109/TASC.2020.2990774.
- [19] S. H. Mao, D. Dorrell, and M. C. Tsai, "Fast analytical determination of aligned and unaligned flux linkage in switched reluctance motors based on a magnetic circuit model," *IEEE Trans. Magn.*, vol. 45, no. 7, pp. 2935–2942, Jul. 2009, doi: 10.1109/TMAG.2009.2016087.
- [20] D. Lin, P. Zhou, S. Stanton, and Z. J. Cendes, "An analytical circuit model of switched reluctance motors," *IEEE Trans. Magn.*, vol. 45, no. 12, pp. 5368–5375, Dec. 2009, doi: 10.1109/TMAG.2009.2024754.
- [21] D. S. Mihic, M. V. Terzic, and S. N. Vukosavic, "A New Nonlinear Analytical Model of the SRM with Included Multiphase Coupling," *IEEE Trans. Energy Convers.*, vol. 32, no. 4, pp. 1322–1334, Dec. 2017, doi: 10.1109/TEC.2017.2707587.
- [22] F. Soares and P. J. C. Branco, "Simulation of a 6/4 switched reluctance motor based on Matlab/Simulink environment," *IEEE Trans. Aerosp. Electron. Syst.*, vol. 37, no. 3, pp. 989–1009, Jul. 2001, doi: 10.1109/7.953252.
- [23] K. N. Srinivas and R. Arumugam, "Dynamic characterization of switched reluctance motor by computer-aided design and electromagnetic transient simulation," *IEEE Trans. Magn.*, vol. 39, no. 3 II, pp. 1806–1812, May 2003, doi: 10.1109/TMAG.2003.809839.
- [24] W. Lu, A. Keyhani, and A. Fardoun, "Neural network-based modeling and parameter identification of switched reluctance motors," *IEEE Trans. Energy Convers.*, vol. 18, no. 2, pp. 284–290, Jun. 2003, doi: 10.1109/TEC.2003.811738.
- [25] Y. Kano, T. Kosaka, and N. Matsui, "Magnetization characteristics analysis of SRM by simplified non-linear magnetic analysis," in *Proceedings of the Power Conversion Conference-Osaka 2002, PCC-Osaka 2002*, 2002, vol. 2, pp. 689–694, doi: 10.1109/PCC.2002.997602.
- [26] L. A. Belfore, "Modeling faulted switched reluctance motors using evolutionary neural networks," *IEEE Trans. Ind. Electron.*, vol. 44, no. 2, pp. 226–233, 1997, doi: 10.1109/41.564161.
- [27] T. Lachman, T. R. Mohamad, and C. H. Fong, "Nonlinear modelling of switched reluctance motors using artificial intelligence techniques," *IEE Proc. Electr. Power Appl.*, vol. 151, no. 1, pp. 53–60, Jan. 2004, doi: 10.1049/ip-epa:20040025.
- [28] H. P. Chi, R. L. Lin, and J. F. Chen, "Simplified flux-linkage model for switched-reluctance motors," in *IEE Proceedings: Electric Power Applications*, May 2005, vol. 152, no. 3, pp. 577–583, doi: 10.1049/ip-epa:20045207.
- [29] W. Ding and D. Liang, "A fast analytical model for an integrated switched reluctance starter/generator," *IEEE Trans. Energy Convers.*, vol. 25, no. 4, pp. 948–956, Dec. 2010, doi: 10.1109/TEC.2010.2052620.

- [30] A. Khalil and I. Husain, "A fourier series generalized geometry-based analytical model of switched reluctance machines," *IEEE Trans. Ind. Appl.*, vol. 43, no. 3, pp. 673–684, May 2007, doi: 10.1109/TIA.2007.895737.
- [31] X. Ding, M. Rashed, C. I. Hill, and S. Bozhko, "Analytical modelling approach for switched reluctance machines with deep saturation," Feb. 2017, doi: 10.1109/ESARS-ITEC.2016.7841411.
- [32] A. Radun, "Analytical calculation of the switched reluctance motor's unaligned inductance," *IEEE Trans. Magn.*, vol. 35, no. 6, pp. 4473–4481, 1999, doi: 10.1109/20.809140.
- [33] S. Li, S. Zhang, T. G. Habetler, and R. G. Harley, "Fast and accurate analytical calculation of the unsaturated phase inductance profile of 6/4 switched reluctance machines," 2016, doi: 10.1109/ECCE.2016.7855107.
- [34] Z. Djelloul-Khedda, K. Boughrara, F. Dubas, and R. Ibtouen, "Nonlinear Analytical Prediction of Magnetic Field and Electromagnetic Performances in Switched Reluctance Machines," *IEEE Trans. Magn.*, vol. 53, no. 7, Jul. 2017, doi: 10.1109/TMAG.2017.2679686.
- [35] J. Kumar, "Application of artificial neural networks to optimization problems in electrical power operation," 1993.
- [36] W. Ding and D. Liang, "Modeling of a 6/4 switched reluctance motor using adaptive neural fuzzy inference system," in *IEEE Transactions on Magnetics*, Jul. 2008, vol. 44, no. 7, pp. 1796–1804, doi: 10.1109/TMAG.2008.919711.
- [37] Z. Lin, D. S. Reay, B. W. Williams, and X. He, "Online modeling for switched reluctance motors using b-spline neural networks," *IEEE Trans. Ind. Electron.*, vol. 54, no. 6, pp. 3317–3322, Dec. 2007, doi: 10.1109/TIE.2007.904009.
- [38] S. Song, M. Zhang, and L. Ge, "A new decoupled analytical modeling method for switched reluctance machine," *IEEE Trans. Magn.*, vol. 51, no. 3, Mar. 2015, doi: 10.1109/TMAG.2014.2363214.
- [39] L. Shen, J. Wu, S. Yang, and X. Huang, "Fast flux linkage measurement for switched reluctance motors excluding rotor clamping devices and position sensors," *IEEE Trans. Instrum. Meas.*, vol. 62, no. 1, pp. 185–191, 2013, doi: 10.1109/TIM.2012.2212598.
- [40] X. Cui, J. Sun, C. Gan, C. Gu, and Z. Zhang, "Optimal design of saturated switched reluctance machine for low speed electric vehicles by subset quasi-orthogonal algorithm," *IEEE Access*, vol. 7, pp. 101086–101095, 2019, doi: 10.1109/ACCESS.2019.2929103.
- [41] K. Diao, X. Sun, G. Lei, Y. Guo, and J. Zhu, "Multiobjective system level optimization method for switched reluctance motor drive systems using finite-element model," *IEEE Trans. Ind. Electron.*, vol. 67, no. 12, pp. 10055–10064, Dec. 2020, doi: 10.1109/TIE.2019.2962483.
- [42] J. W. Lee, H. S. Kim, B. Il Kwon, and B. T. Kim, "New rotor shape design for minimum torque ripple of SRM using FEM," in *IEEE Transactions on Magnetics*, Mar. 2004, vol. 40, no. 2 II, pp. 754–757, doi: 10.1109/TMAG.2004.824803.
- [43] K. Kiyota, T. Kakishima, H. Sugimoto, and A. Chiba, "Comparison of the test result and 3D-FEM analysis at the knee point of a 60 kW SRM for a HEV," *IEEE Trans. Magn.*, vol. 49, no. 5, pp. 2291–2294, 2013, doi: 10.1109/TMAG.2013.2242453.
- [44] M. Abbasian, M. Moallem, and B. Fahimi, "Double-stator switched reluctance machines (DSSRM): Fundamentals and magnetic force analysis," *IEEE Trans. Energy Convers.*, vol. 25, no. 3, pp. 589–597, Sep. 2010, doi: 10.1109/TEC.2010.2051547.

- [45] T. F. Chan, W. Wang, and L. L. Lai, "Performance of an axial-flux permanent magnet synchronous generator from 3-D finite-element analysis," *IEEE Trans. Energy Convers.*, vol. 25, no. 3, pp. 669–676, Sep. 2010, doi: 10.1109/TEC.2010.2042057.
- [46] C. Lu, P. Zhou, D. Lin, B. He, and D. Sun, "Multiply connected 3-D transient problem with rigid motion associated with mbi T-mmb Ω formulation," *IEEE Trans. Magn.*, vol. 50, no. 2, pp. 449–452, 2014, doi: 10.1109/TMAG.2013.2280875.
- [47] P. Zhou, Z. Badics, D. Lin, and Z. J. Cendes, "Nonlinear T- Ω formulation including motion for multiply connected 3-D problems," *IEEE Trans. Magn.*, vol. 44, no. 6, pp. 718–721, Jun. 2008, doi: 10.1109/TMAG.2007.915118.
- [48] D. Lin, P. Zhou, Q. M. Chen, N. Lambert, and Z. J. Cendes, "The effects of steel lamination core losses on 3d transient magnetic fields," in *IEEE Transactions on Magnetism*, Aug. 2010, vol. 46, no. 8, pp. 3539–3542, doi: 10.1109/TMAG.2010.2043509.
- [49] W. Yao, J. M. Jin, and P. T. Krein, "A highly efficient domain decomposition method applied to 3-D finite-element analysis of electromechanical and electric machine problems," *IEEE Trans. Energy Convers.*, vol. 27, no. 4, pp. 1078–1086, 2012, doi: 10.1109/TEC.2012.2216528.
- [50] P. Zhou, B. He, C. Lu, D. Lin, and N. Chen, "Transient simulation of electrical machines using time decomposition method," Aug. 2017, doi: 10.1109/IEMDC.2017.8002034.
- [51] H. Chen, W. Yan, J. J. Gu, and M. Sun, "Multiobjective Optimization Design of a Switched Reluctance Motor for Low-Speed Electric Vehicles with a Taguchi-CSO Algorithm," *IEEE/ASME Trans. Mechatronics*, vol. 23, no. 4, pp. 1762–1774, Aug. 2018, doi: 10.1109/TMECH.2018.2839619.
- [52] B. Anvari, H. A. Toliyat, and B. Fahimi, "Simultaneous Optimization of Geometry and Firing Angles for In-Wheel Switched Reluctance Motor Drive," *IEEE Trans. Transp. Electr.*, vol. 4, no. 1, pp. 322–329, 2017, doi: 10.1109/TTE.2017.2766452.
- [53] W. Tong, *Mechanical design of electric motors*. 2014.
- [54] H. Y. Yang, Y. C. Lim, and H. C. Kim, "Acoustic noise/vibration reduction of a single-phase SRM using skewed stator and rotor," *IEEE Trans. Ind. Electron.*, vol. 60, no. 10, pp. 4292–4300, 2013, doi: 10.1109/TIE.2012.2217715.
- [55] K. N. Srinivas and R. Arumugam, "Analysis and characterization of Switched reluctance motors: Part II - Flow, thermal, and vibration analyses," *IEEE Trans. Magn.*, vol. 41, no. 4, pp. 1321–1332, Apr. 2005, doi: 10.1109/TMAG.2004.843349.
- [56] K. N. Srinivas and R. Arumugam, "Static and dynamic vibration analyses of switched reluctance motors including bearings, housing, rotor dynamics, and applied loads," *IEEE Trans. Magn.*, vol. 40, no. 4 I, pp. 1911–1919, Jul. 2004, doi: 10.1109/TMAG.2004.828034.
- [57] M. Takiguchi, H. Sugimoto, N. Kurihara, and A. Chiba, "Acoustic Noise and Vibration Reduction of SRM by Elimination of Third Harmonic Component in Sum of Radial Forces," *IEEE Trans. Energy Convers.*, vol. 30, no. 3, pp. 883–891, Sep. 2015, doi: 10.1109/TEC.2015.2401398.
- [58] J. W. Ahn, S. J. Park, and D. H. Lee, "Hybrid excitation of SRM for reduction of vibration and acoustic noise," *IEEE Trans. Ind. Electron.*, vol. 51, no. 2, pp. 374–380, Apr. 2004, doi: 10.1109/TIE.2004.825227.

- [59] W. Yan *et al.*, “Design and multi-objective optimisation of switched reluctance machine with iron loss,” *IET Electr. Power Appl.*, vol. 13, no. 4, pp. 435–444, Apr. 2019, doi: 10.1049/iet-epa.2018.5699.
- [60] W. Wu, J. B. Dunlop, S. J. Collocott, and B. A. Kalan, “Design Optimization of a Switched Reluctance Motor by Electromagnetic and Thermal Finite-Element Analysis,” in *IEEE Transactions on Magnetics*, Sep. 2003, vol. 39, no. 5 II, pp. 3334–3336, doi: 10.1109/TMAG.2003.816248.
- [61] Y. Huang, J. Zhu, and Y. Guo, “Thermal analysis of high-speed SMC motor based on thermal network and 3-D FEA with rotational core loss included,” in *IEEE Transactions on Magnetics*, Oct. 2009, vol. 45, no. 10, pp. 4680–4683, doi: 10.1109/TMAG.2009.2023065.
- [62] S. Nategh, O. Wallmark, M. Leksell, and S. Zhao, “Thermal analysis of a PMSRM using partial FEA and lumped parameter modeling,” *IEEE Trans. Energy Convers.*, vol. 27, no. 2, pp. 477–488, 2012, doi: 10.1109/TEC.2012.2188295.
- [63] E. Andriushchenko *et al.*, “Optimization of a 3D-Printed Permanent Magnet Coupling Using Genetic Algorithm and Taguchi Method,” *Electronics*, vol. 10, no. 4, p. 494, Feb. 2021, doi: 10.3390/electronics10040494.
- [64] A. A. Arkadan, M. N. Elbsat, and M. A. Mneimneh, “Particle swarm design optimization of a rotor Synrm for traction applications,” *IEEE Trans. Magn.*, vol. 45, no. 3, pp. 956–959, Mar. 2009, doi: 10.1109/TMAG.2009.2012482.
- [65] J. Y. Lee, J. H. Chang, D. H. Kang, S. Il Kim, and J. P. Hong, “Tooth shape optimization for cogging torque reduction of transverse flux rotary motor using design of experiment and response surface methodology,” in *IEEE Transactions on Magnetics*, Apr. 2007, vol. 43, no. 4, pp. 1817–1820, doi: 10.1109/TMAG.2007.892611.
- [66] K. Diao, X. Sun, G. Lei, G. Bramerdorfer, Y. Guo, and J. Zhu, “Robust Design Optimization of Switched Reluctance Motor Drive Systems Based on System-Level Sequential Taguchi Method,” *IEEE Trans. Energy Convers.*, vol. 36, no. 4, pp. 3199–3207, 2021, doi: 10.1109/TEC.2021.3085668.
- [67] L. Gargalis *et al.*, “Additive Manufacturing and Testing of a Soft Magnetic Rotor for a Switched Reluctance Motor,” *IEEE Access*, p. 1, 2020, doi: 10.1109/ACCESS.2020.3037190.
- [68] H. Tiismus, *Production and Properties of Additively Manufactured Electrical Machine Cores.*
- [69] A. Kallaste, T. Vaimann, and A. Rassõlkin, “Additive Design Possibilities of Electrical Machines,” in *2018 IEEE 59th International Scientific Conference on Power and Electrical Engineering of Riga Technical University (RTUCon)*, 2018, pp. 1–5, doi: 10.1109/RTUCon.2018.8659828.
- [70] H. Tiismus, A. Kallaste, T. Vaimann, and A. Rassõlkin, “Eddy Current Loss Reduction Prospects in Laser Additively Manufactured Soft Magnetic Cores,” *2022 Int. Conf. Electr. Mach.*, pp. 1511–1516, Sep. 2022, doi: 10.1109/ICEM51905.2022.9910679.
- [71] B. Khoshoo, K. J. Islam, H. Suen, P. Kwon, J. P. Lozano, and S. N. Foster, “Eddy Current Loss Reduction in Binder Jet Printed Iron Silicon Cores,” *2022 Int. Conf. Electr. Mach.*, pp. 558–564, Sep. 2022, doi: 10.1109/ICEM51905.2022.9910749.
- [72] A. Credo, E. Kurvinen, I. Petrov, and J. Pyrhonen, “Investigation of Material Combinations for Axially-Laminated Synchronous Machine,” *2022 Int. Conf. Electr. Mach.*, pp. 814–820, Sep. 2022, doi: 10.1109/ICEM51905.2022.9910821.

- [73] R. Notari, M. Pastura, S. Nuzzo, D. Barater, G. Franceschini, and C. Gerada, "AC losses reduction in Hairpin Windings produced via Additive Manufacturing," *2022 Int. Conf. Electr. Mach.*, pp. 1144–1149, Sep. 2022, doi: 10.1109/ICEM51905.2022.9910620.
- [74] "Siemens. Simcenter MAGNET 2D/3D, 2021. [Online]." <https://www.plm.automation.siemens.com/global/en/products/simcenter/magnet.html> (accessed Jun. 28, 2021).
- [75] E. Andriushchenko, J. Kaska, A. Kallaste, A. Belahcen, T. Vaimann, and A. Rassõlkin, "Design Optimization of Permanent Magnet Clutch with Ārtap Framework," *Period. Polytech. Electr. Eng. Comput. Sci. Des. Optim. Perm. Magn. Clutch with Ārtap Framew. Period. Polytech. Electr. Eng. Comput. Sci. (in Press.*
- [76] K. C. Yong, S. Y. Hee, and S. K. Chang, "Pole-shape optimization of a switched-reluctance motor for torque ripple reduction," *IEEE Trans. Magn.*, vol. 43, no. 4, pp. 1797–1800, 2007, doi: 10.1109/TMAG.2006.892292.
- [77] C. Midha, "A Study of Topology Optimization Methods for the Design of Electromagnetic Devices," 2018.
- [78] Y. Hidaka and H. Igarashi, "Topology Optimization of Synchronous Reluctance Motors Considering Localized Magnetic Degradation Caused by Punching," *IEEE Trans. Magn.*, vol. 53, no. 6, Jun. 2017, doi: 10.1109/TMAG.2017.2659721.

Acknowledgements

My sincere gratitude to my supervisors for their continuous support and guidance. I am thankful for help and support that I received from my family along all the way of my PhD study.

This work was supported by the Estonian Research Council with the grant PRG 1827 Additive Manufacturing of Electrical Machines.

Abstract

Design Optimization Methods of Additively Manufactured Switched Reluctance Motor

This Ph.D. dissertation presents switched reluctance motor (SRM) design and optimization. The study focused on the improvement of SRM torque characteristics using topology optimization (TO). In parallel, the TO challenge such as computational complexity was addressed.

Thanks to the rapid growth of advanced power electronics, SRMs have received a close attention from research and industry. Due to their simple and rigid structure, they are now considered as promising motors for various applications. However, SRMs' torque ripple presence slows down their development. Therefore, this thesis was motivated to apply powerful optimization techniques to improve SRM torque characteristics. The aim of this thesis was to optimize design of a SRM in order to increase the average torque, reduce the volume of the core material, and shrink the torque ripple. Additionally, additive manufacturing (AM) was proposed as a capable method of optimal designs production. AM was shown as strong support of motor optimization, thanks to the vast design opportunities that AM provides for motor manufacturing, optimization can be carried out at a more delicate level.

This work started with the review and assessment of the optimization environment elements such as models, methods, and algorithms. The SRMs modelling methods were scrutinized and the superiorities and the drawbacks of them were recognised. Different motor modelling approaches were studied and compared concerning their efficiency. Key optimization methods, models, and algorithms were researched. A comprehensive comparison of various optimization environments was carried out. Moreover, a procedure of the optimization environment section was created baring in mind accuracy of optimization results, computational complexity of the optimization, and manufacturability of optimised motor.

TO was selected as a promising optimization method for SRM's torque quality improvement. To overcome computational burden that TO imposes, a novel optimization approach is proposed in this thesis. The proposed method was a multi-level optimization method and included pre-optimization that could reduce the design space of the TO and consequently, decrease the TO computational complexity. Firstly, design optimization was carried out to increase the average torque of the SRM and reduce the volume of the core material. As a result, the torque characteristic of the motor was improved and the geometry focus shifted on the rotor and stator teeth. Then, a sensitivity analysis (SA) of unique design parameters of the SRM was carried out. The SA provided valuable information regarding the influence of the advance shapes of the rotor and stator teeth on the average torque and torque ripple. The design optimization and SA could help the TO focus on the very important areas of the motor and reduced the TO design space by more than 70%.

The resulting improvement of the SRM torque was significant. Thanks to the proposed approach, the average torque of the motor was increased by 10% while the torque ripple was reduced by 77%. At last, the initial and optimal designs of the SRM were manufactured using AM techniques.

Lühikokkuvõte

Kihtlisandustehnoloogia abil toodetud samm-mootori optimeerimise meetodid

Käesolev doktoritöö käsitleb endas samm-mootori (SRM) projekteerimist ja optimeerimist. Uuringus keskenduti SRM-i pöördemomendi omaduste parandamisele, kasutades topoloogia optimeerimist (TO). Paralleelselt käsitleti ka topoloogia optimeerimisega kaasnevaid probleeme, nagu arvutuslik keerukus.

Tänu jõuelektroonika kiirele arengule on kasvanud ka teadlaste ja tööstuse suur huvi SRMide vastu. Tänu nende lihtsale ja jäigale struktuurile peetakse neid nüüd paljulubavateks mootoriteks erinevate rakenduste jaoks. Samas üheks probleemiks on pöördemomendi pulsatsioon SRMidel, mis piirab nende arengut. Seetõttu võetigi lõputöö eesmärgiks SRM-i pöördemomendi omaduste parandamine kasutades selleks kaasaegseid optimeerimistehnikaid. Lõputöös käsitletaksegi SRM-i konstruktsiooni optimeerimist eesmärgiga suurendada keskmist pöördemomenti, vähendada magnetsüdamik materjali kulu ning vähendada pöördemomendi pulsatsiooni. Kuna optimaalset disainilahendust on keerukas toota traditsiooniliste meetoditega, siis töös pakuti välja ka masina tootmine kihtlisandustehnoloogia (AM) abil. AM on mootori optimeerimisel tugevaks toeks, tänu ulatuslikele disainivõimalustele, mida AM pakub mootori valmistamiseks, kuna optimeerimist saab teostada keerukamal tasemel.

Esmalt teostati töös optimeerimiskeskonna elementide, nagu mudelid, meetodid ja algoritmid, ülevaatamine ja hindamine. Uuriti SRM-i modelleerimismeetodeid ning tuvastati nende eelised ja puudused. Uuriti ja võrreldi erinevaid mootorite modelleerimise lähenemisviise lähtudes nende keerukusest. Viidi läbi sobivate optimeerimismeetodite, mudelite ja algoritmide analüüs, ning teostati erinevate optimeerimiskeskondade põhjalik võrdlus. Lisaks töötati välja protseduur optimeerimiskeskonna jaoks, mis võtaks arvesse optimeerimistulemuste täpsust, optimeerimise arvutuslikku keerukust ja optimeeritud mootori valmistatavust.

SRM-i pöördemomendi kvaliteedi parandamiseks leiti sobivaimaks optimeerimismetoodikaks TO. Töös pakutakse välja uudne optimeerimismetoodika, mis lihtsustaks TO-st tulenevat arvutusliku koormust. Väljapakutud meetodika on mitmetasandiline optimeerimismeetod sisaldades endas eeloptimeerimist, mis vähendab TO projekteerimisruumi ja läbi selle vähendab TO arvutuslikku keerukust. Esmalt teostati disaini optimeerimine, suurendamaks SRM-i keskmist pöördemomenti ja vähendades südamik materjali mahtu. Selle tulemusena paranevad mootori pöördemomendi omadused ning geomeetria fookus nihkub rootori ja staatori hammastele. Seejärel teostatakse SRM-i ainulaadsete konstruktsiooniparameetrite tundlikkuse analüüs (SA). Analüüs annab väärtuslikku teavet rootori ja staatori hammaste kuju mõju kohta keskmisele pöördemomendile ja pöördemomendi pulsatsioonile. Projekteerimise optimeerimine ja SA aitavad TO-l keskenduda mootori väga olulistele piirkondadele ja vähendavad TO projekteerimisruumi mahtu rohkem kui 70% võrra.

Töö tulemuseks on SRM-i pöördemomendi märkimisväärne paranemine. Tänu kavandatud lähenemisviisile suudeti suurendada mootori keskmist pöördemomenti 10% võrra, samas kui pöördemomendi pulsatsioon vähenes 77%. Valmistati ka SRM-i esialgne ja optimaalne prototüüp AM-tehnika abil.

Appendix

Publication I

Andriushchenko E., Mohammadi M. H., Lowther D. A., Heidari H., Kallaste. A. (2022). Topology optimization of a 3D-printed switched reluctance motor. 2022 International Conference on Electrical Machines (ICEM), Valencia, Spain, pp. 1976–1980, 2022.

Topology Optimization of a 3D-Printed Switched Reluctance Motor

E. Andriushchenko, M. H. Mohammadi, D. A. Lowther, H. Heidari, A. Kallaste, A. Khan

Abstract -- The issue of switched reluctance motor (SRM) torque ripple has received close attention in the last decade. One of the most promising methods for addressing the torque ripple problem is topology optimization (TO). Two main challenges of the TO method are the high computational burden and manufacturing constraints. This paper proposes a new three-step approach to SRM optimization which includes initial shape optimization, sensitivity analysis, and TO. The three-step procedure of the SRM optimization significantly reduces the TO design domain, saving the calculation resources and allowing to obtain an optimal design faster. Moreover, the TO is geometrically unrestricted due to the projected use of additive manufacturing techniques for motor fabrication. The current study achieved a notable improvement of the SRM performance: the torque ripple reduction. Moreover, the computational burden for the optimization process saw a considerable decrease.

Index Terms-- Optimization methods, switched reluctance motor, torque ripple, topology optimization.

I. INTRODUCTION

SWITCHED reluctance motors (SRMs) are widely utilized within high-speed and high-performance applications [1]. Thanks to the absence of permanent magnets, the SRM offers an economical and environmentally friendly alternative to the permanent magnet synchronous motor (PMSM). Moreover, the lack of magnets or windings on the rotor makes the SRM advantageous for high-speed and high-temperature applications. Furthermore, SRMs have a great potential to produce high torque density. On the other hand, they suffer from a serious drawback of torque ripple, which leads to vibration and noise during motor operation.

The SRM's torque ripple has long been a question of great interest. It has been discovered that the key reasons for the SRM's torque ripple are the high saturation of the rotor/stator poles and the fringing flux. These two factors affect the inductance profile of the motor and lead to the nonlinear growth of the phase current and phase torque. Several studies have attempted to suppress the torque ripples using simple modifications of the rotor and stator poles [2]–[5]. The major approach of the recent studies is to punch triangle shaped holes on the tip of the rotor to eliminate the fringing flux effect [6]–[8]. Additionally, the control parameters can play a crucial role in torque ripple suppression in SRM. A large and growing body of literature has investigated the influence of the commutation parameters on the torque ripple of the motor [9]. Recently, there has been an increasing number of studies that

pay particular attention to both design and control aspects of the motor. For example, a study on pole-shape optimization has revealed that by changing the air-gap profile, a more steady current curve can be achieved resulting in less torque ripple at the motor's shaft [7].

Recently, researchers have attempted to employ topology optimization (TO) to improve the performance of the motor [10]. The TO has shown itself a powerful tool able to considerably reduce the torque ripple. One of the major issues of TO is its considerable computational burden. To reduce the calculation time, the search space of the TO should be carefully defined. A solution to this problem is suggested in this study. Apart from the computation burden, the conventional manufacturing methods used for the optimized motor can constrain the topological choices. This research proposes additive manufacturing (AM) as a solution that can allow innovation through novel topologies. Moreover, the usage of AM allows to carry out a nearly unrestricted TO in terms of stator and rotor geometry.

This paper presents a new TO methodology, which effectively narrows the search space of the TO and, consequently, accelerates the overall optimization process. The reduction of the search space was achieved using preliminary initial shape optimization and sensitivity analysis. Within the initial shape optimization, the classic geometrical parameters of the motor were optimized. Then, the sensitivity analysis of a group of unique parameters assisted in defining the optimal design space for the TO. Based on the obtained search space, the ON/OFF TO method has been implemented [11].

II. FINITE ELEMENT ANALYSIS OF SRM

A. Problem Statement

The control scheme of a three-phase 6/4-pole SR motor drive is presented in Fig. 1. Traditionally, the SRM is fed by an asymmetric bridge converter, where each phase is controlled independently. A switching pattern directs the DC voltage to one of the phases depending on the rotor's position. To ensure the correct commutation, the 6/4-pole SRM drive includes six position- and current-controlled switches.

Since the operation of SRM is based on reluctance torque the phase inductance of the SRM plays a crucial role in the operation of the motor. Fig. 2 illustrates the variation of the ideal inductance profile for one phase according to the

M. H. Mohammadi, D. A. Lowther, and A. Khan are with the Department of Electrical and Computer Engineering of McGill University, Montréal, Quebec, Canada (e-mail: david.lowther@mcgill.ca).

This research work was supported by the Estonian Research Council under grant PSG137 "Additive Manufacturing of Electrical Machines".

E. Andriushchenko, H. Heidari, and A. Kallaste are with the Department of Electrical Power Engineering and Mechatronics, Tallinn University of Technology, Estonia (e-mail:ekandr@taltech.ee)

position of the rotor. The phase inductance is minimum when the rotor and stator teeth are unaligned. From the beginning of the rotor and stator teeth overlap, the phase inductance starts growing until its maximum value. Near the aligned position of the teeth, the phase inductance experiences a plateau and then symmetrically falls until its minimum value. Fig. 2 shows that the voltage is supplied to the phase at the period of the increasing inductance to produce a positive torque. The torque production can be formulated by the following expression.

$$T = \int_0^i \frac{\partial L(\theta, i)}{\partial \theta} di. \quad (1)$$

Where L represents the phase inductance, i characterizes the instantaneous current and θ denotes to the rotor position.

A key reason for the torque ripples is the nonlinearity of the real inductance profile. The comparison of the ideal and real inductance profiles obtained by finite element (FE) model can be seen in Fig. 2. Due to the variation of the inductance near to the stator and rotor teeth overlap, the torque is produced leading to the nonlinear growth of current and torque ripples. The stator and rotor geometries define the real inductance profile curve. Therefore, the TO of the SRM can be highly beneficial for its performance improvement.

B. Finite Element Analysis

To carry out the optimization, two FE models of the motor were created in 2D within the Simcenter MAGNET software [12]. Fig. 3 illustrates the static and transient models. The static model was used for the real inductance profile and static torque estimation. The model was sufficient for the initial shape optimization and sensitivity analysis, meantime being less computationally demanding compared to the transient model. To further reduce the computational complexity of the static simulation only 1/3rd of the motor was modeled, resulting in a reduction of the calculation time by more than four times. The transient model was created for estimation of the torque ripple. The model simulated the operation of the motor together with the converter. To speed up the overall optimization, the transient model was utilized only within the TO.

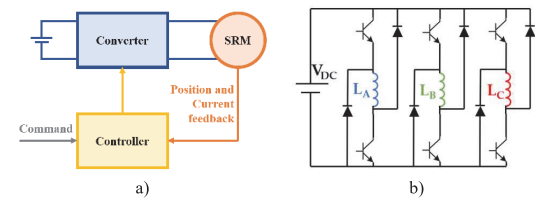


Fig. 1. a) SRM drive; b) asymmetric bridge converter.

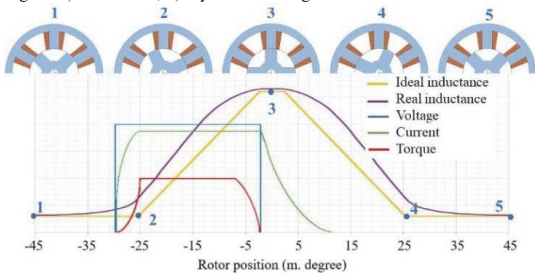


Fig. 2. Ideal and real inductance, voltage, current, and torque profiles.

During design and optimization, automated modeling, solving, and post-processing was required. This was accomplished using MAGNET scripting within the MATLAB optimization process.

C. Initial Design

The initial design of the SRM was created using normally applied geometrical proportions. The motor characteristics and geometrical parameters are listed in Table I. The stator and rotor material was electrical steel with 6.5% silicon content. Since the motor was intended to be 3D printed, the electromagnetic and mass characteristics of the printed sample were taken into account within the model. The average torque of the initial design was 0.77 Nm, the volume of the utilized steel reached 351 cm³, and the torque density achieved 2.19 Nm/m³.

Within the converter model, the choice of the turn-on and turn-off angles depended on the real inductance profile. For all the models, the turn-on angle of each phase was 5° earlier than the beginning of the growing inductance stage. The duration of one phase commutation was 30°.

III. OPTIMIZATION METHODOLOGY

This study proposes a TO procedure with reduced computational burden and the possibility to reach an optimal design faster. The method involved three steps which allowed to compact the search space and carry out the TO. To identify the classic SRM design parameters, the initial shape optimization was carried out. Then, using the Taguchi method, a sensitivity analysis was executed.

The sensitivity analysis of the advanced design parameters helped to define the base shape of the motor. Using the obtained search space and the base design, the TO was accomplished.

A. Initial Shape Optimization

The initial shape optimization of the SRM considered six major geometrical parameters presented in Fig. 4 together with their limits. The optimization model of the SRM is formulated as follows.

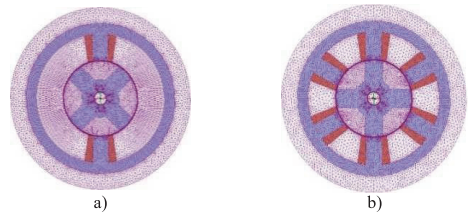


Fig. 3. SRM FE models: a) static model; b) transient model.

TABLE I
MOTOR SPECIFICATIONS

| Specification | Symbol | Value |
|-----------------------------|-------------------|------------|
| Stator outer diameter (mm) | D_{SO} | 120 |
| Stator inner diameter (mm) | D_{SI} | 60 |
| Stator slot depth (mm) | S_D | 21.4 |
| Rotor inner diameter (mm) | D_{RI} | 30.4 |
| Stator/rotor pole angle (°) | β_S/β_R | 23/27.7 |
| Air gap length | a | 0.5 mm |
| Stack length | L | 60 mm |
| Phase resistance | R | 5 Ω |

$$\min f(D_{SO}, D_{SI}, S_D, D_{RI}, \beta_S, \beta_R) = [-T_{peak}, V]^T \quad (2)$$

Where maximization of the peak torque (T_{peak}) and minimization of the volume of the motor steel material (V) are the objectives of the optimization. The initial shape optimization was carried out using the static FE model at the maximum torque rotor position along with the Non-dominated Sorting Genetic Algorithm II (NSGA-II).

The shape optimization flowchart is shown in Fig. 5 (a). The optimization was terminated when the number of complete generations (NG) reached to 10. Fig. 5 (b) presents the Pareto front of the initial shape optimization. Table II lists the optimal design parameters of the motor. It can be seen from the table, that the torque density achieved a 20% improvement. Moreover, the volume of the stator and rotor material was reduced by 10%. The initial shape optimization allowed to fix the main dimensions of the motor, thereby, decrease the search space by 10% for the further optimization steps.

B. Sensitivity Analysis

To reduce the TO design space and find the most crucial design parameters of the SRM, a sensitivity analysis was accomplished. The sensitivity analysis used a simplified static model of the motor along with the Taguchi design of experiments (DOE) method. The Taguchi DOE is a widely applied sensitivity analysis approach that ensures low computational complexity and robust results. The Taguchi method is a statistical approach that helps to explore design spaces. For a particular number of design parameters and their levels, Taguchi proposed a particular orthogonal array that consists of a minimum necessary combinations of the design parameters enough to analyze the results. The detailed explanation of the Taguchi method application is presented in [13]. Using the Taguchi DOE, the six unique geometrical parameters chosen through the literature review were analyzed together with their influence on the average torque and torque ripple.

The parameters (i.e. control factors) utilized within the sensitivity analysis are presented in Fig. 6 (a). The design space of the sensitivity analysis was sampled based on the parameters number and their levels using the L_{25} (65) design matrix (i.e. orthogonal array) proposed by Taguchi.

The control factors, as well as their levels, are listed in Table III. For each design of the L_{25} (65) matrix, a static 2D simulation was carried out at different positions to obtain a full curve of the static torque. The peak-to-peak values of the average torque and torque ripple at zero speed were calculated for each factor and level.

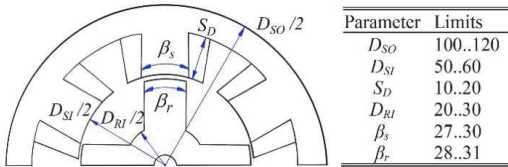


Fig. 4. Shape optimization parameters.

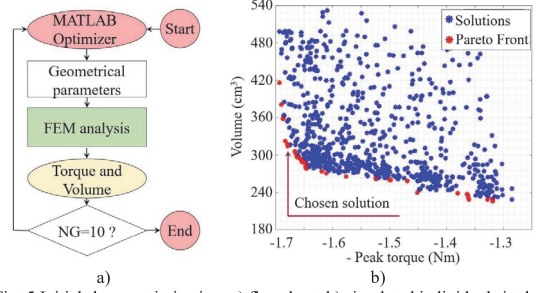


Fig. 5 Initial shape optimization: a) flowchart; b) simulated individuals in the objectives plane and Pareto front.

$$M_{ij}(f) = \frac{1}{n} \cdot \sum f(i, j) \quad (3)$$

Where i represents the parameter number, j shows the level number, n is the number of experiments, and $f(i, j)$ denoted the value of an objective function. To explore the effect of each parameter on the objective function, the sums of squares were assessed as follows.

$$SS_{ij}(f) = n \cdot \sum (M_{ij} - M_f)^2 \quad (4)$$

Where M_f is the total mean value of the objective function. The results of the sensitivity analysis are shown in Fig. 7. It can be seen that the stator pole angle and airgap shift had a major influence on the average torque. Moreover, the rotor pole and additional tooth angles had a major impact on the torque ripple.

The trade-off design and the search space for the TO were selected as shown in Fig. 6 (b). Thanks to the proposed procedure, the design space was reduced considerably. Through the sensitivity analysis, it had been revealed that only 25% of the motor geometry had a considerable influence on its performance.

C. Topology Optimization

The ON/OFF method of TO was employed in this study. The method operated on 320 discrete design variables. Each design variable represented a particular cell within the defined design space, which had a material property able to switch from air to steel.

A single-objective optimization was performed to minimize the torque ripple. The optimization utilized transient models of the SRM operation at the speed of 500°/sec along with the NSGA-II. The number of individuals within the NSGA-II was set as 200 and number of generations was 5.

TABLE II
OPTIMAL PARAMETERS

| Parameter | Notation | Limits |
|--------------------------------------|-----------|--------|
| Stator outer diameter (mm) | D_{SO} | 103 |
| Stator inner diameter (mm) | D_{SI} | 60 |
| Stator slot depth (mm) | S_D | 14.8 |
| Rotor inner diameter (mm) | D_{RI} | 22 |
| Stator pole angle (°) | β_S | 28.5 |
| Rotor pole angle (°) | β_R | 29.1 |
| Volume (cm ³) | V | 315 |
| Average torque (Nm) | T | 0.84 |
| Torque density (kNm/m ³) | T/V | 2.67 |

TABLE III
CONTROL FACTORS

| Parameter | Notation | Factor | Level | | | | |
|-------------------------------|----------------------------|--------|-------|-------|------|-------|----|
| | | | 1 | 2 | 3 | 4 | 5 |
| Stator pole angle (°) | β_s | X_1 | 25 | 28.75 | 32.5 | 36.25 | 40 |
| Stator pole angle at core (°) | $\alpha_s = \beta_s - X_2$ | X_2 | 5 | 7.5 | 10 | 12.5 | 15 |
| Rotor pole angle (°) | β_r | X_3 | 25 | 28.75 | 32.5 | 36.25 | 40 |
| Rotor pole angle at core (°) | $\alpha_r = \beta_r + X_4$ | X_4 | 25 | 31.25 | 37.5 | 43.75 | 50 |
| Airgap shift | ε | X_5 | 0 | 0.25 | 0.5 | 0.75 | 1 |
| Additional tooth angle (°) | β_{r+} | X_6 | 0 | 3.75 | 7.5 | 11.25 | 15 |

It is important to highlight that this TO was accomplished as a test run to determine the convergence of the GA.

Fig. 8 presents the results of the optimization. The obtained geometry shows that the material density of the stator teeth was higher on the side of the overlap beginning. Moreover, the airgap profile was descending. The density of the rotor teeth material was relatively constant. It can be concluded that the TO could be run for more generations in order to achieve a more specific shape. Nevertheless, the obtained geometry offered a considerable improvement: the torque ripple dropped by more than 50%, while the average torque decreased by 30%.

IV. CONCLUSION

This research work aimed to introduce an optimization methodology which reduces computational complexity. The computational burden reduction was achieved by narrowing the TO search space using preliminary shape optimization and sensitivity analysis. The reduction of the TO design space was more than 75%, which led to a notable decrease of the TO computational burden. Moreover, the improvement of the SRM performance was significant. The obtained geometry of the SRM suggests exploring of the convergence of the TO in order to achieve more specific shapes.

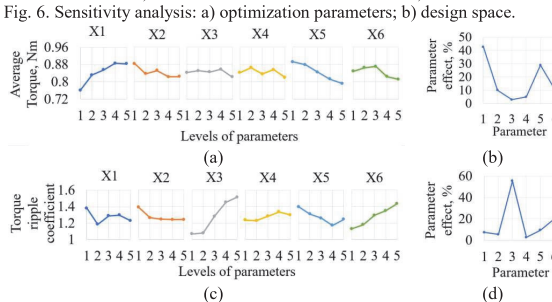
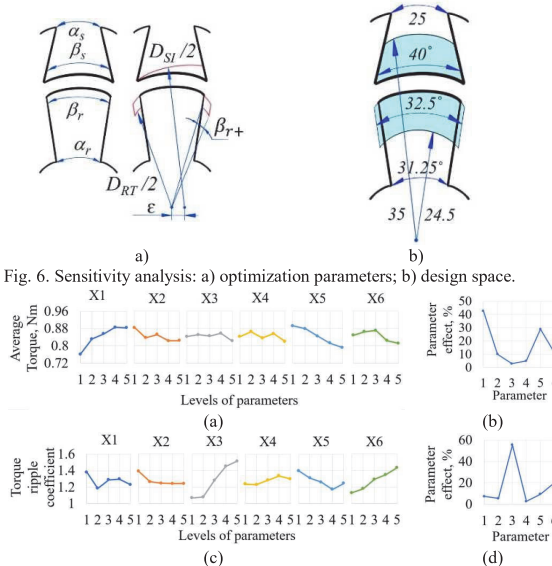


Fig. 7. Sensitivity analysis results: a) peak-to-peak values of average torque; b) parameters' effect on average torque; c) peak-to-peak values of torque ripple; d) parameters' effect on torque ripple.

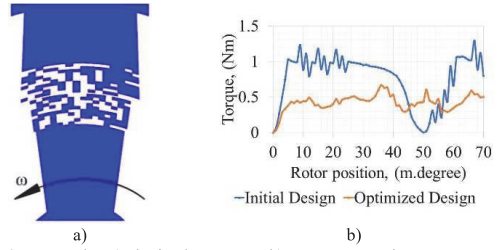


Fig. 8. TO results: a) obtained geometry; b) torque comparison.

Moreover, the question raised by this study is manufacturability of the topologically optimized designs. It is important to highlight that the structural integrity and losses within a topologically optimized 3D printed motor are needed to be taken into account. Therefore, in the future study, additive manufacturing possibilities and restrictions will be studied and addressed within the topology optimization.

V. REFERENCES

- [1] W. Ding and D. Liang, "Modeling of a 6/4 switched reluctance motor using adaptive neural fuzzy inference system," in *IEEE Transactions on Magnetics*, Jul. 2008, vol. 44, no. 7, pp. 1796–1804, doi: 10.1109/TMAG.2008.919711.
- [2] C. Gan, J. Wu, M. Shen, S. Yang, Y. Hu, and W. Cao, "Investigation of skewing effects on the vibration reduction of three-phase switched reluctance motors," *IEEE Trans. Magn.*, vol. 51, no. 9, Sep. 2015, doi: 10.1109/TMAG.2015.2441035.
- [3] A. M. Omekanda, "Robust torque and torque-per-inertia optimization of a switched reluctance motor using the Taguchi methods," *IEEE Trans. Ind. Appl.*, vol. 42, no. 2, pp. 473–478, Mar. 2006, doi: 10.1109/TIA.2006.870031.
- [4] N. K. Sheth and K. R. Rajagopal, "Optimum Pole Arcs for a Switched Reluctance Motor for Higher Torque with Reduced Ripple," *IEEE Trans. Magn.*, vol. 39, no. 5 II, pp. 3214–3216, Sep. 2003, doi: 10.1109/TMAG.2003.816151.
- [5] H. Chen, W. Yan, J. J. Gu, and M. Sun, "Multiobjective Optimization Design of a Switched Reluctance Motor for Low-Speed Electric Vehicles with a Taguchi-CSO Algorithm," *IEEE/ASME Trans. Mechatronics*, vol. 23, no. 4, pp. 1762–1774, Aug. 2018, doi: 10.1109/TMECH.2018.2839619.
- [6] J. W. Lee, H. S. Kim, B. Il Kwon, and B. T. Kim, "New rotor shape design for minimum torque ripple of SRM using FEM," in *IEEE Transactions on Magnetics*, Mar. 2004, vol. 40, no. 2 II, pp. 754–757, doi: 10.1109/TMAG.2004.824803.
- [7] K. C. Yong, S. Y. Hee, and S. K. Chang, "Pole-shape optimization of a switched-reluctance motor for torque ripple reduction," *IEEE Trans. Magn.*, vol. 43, no. 4, pp. 1797–1800, 2007, doi: 10.1109/TMAG.2006.892292.
- [8] G. Li, J. Ojeda, S. Hlioui, E. Hoang, M. Lecrivain, and M. Gabsi, "Modification in rotor pole geometry of mutually coupled switched reluctance machine for torque ripple mitigating," *IEEE Trans. Magn.*, vol. 48, no. 6, pp. 2025–2034, 2012, doi: 10.1109/TMAG.2011.2179307.
- [9] A. M. Omekanda, "A new technique for multidimensional performance optimization of switched reluctance motors for vehicle propulsion," *IEEE Trans. Ind. Appl.*, vol. 39, no. 3, pp. 672–676, May 2003, doi: 10.1109/TIA.2003.810632.
- [10] H. Zhang and S. Wang, "Topology Optimization of Rotor Pole in Switched Reluctance Motor for Minimum Torque Ripple," <http://dx.doi.org/10.1080/15325008.2017.1310769>, vol. 45, no. 8, pp. 905–911, May 2017, doi: 10.1080/15325008.2017.1310769.
- [11] C. Midha, "A Study of Topology Optimization Methods for the Design of Electromagnetic Devices," 2018.
- [12] "Siemens. Simcenter MAGNET 2D/3D, 2021. [Online]." <https://www.plm.automation.siemens.com/global/en/products/simcenter/magnet.html> (accessed Jun. 28, 2021).
- [13] E. Andriushchenko et al., "Optimization of a 3D-Printed Permanent Magnet Coupling Using Genetic Algorithm and Taguchi Method," *Electronics*, vol. 10, no. 4, p. 494, Feb. 2021, doi: 10.3390/electronics10040494.

VI. BIOGRAPHIES

Ekaterina Andriushchenko received her B.Sc. and M.Sc. degrees in mechanical engineering from Peter the Great St. Petersburg Polytechnic University, Russia, in 2013 and 2019 respectively. She is currently working toward the Ph.D. degree in electrical engineering with Tallinn University of Technology.

Her current research interest is design optimization of electrical machines.

Mohammad Hossain Mohammadi (Member, IEEE) received the B.Sc. (Eng) degree in electrical engineering from American University in Dubai, United Arab Emirates, in 2013, with the Valedictorian Award, and the M.Sc. and Ph.D. degrees in electrical engineering from McGill University, Montréal, Canada, in 2015 and 2019, respectively. He is currently a Postdoctoral Research Scientist with the Renewable Energy Integration Group, CanmetENERGY, Natural Resources Canada, leading the development of synthetic benchmarks representative of the Canadian grid. His other research interests include modeling, design, optimization, and control of low-frequency electromagnetic devices, applied machine learning, and statistical analysis. He has been an Active Volunteer in the IEEE Montreal Section, since 2014.

David Alister Lowther (Life Fellow, IEEE), obtained a B.Sc. (Eng) degree from Kings College, London and then his Ph.D. degree in 1973 from Brighton University in the United Kingdom for research related to the design of linear induction motors. He then moved to Imperial College, London as a Postdoctoral Researcher before finally taking up an academic post at McGill University in 1979, where he is currently a Professor of electrical engineering. From 1998 to 2006, he was the Chair of the Electrical and Computer Engineering Department and was President of the McGill Association of University Teachers in 2015. His research interests involve the analysis and design of low frequency electromagnetic devices including the numerical solution of the field equations, result evaluation, design optimization and the

use of knowledge-based techniques to implement a design process. He has over 300 publications in the area and currently has a team of about 7 research students. He was a founder and President of Infolytica Corporation, a company specializing in the development of computer based tools for the analysis and design of low frequency devices, until its acquisition in 2017 by Mentor Graphics. He is currently a Technical Director with the Mechanical Analysis Division of Mentor Graphics. In addition, he was a founder member of the International Compumag Society and is currently its President. He is also a member of the International Steering Committee of the IEEE CEFC conference, among many others. He was the Chair of the 2015 Compumag conference held at McGill University. Dr. Lowther is a Fellow of the IET, a Fellow of the Canadian Academy of Engineering and a Fellow of the IEEE.

Hamidreza Heidari was born in Zanjan, Iran, in 1989. He received the B.Sc. and M.Sc. degrees in electronic engineering from the University of Zanjan, Zanjan, Iran. He is currently working toward the Ph.D. degree in electrical engineering with Tallinn University of Technology.

His current research interests include analysis and control of electric machines.

Ants Kallaste received his B.Sc., M.Sc., Ph.D., and Doctor (Tech.) degrees from degrees in electrical engineering from Tallinn University of Technology, Estonia, in 2004, 2006, 2013, 2021 respectively. He is currently a professor of electrical machines in Tallinn University of Technology, Department of Electrical Power Engineering and Mechatronics. He is holding the position of Head of Electrical Machines Research Group. He is the member of IEEE and Estonian Society of Moritz Hermann Jacobi.

His main research interest is design of electrical machines.

Arbaaz Khan completed his B.Sc. (Eng) in Electrical and Electronics Engineering from Birla Institute of Tech (BIT, Mesra) in 2012. He joined Defence Institute of Advanced Technology (DIAT) to pursue his M.Sc. During his master's, he was selected to work in DRDO lab at Pune. He received his Ph.D. degree in electrical engineering from McGill University. His main interests lie in electromagnetic analysis and optimization.

Publication II

Andriushchenko E., Kallaste A., Mohammadi M. H., Lowther D. A., Heidari H. (2022). Sensitivity analysis for multi-objective optimization of switched reluctance motors. *MDPI Machines* 10(7), 559.

Article

Sensitivity Analysis for Multi-Objective Optimization of Switched Reluctance Motors

Ekaterina Andriushchenko ^{1,*} , Ants Kallaste ¹ , Mohammad Hossain Mohammadi ² , David A. Lowther ² and Hamidreza Heidari ¹ 

¹ Department of Electrical Power Engineering and Mechatronics, Tallinn University of Technology, Ehitajate tee 5, 12616 Tallinn, Estonia; ants.kallaste@taltech.ee (A.K.); haheid@taltech.ee (H.H.)

² Department of Electrical and Computer Engineering, McGill University, Montréal, QC H3A 0G4, Canada; mohammad.mohammadi@mail.mcgill.ca (M.H.M.); david.lowther@mcgill.ca (D.A.L.)

* Correspondence: ekandr@taltech.ee

Abstract: The main issue of the switched reluctance motor (SRM) is its noise and vibration caused by high torque ripples on the rotor's shaft. Many methods have been developed for improving the torque characteristic of the SRM. For example, design optimization is one of the promising approaches to the noise and vibration reduction of the SRM. Particularly, topology optimization (TO) of the stator and rotor can be highly beneficial to addressing the torque ripple issue. However, the TO of the SRM appears to be computationally demanding. To overcome this issue, this study proposes a method aiming to reduce the computational complexity of the TO through the reduction of the design space. Particularly, this paper presents a sensitivity analysis of a list of unique design parameters of the SRM and their influence on the average torque of the motor and the torque ripple of the motor. By applying the sensitivity analysis, the design space of the TO could be reduced, leading to a considerable decrease in the TO computational burden. Additionally, valuable conclusions on the geometrical parameters' influences on the SRM torque and torque ripple have been drawn.



Citation: Andriushchenko, E.; Kallaste, A.; Mohammadi, M.H.; Lowther, D.A.; Heidari, H. Sensitivity Analysis for Multi-Objective Optimization of Switched Reluctance Motors. *Machines* **2022**, *10*, 559. <https://doi.org/10.3390/machines10070559>

Academic Editor: Jose Alfonso Antonino-Daviu

Received: 5 June 2022

Accepted: 8 July 2022

Published: 11 July 2022

Publisher's Note: MDPI stays neutral with regard to jurisdictional claims in published maps and institutional affiliations.



Copyright: © 2022 by the authors. Licensee MDPI, Basel, Switzerland. This article is an open access article distributed under the terms and conditions of the Creative Commons Attribution (CC BY) license (<https://creativecommons.org/licenses/by/4.0/>).

Keywords: design of experiments; electric motors; optimization; optimization methods; switched reluctance motor; Taguchi methods

1. Introduction

Recently, there has been increasing interest in switched reluctance motors (SRMs) due to the benefits they provide. Within the SRMs' structure, no permanent magnets or rotor windings are used. For this reason, the SRMs are highly suitable for high-speed and high-temperature applications. However, the performance of the SRMs is limited by high torque ripple and consequent vibration and noise [1,2].

Previous research has established that the design of the SRM plays an important role in addressing the issue of the torque ripple [3–5]. Many studies on SRM have utilized various design optimization techniques to achieve high and stable torque characteristics. Several authors have investigated the possibilities of rotor pole modifications to reduce the torque ripples [6–10]. Another group of studies presents the optimization of classic linear and angular dimensions of the motor [11,12]. The majority of the methods propose simple yet effective modifications of the rotor and stator, aiming to reduce the fringing flux effect and avoid the oversaturation of the pole's tips. Nevertheless, a wider search for more beneficial shapes is possible with topology optimization (TO).

Nowadays, TO has been shown as a feasible approach for electric motor improvement. Many researchers have successfully obtained advantageous shapes of the motors, enhancing their performance characteristics [13,14]. In this sense, SRMs are not an exception. A considerable improvement in the torque and reduction of the torque ripple of the SRMs have been achieved using TO techniques [15,16]. Yet, a key challenge of the TO application is its high computational complexity. This is especially critical if a finite element model is

utilized to calculate the objective function. For instance, the application of the ON/OFF topology optimization method requires a high-density discretization of the motor geometry. The discretization of the motor geometry defines the number of optimization parameters. To carry out TO for the SRM considering all the core body, around 1500 discrete parameters should be involved. This leads to a high number of calculations being needed to analyze the influences of these parameters on the objective function [17].

To overcome the issue of the high computational complexity of the TO, many methods have been developed by researchers in the fields of electromagnetic calculations and motor design. The first group of researchers attempts to replace a FE model of the electrical machine with a surrogate model [18]. The surrogate model represents the motor FE model with high precision but requires the application of complex and computationally demanding methods. Another group of researchers defined crucial areas of the motor geometry based on the fringing flux behavior [13]. Yet, the defined crucial areas are mainly defined approximately and can lead to an improper design space definition.

This paper proposes a method that helps to minimize the design space of the SRM TO using sensitivity analysis (SA). The method involved the definition of the potentially crucial geometrical parameters of the SRM based on a literature review. Then, the SA was applied to determine which parameters have a major impact on the average torque and torque ripple of the motor. Lastly, based on the results of the SA, an optimal and minimal design space of the motor was defined to be utilized within the TO. The SA was accomplished using the Taguchi method. For many years this method has been applied for different purposes, from sensitivity analysis and robust optimization to the design of experiments. It has been recalled by many scientists as a relatively simple, fast, and reliable approach to the SA for motor design problem.

The proposed approach helps to efficiently reduce the design domain of the TO, and consequently decrease the computational complexity of the TO. This allows the speeding up of the overall SRM development and optimization process. To the authors' knowledge, there have been no studies focused on the TO design domain definition using the Taguchi method. Additionally, this study provides a comprehensive overview of the SRM's geometric parameters and their influences on the average torque and torque ripple.

The paper is organized as follows. First, the structure and operation principle of the motor are discussed in Section 2. Then, Section 2 gives insights into the torque ripple origins and considers the SRM's geometrical parameters. Section 3 is dedicated to the design model definition and Taguchi method's theory with its application. The following chapter concentrates on the results of the SA and the selection of the optimal design space of the TO. Lastly, Section 5 concludes and discusses the research work.

2. Switched Reluctance Motor

2.1. SRM Working Principle

This section briefly introduces the basics of the SRMs which are essential for the average torque and torque ripple improvement. The basic structure, operation principle, electromagnetic characteristics, and control are covered in the following paragraphs.

SRMs have been widely applied for electric propulsion, fan, pump, and servo applications. They possess a simple, robust structure without windings on the rotor, which makes them beneficial for high-speed and high-temperature applications.

There is a list of SRM structures that are primarily defined by the number of stator phases. In this paper, a three-phase 6-stator-pole and 4-rotor-pole SRM is considered. A simplified structure of the motor is presented in Figure 1. As can be seen in the figure, the stator carries the windings of three phases (A, B, and C) and the rotor has a simple 4-pole or 4-tooth structure.

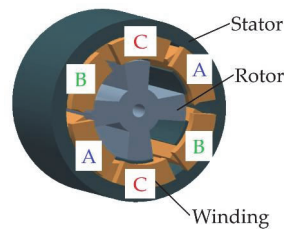


Figure 1. Three-phase 4/6 pole SRM structure.

The working principle of the motor is based on the rule of minimum reluctance. This rule is closely connected to the term “phase reluctance” or the opposite of it—“phase inductance.” During the motor operation phase, inductances are constantly changing depending on the effective airgap length between the rotor and stator poles as a function of the rotor position. The operation principle of the SRM is presented in Figure 2, where red is dedicated to the energized phase C, green the energized phase B, and blue the energized phase A. Additionally, Figure 3 gives a detailed representation of the ideal phase inductance variation in relation to the rotor position. The involved stator and rotor teeth are marked with red. As can be seen, the phase inductance is minimum when the rotor teeth are not aligned with the considered stator teeth. When the considered phase is excited, the rotor teeth try to align themselves with the stator teeth to decrease the reluctance (increase the inductance) by reducing the effective air gap length. When the teeth of the stator and rotor are aligned, the phase inductance appears at its maximum. To ensure continuous rotation and operation of the motor, one phase gets turned on after other switches off. Prior to the area of maximum inductance, the phase voltage switches off and the current falls to zero. If the voltage continues to be supplied to the considered phase, a negative torque will be produced.

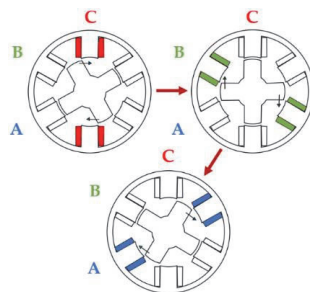


Figure 2. SRM operation principle.

As shown in Figure 3, the DC-voltage is supplied to a phase at the rotor position when the inductance is at its growing phase. To illustrate this process mathematically, the following equation can be considered.

$$T(\theta, i) = \int_0^i \frac{\partial L(\theta, i)}{\partial \theta} di. \quad (1)$$

where T is the produced phase torque, θ denotes the rotor position angle, and i is the phase current.

To maintain continuous torque production, the control scheme of a three-phase 6/4-pole SR motor drive is applied (see Figure 4). Usually, the SRM is run by an asymmetric bridge converter, where each phase is controlled independently. A switching pattern directs the DC voltage to one of the phases depending on the rotor’s position. For this purpose, the SRM drive often comprises six position-controlled and current-controlled switches.

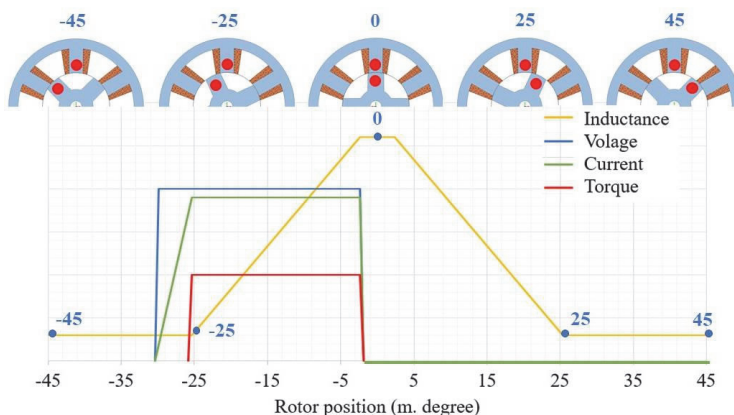


Figure 3. Ideal inductance profile of one SRM phase.

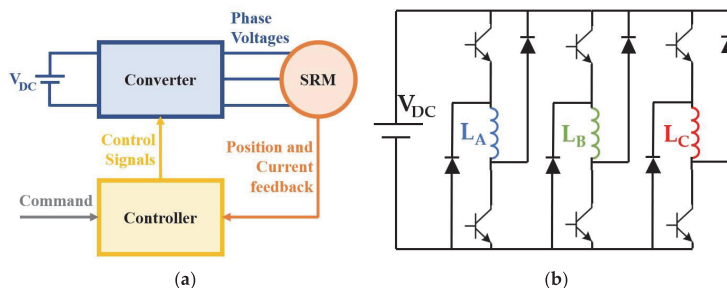


Figure 4. SRM drive: (a) SRM drive concept; (b) asymmetric bridge converter. L_{A-C} denote to the phase inductances.

Traditionally, the commutation pattern of the SRM motor is defined based on the static representation of the phase inductance profile. Assuming the symmetry of the stator and rotor poles, the classic commutation pattern for the 6/4 pole SRM can be illustrated by Figure 5. It is important to highlight that a phase winding should be excited during of the phase inductance growth. Therefore, the duration of the phase voltage application is 30° of the mechanical position of the motor.

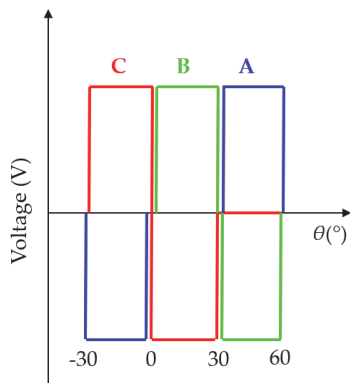


Figure 5. Commutation pattern of three-phase SRM drive.

2.2. Torque Ripple

A main challenge of the SRM drive is high levels of vibration and noise during operation. It has been revealed that the key reasons for the SRM's vibrations are the unstable, fluctuating torque at the motor shaft. Numerous studies have proved that the SRM's torque ripples are mainly caused by the fringing flux which appears just before the rotor and stator teeth overlap, as shown in Figure 6. The consequence of the fringing flux is the nonlinear growth of the phase inductance profile, which triggers the torque also to grow nonlinearly. The nonlinearity of the magnetic torque negatively influences the phase current and leads to unstable torque production. Figure 7 illustrates the described process graphically.

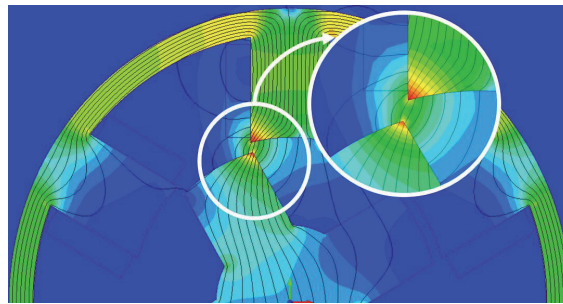


Figure 6. Fringing flux at the beginning of overlap.

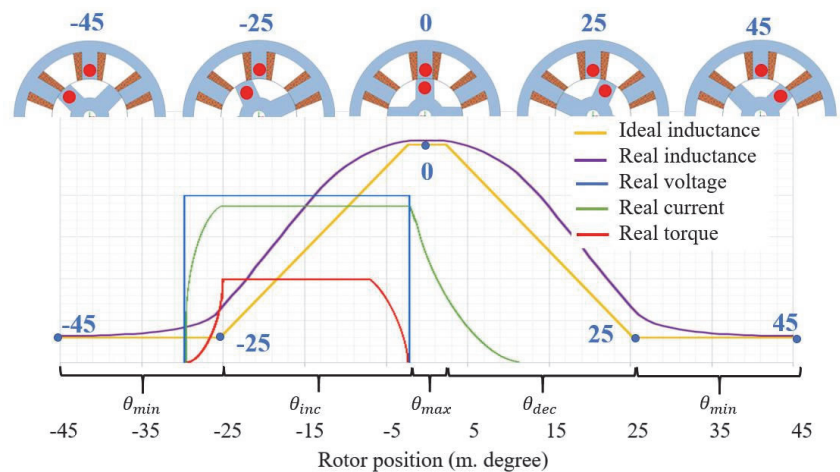


Figure 7. Ideal and real phase inductance comparison.

There are various methods in the literature that address the torque ripple issue from different points of view. The most well-known approaches are motor design modification and control algorithm adjustment. It has been shown that particular geometries of the rotor and stator poles reduce the fringing flux, improve the inductance profile, and consequently, suppress the torque ripples. These geometries are considered in the following section.

2.3. Geometrical Parameters of SRM

This section describes in detail the crucial geometrical parameters of the SRM which are illustrated in Figure 8. In the figure, D_{RT} is the diameter of the rotor additional teeth and D_{SJ} is the stator inner diameter.

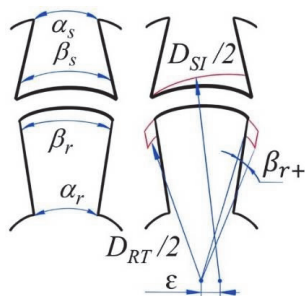


Figure 8. Design parameters.

The phase inductance profile of the SRM is highly dependent on the geometry of the rotor, stator, and the airgap—particularly, on the rotor and stator pole angles, β_r , β_s . The duration of the minimum inductance θ_{min} , the duration of the maximum inductance θ_{max} , and the duration of the growing θ_{inc} and falling inductance θ_{dec} phases can be defined as follows.

$$\begin{cases} \theta_{min} = (\alpha - (\beta_s + \beta_r))/2 \\ \theta_{max} = \beta_r - \beta_s \\ \theta_{inc} = \theta_{dec} = \beta_s \end{cases} \quad (2)$$

where $\alpha = 2\pi/N_r$ is a rotor pole pitch and N_r is the number of the rotor poles.

The stator and rotor pole angles at the core (α_s , α_r , respectively) have an indirect influence on the torque ripple minimization. It has been shown by many studies that the variation of α_s and α_r creates beneficial sharp angles at the beginning of stator and rotor teeth overlap, avoiding the fringing flux appearance [10] and reducing the torque ripple.

The additional tooth angle β_{r+} proposes a similar solution to α_s and α_r . The additional tooth angle makes a big difference in terms of the wider distributed magnetic flux saturation. Moreover, this parameter addresses torque fall during the excitation transition.

One of the key design parameters influencing the inductance profile is the air-gap shape between the rotor and stator poles. As illustrated in Figure 8, air-gap shift ϵ helps achieving a variable air-gap length (L_{ag}) with a bigger value at the beginning of the overlap and a smaller value at the end of the overlap. Applying an appropriate value of the air-gap shift allows one to obtain the torque, which grows together with the teeth overlap.

In this sensitivity analysis, the vector of the design parameters is defined as follows:

$$x = [\beta_s, \alpha_s, \beta_r, \alpha_r, \epsilon, \beta_{r+}] \quad (3)$$

To avoid unfeasible designs, geometrical constraints are set for the entire space, denoted by \mathcal{F}_Δ .

$$\mathcal{F}_\Delta = \begin{cases} 25^\circ \leq \beta_s \leq 40^\circ \\ \beta_s - 5^\circ \leq \alpha_s \leq \beta_s - 15^\circ \\ 25^\circ \leq \beta_r \leq 40^\circ \\ \beta_r + 25^\circ \leq \alpha_r \leq \beta_r + 50^\circ \\ 0 \text{ mm} \leq \Delta \leq 1 \text{ mm} \\ 0^\circ \leq 2\Delta\beta_{r+} \leq 15^\circ \end{cases} \quad (4)$$

3. Case Study

3.1. Design Model of SRM

With the aim of studying the defined design parameters and carrying out the SA, the design model of the motor was created within the Simcenter MAGNET software. Only 1/3 of the motor was modeled in 2D to reduce the computational complexity. The static simulation was carried out and resulted in a full torque curve being obtained. The SRM's FE model is presented in Figure 9. The mesh characteristics of the model were as follows:

maximum element size: 1, curvature refinement angle: 1. Only one phase of the motor was included in the static model. The full stator core and rotor were modelled to close the magnetic circle. The coils specifications were the following: 257 number of turns, strand area: 0.326 mm².

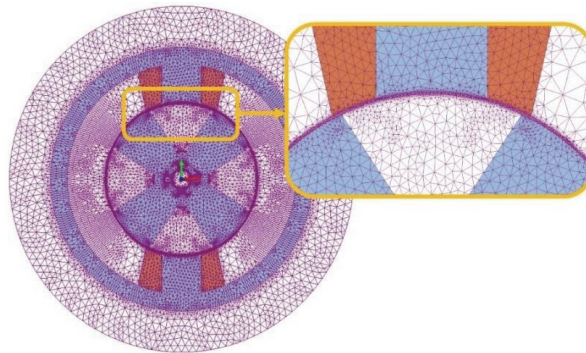


Figure 9. SRM's 2D FE model for one phase.

The specifications and geometry characteristics of the SRM's initial design are presented in Table 1 and Figure 10. The torque ripple coefficient (Table 1) was calculated as follows.

$$T_r = \frac{T_{max} - T_{min}}{T_{av}} \quad (5)$$

It is important to mention that prior to the SA, the main geometry characteristics were optimized with respect to the average torque. The material of the stator and rotor core was electrical steel with 6.5% silicon content. It was projected that the SRM would be manufactured using additive manufacturing techniques. Therefore, the electromagnetic characteristics of a printed sample were utilized in the FE model (see Figure 11).

In order to assess the torque ripple of the SRM, a full curve of the torque had to be obtained. Therefore, each design was simulated at different positions, as shown in Figure 12. The simulations were carried out starting at the position -45° to 0° with the step of 1° .

3.2. Taguchi Method

In this paper, the SA of the design parameters was carried out using the Taguchi method and analysis of variance (ANOVA). Detailed descriptions of the Taguchi and ANOVA methods are presented in the following papers [11,12,19].

Table 1. Motor specifications and geometry characteristics.

| Specification/Geometry Characteristic | Symbol | Value |
|---------------------------------------|-------------------|--------------------|
| Phase resistance | R | 5 Ω |
| Stack length | L | 60 mm |
| Stator outer diameter | D_{SO} | 103 mm |
| Stator inner diameter | D_{SI} | 60 mm |
| Stator slot depth | S_D | 14.8 mm |
| Rotor inner diameter | D_{RI} | 22 mm |
| Stator/rotor pole angle | β_S/β_R | 28.5/29.1 $^\circ$ |
| Air-gap length | a | 0.25 mm |
| Average three-phase torque | T_{av} | 1.34 Nm |
| Torque ripple coefficient | K | 2.03 |

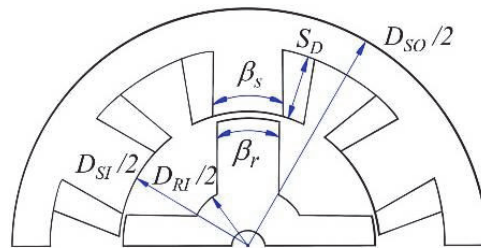


Figure 10. Geometry of the SRM's initial design.

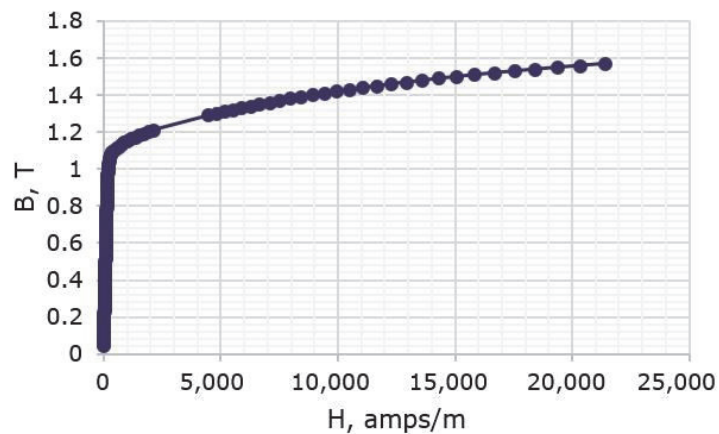


Figure 11. B-H curve of printed steel [19,20].

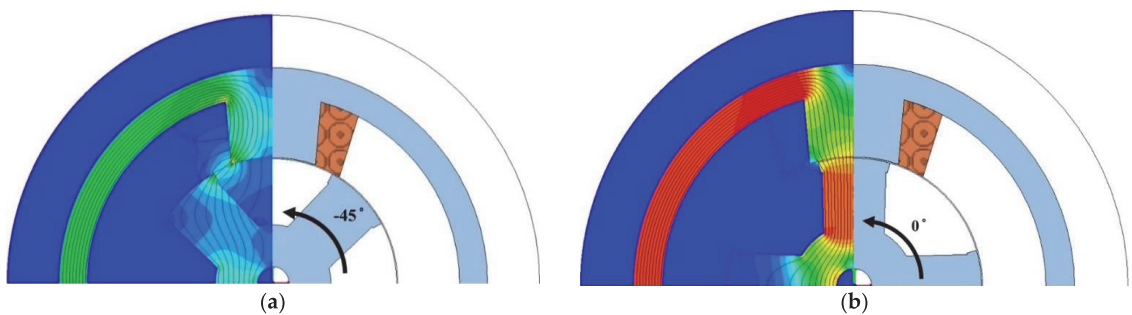


Figure 12. Static simulation positions (a) beginning position; (b) end position.

The Taguchi method provided a plan of experiments for the SA with a reduced number of required simulations. Moreover, by employing the Taguchi method, the best level of each variable could be defined. Then, the ANOVA helped to define the influence of each variable on the objective function.

The Taguchi approach is a statistical method that helps to effectively discover the parameter space. For a certain number of design parameters and their levels, Taguchi proposed a certain orthogonal array consisting of the minimum necessary combinations of the design parameters to be able to fully analyze the results. Each combination of the design parameters is called an experiment. Aiming to obtain the values of the objective functions, these experiments can be both carried out as real tests or simulations. Then, based on the results of the Taguchi experiments, the ANOVA can be carried out [19]. The

sensitivity analysis was carried out using the six design parameters discussed in Section 4. The design parameters or so-called “control factors” were sampled within the design space, as shown in Table 2.

Table 2. Design parameters’ sampling.

| Design Parameter/Control Factor | Symbol | Factor | Level | | | | |
|---------------------------------|----------------------------|--------|-------|-------|------|-------|----|
| | | | 1 | 2 | 3 | 4 | 5 |
| Stator pole angle (°) | $\beta_s = X_1$ | X_1 | 25 | 28.75 | 32.5 | 36.25 | 40 |
| Stator pole angle at core (°) | $\alpha_s = \beta_s - X_2$ | X_2 | 5 | 7.5 | 10 | 12.5 | 15 |
| Rotor pole angle (°) | $\beta_r = X_3$ | X_3 | 25 | 28.75 | 32.5 | 36.25 | 40 |
| Rotor pole angle at core (°) | $\alpha_r = \beta_r + X_4$ | X_4 | 25 | 31.25 | 37.5 | 43.75 | 50 |
| Airgap shift, mm | $\varepsilon = X_5$ | X_5 | 0 | 0.25 | 0.5 | 0.75 | 1 |
| Additional tooth angle (°) | $\beta_{r+} = X_6/2$ | X_6 | 0 | 3.75 | 7.5 | 11.25 | 15 |

Based on the number of parameters and their levels, Taguchi proposed the design matrix constituted of a minimum and a sufficient number of experiments. For six parameters and five levels of each, a matrix $L_{25} (6^5)$ of twenty-five experiments was utilized. In case of the full factorial experiment, the 7776 experiments would have been required. The orthogonal array or matrix of experiments is presented in Table 3.

Table 3. Taguchi orthogonal array $L_{25} (6^5)$ for 6 control factors and 5 levels and simulation results.

| Experiment | Control Factor | | | | | | Average Torque | Torque Ripple Coefficient |
|------------|----------------|-------|-------|-------|-------|-------|----------------|---------------------------|
| | X_1 | X_2 | X_3 | X_4 | X_5 | X_6 | | |
| 1 | 1 | 1 | 1 | 1 | 1 | 1 | 0.851 | 1.22 |
| 2 | 1 | 2 | 2 | 2 | 2 | 2 | 0.838 | 1.06 |
| 3 | 1 | 3 | 3 | 3 | 3 | 3 | 0.790 | 1.36 |
| 4 | 1 | 4 | 4 | 4 | 4 | 4 | 0.716 | 1.55 |
| 5 | 1 | 5 | 5 | 5 | 5 | 5 | 0.614 | 1.73 |
| 6 | 2 | 1 | 2 | 3 | 4 | 5 | 0.808 | 1.16 |
| 7 | 2 | 2 | 3 | 4 | 5 | 1 | 0.792 | 1.06 |
| 8 | 2 | 3 | 4 | 5 | 1 | 2 | 0.899 | 1.37 |
| 9 | 2 | 4 | 5 | 1 | 2 | 3 | 0.850 | 1.39 |
| 10 | 2 | 5 | 1 | 2 | 3 | 4 | 0.812 | 0.95 |
| 11 | 3 | 1 | 3 | 5 | 2 | 4 | 0.887 | 1.53 |
| 12 | 3 | 2 | 4 | 1 | 3 | 5 | 0.829 | 1.55 |
| 13 | 3 | 3 | 5 | 2 | 4 | 1 | 0.837 | 1.19 |
| 14 | 3 | 4 | 1 | 3 | 5 | 2 | 0.796 | 0.92 |
| 15 | 3 | 5 | 2 | 4 | 1 | 3 | 0.930 | 1.25 |
| 16 | 4 | 1 | 4 | 2 | 5 | 3 | 0.936 | 1.52 |
| 17 | 4 | 2 | 5 | 3 | 1 | 4 | 0.878 | 1.72 |
| 18 | 4 | 3 | 1 | 4 | 2 | 5 | 0.907 | 1.30 |
| 19 | 4 | 4 | 2 | 5 | 3 | 1 | 0.855 | 0.92 |
| 20 | 4 | 5 | 3 | 1 | 4 | 2 | 0.856 | 1.02 |
| 21 | 5 | 1 | 5 | 4 | 3 | 2 | 0.935 | 1.52 |
| 22 | 5 | 2 | 1 | 5 | 4 | 3 | 0.847 | 0.94 |
| 23 | 5 | 3 | 2 | 1 | 5 | 4 | 0.826 | 1.00 |
| 24 | 5 | 4 | 3 | 2 | 1 | 5 | 0.901 | 1.43 |
| 25 | 5 | 5 | 4 | 3 | 2 | 1 | 0.910 | 1.26 |

Using the Taguchi orthogonal array, twenty-five experiments were carried out, and the results are listed in Table 3 as well.

The peak-to-peak values of the average torque and torque ripple at zero speed were calculated for each factor and level.

$$M_{ij}(f) = \frac{1}{n} \cdot \sum f(i, j) \tag{6}$$

where i denotes the parameter number, j represents the level number, n is the number of experiments, and $f(i, j)$ is the value of an objective function.

To study the effect of each parameter on the objective function, the sums of squares were calculated as follows.

$$SS_{ij}(f) = n \cdot \sum (M_{ij} - M_f)^2 \quad (7)$$

where M_f is the total mean value of the objective function.

4. Results

4.1. Results of the Sensitivity Analysis

The results of the sensitivity analysis, such as peak-to-peak values of the average torque and torque ripple, are shown in Figures 13 and 14. Moreover, Figure 15 presents the overall influences of the design parameters on the objective functions.

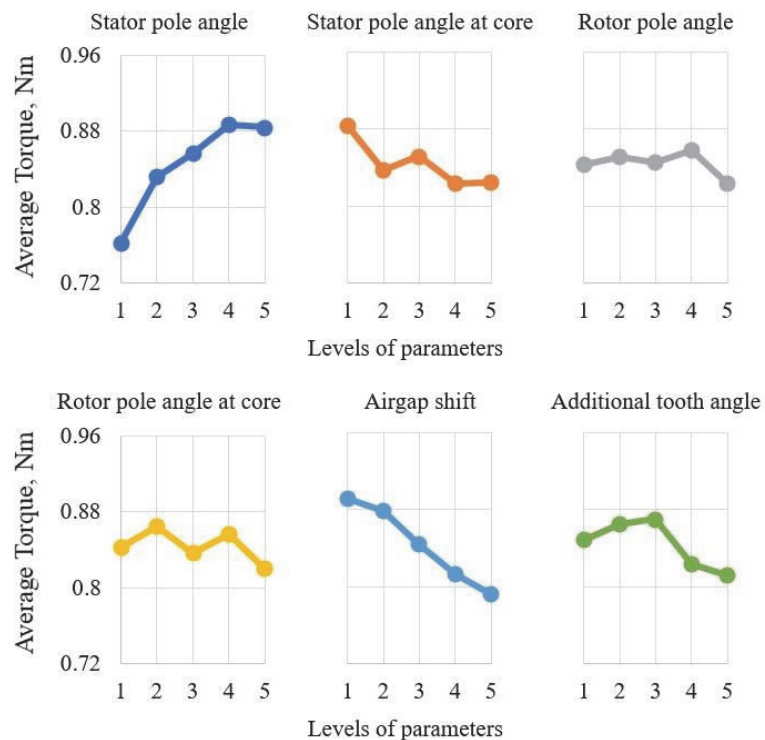


Figure 13. Peak-to-peak values of the average torque.

It can be seen in the graphs above (see Figures 13 and 15a) that the stator pole angle and the airgap shift variations have major influences on the average torque. The parameter effect value of the stator pole angle (X_1) and airgap shift (X_5) are 42% and 28%, respectively. Figure 13 suggests that the growth of the stator pole angle makes the average torque increase rapidly. This fact correlates with Equation (2), which defines θ_{inc} and the duration of torque production as a direct function of the stator pole angle. Meanwhile, the growth in the airgap shift reduces the average torque. One of the reasons could be a torque fall at the beginning of the overlap. On the other hand, the average torque has a nonlinear response to the change in the stator pole angle at the core and additional tooth angle on the rotor. There was a slight reaction noticed from the change in the rotor pole angle and the rotor tooth angle at the core.

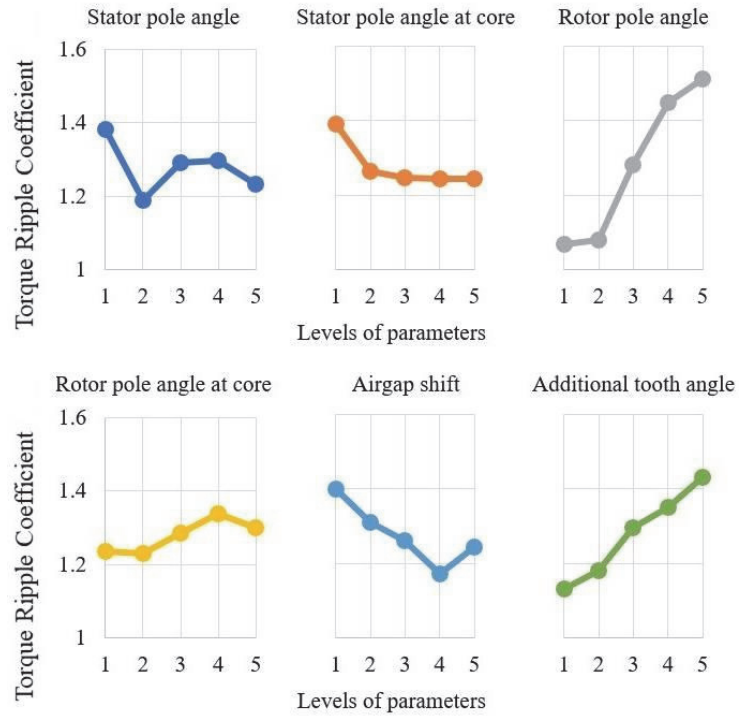


Figure 14. Peak-to-peak values of the torque ripple.

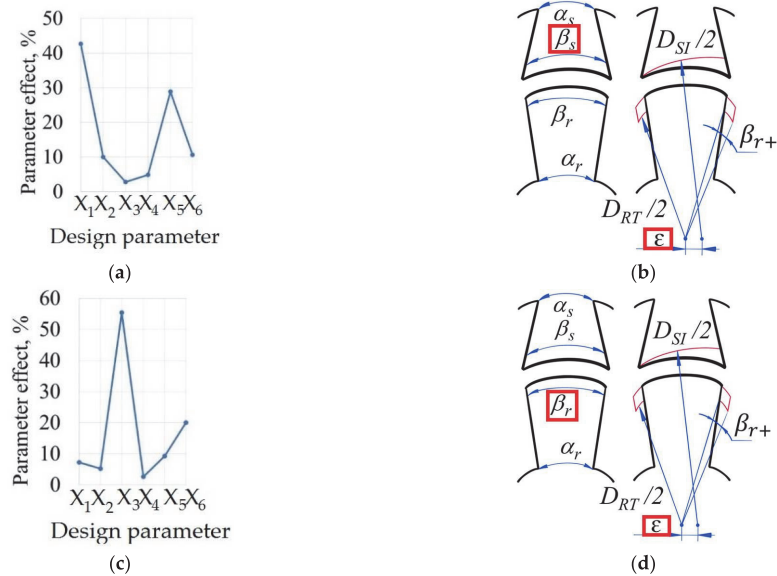


Figure 15. Control factors' effects on the objectives: (a) average torque; (b) most influential parameters on average torque; (c) torque ripple; (d) most influential parameters on torque ripple.

If we now turn to the torque ripple analysis, we can conclude that the rotor pole angle has a principal influence on the torque ripple (see Figures 14 and 15c). The parameter effect

value of the rotor pole angle (X_3) is more than 50%. Particularly, with the growth of the rotor pole angle, the torque ripple swiftly increases. The same tendency can be noticed for the growth of the additional tooth angle. This fact correlates with Equation (2), which illustrates that the duration of the maximum inductance θ_{max} grows together with the rotor pole angle. One of the reasons that torque ripple increases along with the rotor pole angle could be that the SRM reaches the maximum inductance too fast and moves to a phase with no positive torque production. The air gap shift had a positive influence on the torque ripple reduction, as was expected. On the other hand, the advance in the stator pole angle and the reduction in the stator angle on the core slightly reduced the torque ripple.

It is worth taking a look at additional graphs which illustrate the influences of the changes in stator pole angle X_1 , airgap shift X_5 , and rotor pole angle X_3 on the average torque. For that reason, Figure 16 presents the static torque curve for designs 1, 6, 11, 16, and 21 with the stator pole angle levels 1, 2, 3, 4, and 5, respectively (see Table 3).

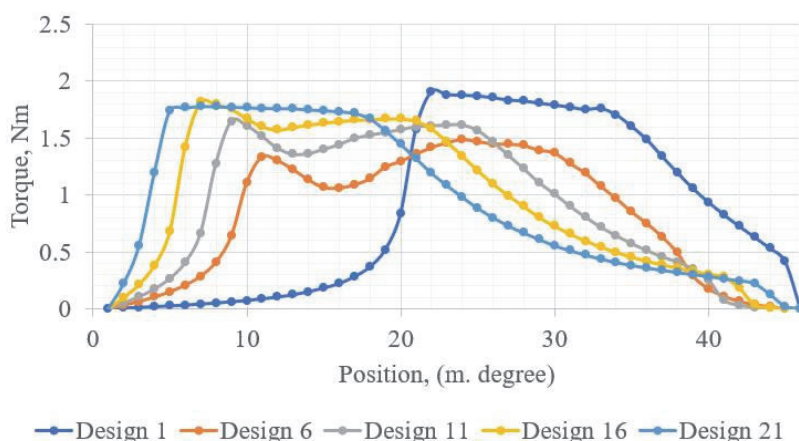


Figure 16. Static torque curve for Taguchi designs with different levels of stator pole angle.

It can be seen in the graph above that the increase in the stator pole angle leads to a wider area of torque production and consequent larger average torque. The drop in the torque at the beginning of the overlap in designs 6, 11, and 16 attracts particular attention. It may indicate the coefficient of the rotor pole angle X_3 and rotor additional angle X_6 , which are higher in designs 6, 11, and 16.

Figure 17 presents the variation in the static torque with the change in both air-gap shift X_5 and rotor pole angle X_3 . It is apparent from the figure that the average torque decreases. On the other hand, the area of the torque production shifted to the beginning of the overlap due to the growth of the rotor pole angle. Therefore, the area of zero torque enlarges at the end of the growing inductance phase when $\theta_{max} = [30, 45]$. It is important to highlight that the biggest improvement in the width of the torque and constancy of the torque at its maximum can be noticed between Design 1 and Design 2; $\theta_{max} = [18, 30]$ and $\theta_{max} = [22, 32]$, respectively. Due to the introduction of the airgap shift, the torque in design 2 became more stable at its maximum. However, further increase in the air-gap shift did not have a positive influence on the torque characteristic due to the possible influences of other parameters, such as additional tooth angle X_6 .

Due to the coefficient of the analyzed parameters on the resultant torque, it is important to keep in mind that Figures 16 and 17 should be considered only together with Figures 13 and 14.

The findings of the analysis of the results can be summarized as follows.

1. Stator pole angle has a major influence on the average torque. The increase in the stator pole angle leads to a wider torque production region and higher average torque.

2. The growth of the airgap shift has a positive influence on the torque ripple reduction and a negative influence on the average torque. The airgap shift raises the torque at the end of the growing inductance phase. However, the air-gap shift is a sensitive parameter, and its value should be selected carefully.
3. The increase in the rotor pole angle has a negative effect on the torque ripple. With the growth of the rotor pole angle, the torque curve shifts to the beginning of the torque production phase. To avoid the torque ripple with the increase in the rotor pole angle, the control turn-on and turn-off angles should be adjusted according to the area of torque production.
4. The introduction of the rotor pole angle within this SRM design leads to an increase in torque ripples. The possible explanation can be an improper selection of its values.

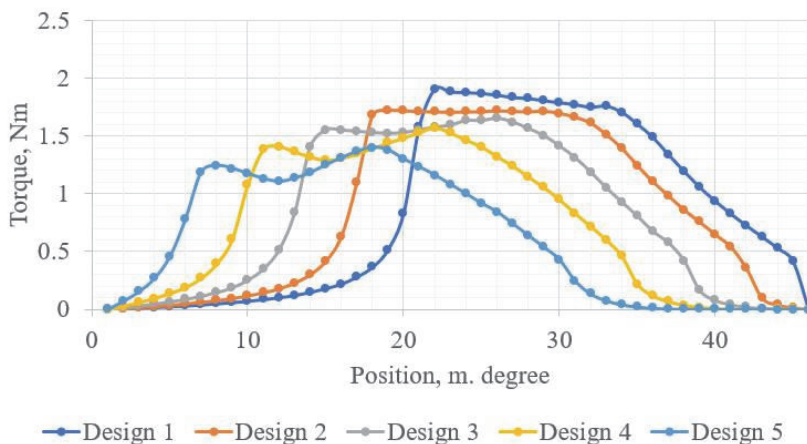


Figure 17. Static torque curve for Taguchi designs with different levels of air-gap shift and rotor pole angle.

4.2. Topology Optimization Design Space Definition

With the aim of reducing the computational load during the topology optimization, the base design can be defined using the SA results. Moreover, the design domain of the topology optimization can be created based on the results presented in Section 3.

Table 4 and Figure 18 summarize the optimal designs according to the Taguchi SA. Based on Figures 13–17, the best control factor sets in terms of average torque improvement and torque ripple reduction were chosen: first optimal design and second optimal design, respectively. The trade-off between these designs is defined in Table 4 as well. The trade-off design performed the average one-phase torque of 0.875 Nm, the total average torque of 1.31 Nm, and the torque ripple coefficient of 1.48.

Table 4. Optimal designs according to the Taguchi SA.

| Control Factor | 1st Optimal Design | 2nd Optimal Design | Trade-Off Design |
|----------------|--------------------|--------------------|------------------|
| X1 | 4 | 2 | 5 |
| X2 | 1 | 5 | 3 |
| X3 | 4 | 1 | 2 |
| X4 | 2 | 2 | 2 |
| X5 | 1 | 4 | 2 |
| X6 | 3 | 1 | 2 |

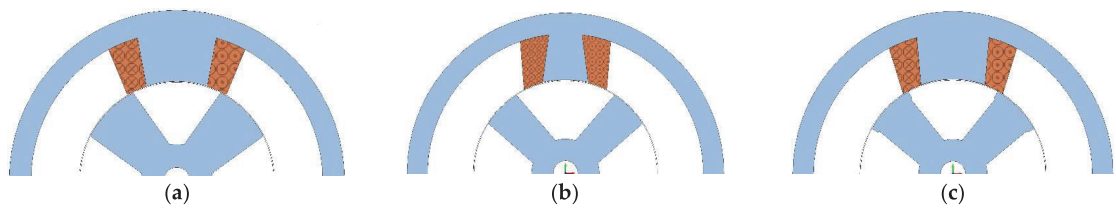


Figure 18. (a) First optimal design; (b) second optimal design; (c) trade-off design.

To determine the design domain of the topology optimization, the following steps were performed:

1. Stator pole angle was set to 40° , pursuing the best combination of maximum average torque and minimum torque ripple.
2. Stator pole angle at the core was set to 30° , insuring almost the lowest torque ripple and reasonably high torque.
3. The rotor pole angle and rotor pole angle at the core were set to 28.75° and 60° , respectively, trying to achieve the minimum torque ripple and keep the average torque ripple at the average level.
4. Due to the high influence of the airgap shift and the low influence of the core angles on the objective functions, the depth of the TO domain was set to 5 mm.
5. The possible additional angle for the rotor teeth was set to $\pm 1.875^\circ$ due to the highly negative influence of the additional teeth after 1.875 on both the average torque and torque ripple.

The base design for the future topology optimization will possess the following vector of the design parameters:

$$x = [40, 10, 28.75, 31.25, 0, 0] \quad (8)$$

Based on the results of the sensitivity analysis, the design domain of the topology optimization is defined in Figure 19a. Additionally, the torque comparison between the initial design and the trade-off design is presented in Figure 19b.

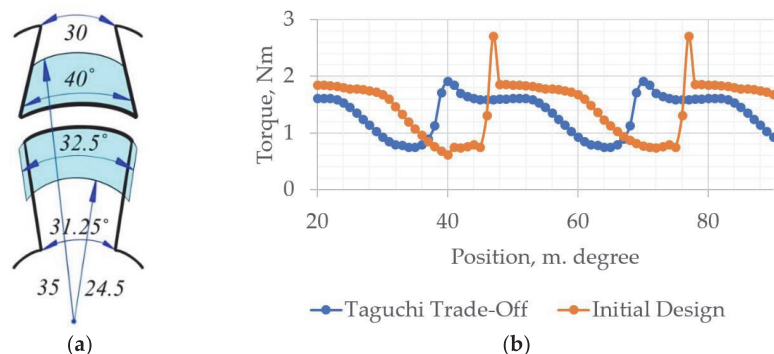


Figure 19. (a) Topology optimization design domain; (b) Torque comparison of initial and trade-off designs.

5. Conclusions

TO can be used as a powerful tool for design optimization while pursuing high performance for an SRM. On the other hand, TO is computationally expensive and geometrically restricted. To overcome the geometry restrictions, additive manufacturing techniques are proposed to be used for the optimized SRM. To overcome the issue of the computational complexity of the TO, the present research proposed a method of the TO design space

reduction. To reduce the design domain of the SRM TO, and consequently reduce its computational burden, this research carried out SA to identify the minimum necessary design domain. To carry out the SA, the authors applied the Taguchi approach. The proposed method allowed the reduction of the design domain of the future TO considerably. Thanks to the applied SA, the most crucial areas of the three-phase SRM for future optimization were identified. Thereafter, the SA helped to define the TO design space that included only 25% of the whole body of the SRM. Thanks to the obtained minimum necessary design space of the motor, the computational complexity of the future TO was reduced by more than a half. The proposed method has significant implications for the TO computational burden reduction. Additionally, the proposed approach can be utilized for SRMs with different numbers of phases, stators, and rotor poles. Moreover, the presented SA of the motor design parameters can give a good overview of their influences on the average torque of the SRM and its torque ripple.

A natural progression of this work is to study the possibilities and restrictions of additive manufacturing for producing a topologically optimized SRM. As the second step, we plan to carry out TO with respect to the results of the SA and additive manufacturing potentials and constraints. After obtaining the topologically optimized SRM, a prototype is to be manufactured and tested. More broadly, this research work could also focus on the application of the proposed approach for other motors' TO.

Author Contributions: Conceptualization, E.A. and M.H.M.; methodology, E.A.; software, E.A. and H.H.; validation, E.A., M.H.M. and D.A.L.; formal analysis, E.A.; investigation, E.A.; resources, E.A.; data curation, E.A.; writing—original draft preparation, E.A.; writing—review and editing, H.H. and A.K.; visualization, E.A.; supervision, M.H.M., D.A.L. and A.K.; project administration, A.K.; funding acquisition, A.K. All authors have read and agreed to the published version of the manuscript.

Funding: This research was funded by the Estonian Research Council with grant PSG137, “Additive Manufacturing of Electrical Machines.”

Conflicts of Interest: The authors declare no conflict of interest.

References

1. Rahman, K.M.; Fahimi, B.; Suresh, G.; Rajarathnam, A.V.; Ehsani, M. Advantages of switched reluctance motor applications to EV and HEV: Design and control issues. *IEEE Trans. Ind. Appl.* **2000**, *36*, 111–121. [\[CrossRef\]](#)
2. Li, S.; Zhang, S.; Habetler, T.G.; Harley, R.G. Modeling, design optimization, and applications of switched reluctance machines—A review. *IEEE Trans. Ind. Appl.* **2019**, *55*, 2660–2681. [\[CrossRef\]](#)
3. Madhavan, R.; Fernandes, B.G. Performance improvement in the axial flux-segmented rotor-switched reluctance motor. *IEEE Trans. Energy Convers.* **2014**, *29*, 641–651. [\[CrossRef\]](#)
4. Lin, Z.; Reay, D.S.; Williams, B.W.; He, X. Online modeling for switched reluctance motors using b-spline neural networks. *IEEE Trans. Ind. Electron.* **2007**, *54*, 3317–3322. [\[CrossRef\]](#)
5. Ma, C.; Qu, L. Design Considerations of Switched Reluctance Motors with Bipolar Excitation for Low Torque Ripple Applications. In Proceedings of the 2013 IEEE Energy Conversion Congress and Exposition, Denver, CO, USA, 15–19 September 2013; Available online: <https://digitalcommons.unl.edu/electricalengineeringfacpub/295> (accessed on 14 March 2022).
6. Wang, W.; Luo, M.; Cosoroaba, E.; Fahimi, B.; Kiani, M. Rotor shape investigation and optimization of double stator switched reluctance machine. *IEEE Trans. Magn.* **2015**, *51*, 8103304. [\[CrossRef\]](#)
7. Lee, J.W.; Kim, H.S.; Kwon, B.I.; Kim, B.T. New rotor shape design for minimum torque ripple of SRM using FEM. *IEEE Trans. Magn.* **2004**, *40*, 754–757. [\[CrossRef\]](#)
8. Li, G.-J.; Ojeda, J.; Hlioui, S.; Hoang, E.; Lecrivain, M.; Gabsi, M. Modification in rotor pole geometry of mutually coupled switched reluctance machine for torque ripple mitigating. *IEEE Trans. Magn.* **2012**, *48*, 2025–2034. [\[CrossRef\]](#)
9. Choi, Y.K.; Yoon, H.S.; Koh, C.S. Pole-shape optimization of a switched-reluctance motor for torque ripple reduction. *IEEE Trans. Magn.* **2007**, *43*, 1797–1800. [\[CrossRef\]](#)
10. Sheth, N.; Rajagopal, K. Optimum Pole Arcs for a Switched Reluctance Motor for Higher Torque with Reduced Ripple. *IEEE Trans. Magn.* **2003**, *39*, 3214–3216. [\[CrossRef\]](#)
11. Chen, H.; Yan, W.; Gu, J.J.; Sun, M. Multiobjective Optimization Design of a Switched Reluctance Motor for Low-Speed Electric Vehicles with a Taguchi-CSO Algorithm. *IEEE/ASME Trans. Mechatron.* **2018**, *23*, 1762–1774. [\[CrossRef\]](#)
12. Omekanda, A.M. Robust torque and torque-per-inertia optimization of a switched reluctance motor using the Taguchi methods. *IEEE Trans. Ind. Appl.* **2006**, *42*, 473–478. [\[CrossRef\]](#)

13. Hidaka, Y.; Igarashi, H. Topology Optimization of Synchronous Reluctance Motors Considering Localized Magnetic Degradation Caused by Punching. *IEEE Trans. Magn.* **2017**, *53*, 7000804. [[CrossRef](#)]
14. Sato, S.; Sato, T.; Igarashi, H. Topology optimization of synchronous reluctance motor using normalized gaussian network. *IEEE Trans. Magn.* **2015**, *51*, 8200904. [[CrossRef](#)]
15. Zhang, H.; Wang, S. Topology Optimization of Rotor Pole in Switched Reluctance Motor for Minimum Torque Ripple, Electric Power Components and Systems. *Electr. Power Compon. Syst.* **2017**, *45*, 905–911. [[CrossRef](#)]
16. Okamoto, Y.; Hoshino, R.; Wakao, S.; Tsuburaya, T. Improvement of torque characteristics for a synchronous reluctance motor using MMA-based topology optimization method. *IEEE Trans. Magn.* **2017**, *54*, 7203104. [[CrossRef](#)]
17. Ishikawa, T.; Yonetake, K.; Kurita, N. An optimal material distribution design of brushless DC motor by genetic algorithm considering a cluster of material. *IEEE Trans. Magn.* **2011**, *47*, 1310–1313. [[CrossRef](#)]
18. DWhite, D.A.; Arrighi, W.J.; Kudo, J.; Watts, S.E. Multiscale topology optimization using neural network surrogate models. *Comput. Methods Appl. Mech. Eng.* **2019**, *346*, 1118–1135. [[CrossRef](#)]
19. Andriushchenko, E.; Kallaste, A.; Belahcen, A.; Vaimann, T.; Rassölkin, A.; Heidari, H.; Tiismus, H. Optimization of a 3D-Printed Permanent Magnet Coupling Using Genetic Algorithm and Taguchi Method. *Electronics* **2021**, *10*, 494. [[CrossRef](#)]
20. Andriushchenko, E.; Kaska, J.; Kallaste, A.; Belahcen, A.; Vaimann, T.; Rassölkin, A. Design Optimization of Permanent Magnet Clutch with Ärtap Framework. *Period. Polytech. Electr. Eng. Comput. Sci.* **2021**, *65*, 106–112. [[CrossRef](#)]

Publication III

Andriushchenko E., Kallaste A., Belahcen A., Vaimann T., Rassolkin A., Heidari H., Tiismus H. (2021). Optimization of a 3D-printed permanent magnet coupling using genetic algorithm and Taguchi method. *MDPI Electronics* 10(4), 494.

Article

Optimization of a 3D-Printed Permanent Magnet Coupling Using Genetic Algorithm and Taguchi Method

Ekaterina Andriushchenko ^{1,*}, Ants Kallaste ¹, Anouar Belahcen ^{1,2}, Toomas Vaimann ^{1,3}, Anton Rassõlkin ^{1,3}, Hamidreza Heidari ¹ and Hans Tiismus ¹

- ¹ Department of Electrical Power Engineering and Mechatronics, Tallinn University of Technology, Ehitajate tee 5, 12616 Tallinn, Estonia; ants.kallaste@taltech.ee (A.K.); anouar.belahcen@taltech.ee (A.B.); toomas.vaimann@taltech.ee (T.V.); anton.rassolkin@taltech.ee (A.R.); haheid@taltech.ee (H.H.); hans.tiismus@taltech.ee (H.T.)
- ² Department of Electrical Engineering and Automation, Aalto University, P.O. Box 15500 Aalto, Finland
- ³ Faculty of Control Systems and Robotics, ITMO University, 197101 Saint Petersburg, Russia
- * Correspondence: ekandr@taltech.ee; Tel.: +372-5614-0410

Abstract: In recent decades, the genetic algorithm (GA) has been extensively used in the design optimization of electromagnetic devices. Despite the great merits possessed by the GA, its processing procedure is highly time-consuming. On the contrary, the widely applied Taguchi optimization method is faster with comparable effectiveness in certain optimization problems. This study explores the abilities of both methods within the optimization of a permanent magnet coupling, where the optimization objectives are the minimization of coupling volume and maximization of transmitted torque. The optimal geometry of the coupling and the obtained characteristics achieved by both methods are nearly identical. The magnetic torque density is enhanced by more than 20%, while the volume is reduced by 17%. Yet, the Taguchi method is found to be more time-efficient and effective within the considered optimization problem. Thanks to the additive manufacturing techniques, the initial design and the sophisticated geometry of the Taguchi optimal designs are precisely fabricated. The performances of the coupling designs are validated using an experimental setup.

Keywords: design optimization; genetic algorithms; Taguchi designs; electromagnetic coupling; additive manufacturing



Citation: Andriushchenko, E.; Kallaste, A.; Belahcen, A.; Vaimann, T.; Rassõlkin, A.; Heidari, H.; Tiismus, H. Optimization of a 3D-Printed Permanent Magnet Coupling Using Genetic Algorithm and Taguchi Method. *Electronics* **2021**, *10*, 494. <https://doi.org/10.3390/electronics10040494>

Academic Editor: Hamid Reza Karimi

Received: 19 January 2021
Accepted: 18 February 2021
Published: 20 February 2021

Publisher's Note: MDPI stays neutral with regard to jurisdictional claims in published maps and institutional affiliations.



Copyright: © 2021 by the authors. Licensee MDPI, Basel, Switzerland. This article is an open access article distributed under the terms and conditions of the Creative Commons Attribution (CC BY) license (<https://creativecommons.org/licenses/by/4.0/>).

1. Introduction

The term permanent magnet (PM) coupling or clutch refers to a device that is used to transmit torque between two shafts without mechanical contact. Torque transmission is served by the magnetic field induced by PMs placed on the driving member. Throughout the years, PM couplings have been widely employed in blowers and compressors, conveyors and pumps, and food processing equipment due to their unique qualities [1,2]. For instance, the highlighted features of the PM couplings are the ability to transmit torque through a separator and easy maintenance. Still, there are several important aspects to take into account in PM couplings design. Among these concerns, mass characteristics, transmitted torque, and their balance remain challenging.

Nowadays, the design optimization is extensively used for enhancing the performance of PM couplings. The majority of the studies on PM coupling optimization have utilized coupling dimensions as optimization parameters [3–5]. On the other hand, the optimization of coupling shapes may propose a better improvement of the device performance.

Researchers have been avoiding the optimization of coupling shapes due to the restricted abilities of conventional manufacturing techniques. Presently, additive manufacturing (AM) is considered a constructive alternative to the conventional ways of fabrication [6–9]. Being a flexible and low-material waste technique, the AM can construct

geometrically intricate components. Overall, the AM techniques provide an opportunity to discover more favorable shapes of PM couplings and greatly enhance their performance.

To date, several methods have been developed to optimize the design of electrical machines and devices. The direct and indirect optimization methods (DOM and IOM), multi-level optimization methods, and robust optimization methods are the main approaches. In this study, two methodological approaches are selected: the DOM accompanied by the genetic algorithm (GA) and the Taguchi optimization method [10,11]. The DOM presents a clear and intuitive structure, since it simply utilizes a finite element model (FEM) along with the GA [12–16]. The unique features of the GA, such as the ability to obtain the global minimum, handle non-analytic formulation of optimization problems, and high flexibility, justify its popularity among researchers. This algorithm not only considerably narrows the solution space during optimization but also presents an impressive searching ability. Regardless of the great advantages of DOM-GA optimization, it often appears time-consuming [17–19]. In contrast with the DOM-GA, the Taguchi method requires a considerably lower number of calculations that significantly reduces the execution time [20]. This method takes into account the manufacturing variations of the optimization parameters within the optimization model and, consequently, reaches the high reliability of the optimization results [21–23]. However, far too little attention has been paid to the Taguchi method within the design optimization of electromagnetic devices.

This paper aims to carry out the optimization of the PM coupling shapes with the following optimization objectives: minimization of the coupling volume and maximization of the transmitted torque. Additionally, the study compares the DOM-GA and the Taguchi method in terms of the obtained optimization results and the required execution time. The importance and originality of this study is that it explores complex shapes of the PM coupling design and proposes a great improvement of the device performance. Moreover, the comparative analysis of the DOM-GA and Taguchi method should make an important contribution to the field of design optimization of electromagnetic devices.

The paper is organized as follows. First, the initial design of the PM coupling and definition of the optimization model is presented in Sections 2 and 3, respectively. It will then go on to Section 4, which is dedicated to GA optimization, and Section 5, which presents the Taguchi optimization. Next, Section 6 provides a comprehensive comparison of the applied optimization methods. Then, Section 7 describes the experimental setup and provides the test results for the initial and optimal designs of the coupling, respectively. Finally, the discussion and conclusion of the study are presented in Section 8.

2. Permanent Magnet Coupling Design

This paper considers an optimization problem of a face type PM coupling. Before proceeding to the optimization, it is important to overview the concept of the PM coupling design and operation principle. To illustrate the structure of the coupling, Figure 1 is presented. The figure shows two main components of the coupling: driving and driven members. The driving member possesses magnetic teeth, while the driven member has steel teeth. Along with the structure, Figure 1 demonstrates the main dimensions of the coupling. Additionally, Figure 1 shows the angle of deviation of the coupling members θ . To demonstrate θ , the centers of the disks C1 and C2 are specified. Table 1 lists the main parameters of the coupling geometry.

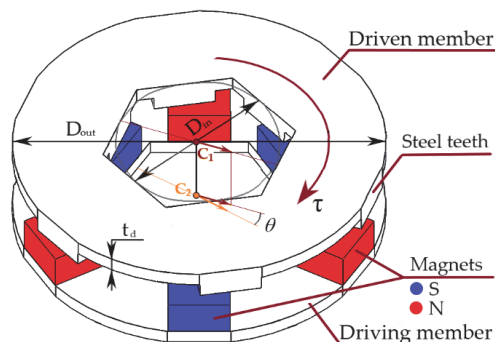


Figure 1. The initial design of the permanent magnet (PM) coupling.

Table 1. Coupling specifications.

| Dimension/Materials | Value |
|------------------------------|---------|
| Outer diameter D_{out} | 30 mm |
| Inner diameter D_{in} | 12.5 mm |
| Thickness of the disks t_d | 1.2 mm |
| Steel teeth height | 1.6 mm |
| Steel teeth width | 5 mm |
| Steel teeth length | 8 mm |
| Magnets thickness | 3 mm |
| Magnets width | 5 mm |
| Magnets length | 8 mm |
| Air gap | 1.5 mm |

The operation concept of the PM coupling is based on the attraction efforts that appear between the magnets placed on the driving disk and the driven member made of steel. The magnetic torque induced in the driven disk depends on the angle of deviation of the coupling members θ , magnetic flux density B , and magnetic field intensity H [24]:

$$\tau = \frac{\delta \int_V \int_0^H B dH dV}{\delta \theta} \tag{1}$$

For prototyping, the steel material with 6.5% silicon content was utilized for the disks and driven member’s teeth. The neodymium magnets N52 (Sintered Nd-Fe-B) were employed to provide the magnetic force.

The finite element analysis of the coupling initial design was carried out through Symcenter MagNet. According to the initial design modelling, the volume of the coupling was $2.31 \times 10^{-6} \text{ m}^3$ and the maximum magnetic torque was $73.0 \times 10^{-3} \text{ Nm}$. Figure 2 presents the dependence of the torque on the angle of deviation. The static simulation results and their approximation are provided. The approximation was carried out by fitting the smoothing spline within the Matlab Curve Fitting Toolbox.

It is important to notice that the magnetic torque reached its maximum when the angle of deviation of the coupling members θ was 17° . Therefore, this position was chosen for static simulations within the optimization.

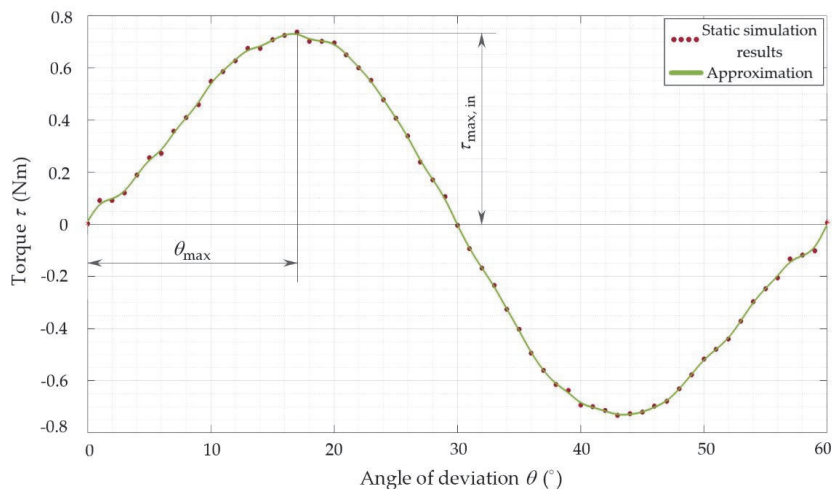


Figure 2. Magnetic torque versus angle of deviation of the initial design of the coupling.

3. Permanent Magnet Coupling Optimization Model

Figure 3 shows the distribution of the magnetic flux density obtained through the MagNet for the initial design of the coupling. It can be seen that the flux density saturation is quite low in particular areas of the coupling disks. Here, the low saturation is a sign that the material of the coupling is not utilized efficiently. Therefore, the coupling design needs to be improved to enhance the effectiveness of material usage. For this purpose, the design optimization can be employed.

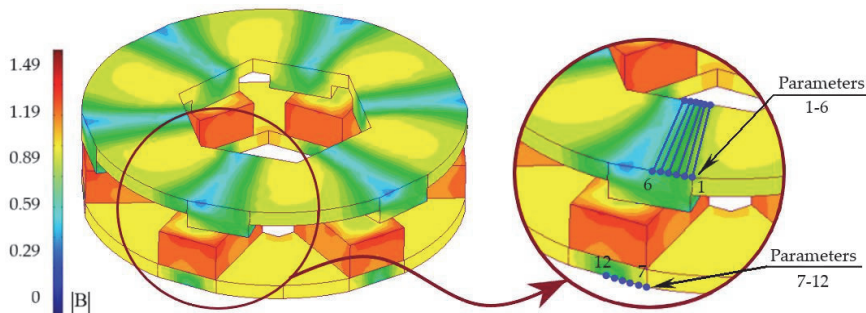


Figure 3. Initial design of the coupling with the distribution of magnetic flux density and illustration of the optimization parameters.

Many researchers have optimized PM couplings paying particular attention to the torque output and volume of the utilized materials [1,4]. Traditionally, linear dimensions, such as diameters of the disks or sizes of magnets, are chosen as optimization parameters. This might be due to the restrictions of the conventional methods of fabrication on design production.

Since AD techniques allow producing complex geometry, the search for optimal dimensions can be replaced with the search for optimal shapes. Therefore, this paper aims to obtain an optimal shape of the PM coupling disks to minimize the material usage and maximize the transmitted torque.

In solving an optimization problem, the first step is to create an optimization model, which involves defining objectives, constraints, and parameters. This study considers the optimization problem, in which the objective functions were non-analytical. More

specifically, the volume and the magnetic torque were obtained using FEA within Simcenter MAGNET. The optimization problem was unconstrained. To find an optimal shape of the clutch disks, the vector of optimization parameters was formed by twelve elements, which represented geometrical locations of the points. Figure 3 shows a set of the geometrical points used as the optimization parameters. As can be noted, the points were placed within the area of low saturation of the coupling disks. Within this area, the material could be potentially removed in order to increase the effectiveness of material usage. The demonstrated set was repeated along the circumference of the coupling disks. Within the optimization, the variation of the parameters had the following limits: [0 . . . 1] mm. The disks' general thicknesses t_d were not included in the group of the optimization parameters, since they were minimized beforehand and their further reduction negatively influenced the torque.

4. Optimization Using Genetic Algorithm

4.1. Genetic Algorithm

To carry out a multi-objective optimization, an optimization model should be formulated in the following view:

$$\begin{aligned} &\text{minimize } f(x) = [f_1(x), f_2(x), \dots, f_n(x)]^T, \\ &\text{subject to } g_i(x) \leq 0, i = \{1 \dots m\}, \\ &\quad h_j(x) = 0, j = \{1 \dots p\}, \end{aligned} \tag{2}$$

where the vector $f(x)$ is formed from objective functions, and the vector x presents a set of k optimization parameters. The functions $g_i(x)$ and $h_j(x)$ are constraint functions.

In solving multi-objective problems (MOPs), the ultimate goal is to find good compromises between the objective functions. Traditionally, this goal is achieved using the concept of Pareto Optimality.

To understand the idea of the Pareto Optimality, several definitions should be presented. First, a classic definition of Pareto Optimal Solution can be expressed as follows. A solution $x \in \Omega$ is called a Pareto Optimal Solution if there is no $x' \in \Omega$ for which the objective vector $f_k(x')$ dominates $f_k(x)$. Here, Ω implies the feasible region of the optimization problem. The feasible region is an area of the parameter space, where all constraints are satisfied. Second, Pareto Dominance can be defined as follows. A vector $f_k(x)$ is said to dominate another vector $f_k(x')$ only if $f_k(x)$ is partially less than $f_k(x')$.

Essentially, the main functions of the multi-objective genetic algorithm (MOGA) are to obtain a set of Pareto Optimal Solutions (P^*). The set P^* is a set of optimal values of the optimization parameters. Mathematically, the Pareto Optimal Set can be defined as follows [19]:

$$P^* := \{x \in \Omega \mid \neg \exists x' \in \Omega \mid f(x') \leq f(x)\}, \tag{3}$$

The second function of the MOGA is to construct the Pareto Front (PF^*). At first, many points within the feasible region should be calculated. If the number of the points is high enough, the GA finds the non-dominated points and identifies PF^* :

$$PF^* := \{u = f(x) \mid x \in P^*\}. \tag{4}$$

The procedure that allows the MOGA to explore the solution space is presented in Algorithm 1 [19]. The specific terms used within the MOGA procedure are the following:

- The term "gene" implies an optimization parameter;
- The term "individual" defines a set of optimization parameters;
- The term "population" presents a group of different parameter sets.

Algorithm 1 MOGA

```

1: Initialize Population;
2: Evaluate Objective Values;
3: Assign Rank based on Pareto Dominance;
4: Compute Niche Count;
5: Assign Linearly Scaled Fitness;
6: Assign Shared Fitness;
7: for  $i = 1$  to number of Generations do;
8:     Tournament Selection;
9:     Single-Point Crossover;
10:    Uniform Mutation;
11:    Evaluate Objective Values;
12:    Assign Rank based on Pareto Dominance;
13:    Compute Niche Count;
14:    Assign Linearly Scaled Fitness;
15:    Assign Shared Fitness;
16: end.

```

The first steps in the MOGA are to generate the initial population and to compute the values of optimization objectives. The next phase involves ranking based on the Pareto Dominance and assigning the fitness values using the niching technique. Fitness value expresses how “good” an individual is. It is a positive real value and, therefore, is often easier to use than the values of the objectives. The niching technique (also called the fitness sharing technique) is responsible for maintaining diversity in the population. To use the niching technique, the size of the neighborhood (niche radius) of each individual should be calculated first. Then, the linearly scaled fitness value of each individual is decreased proportionally to the number of individuals sharing the same neighborhood.

Using the obtained fitness values, the cycle of the evolutionary search starts with the following operators: selection, crossover, and mutation. The general functions of these operators are the following:

- The selection operator selects individuals from the current population based on their fitness values; the selected individuals are called “parents”;
- The crossover operator is applied to the “parents” to create new individuals called “offspring”;
- The mutation operator broadens the search space by making changes in the current population; then, the “offspring” and mutated individuals form a new generation.

There are many types of selection, crossover, and mutation operators. In this optimization problem, the tournament selection, single-point crossover, and uniform mutation were used. Figure 4 illustrates the basic ideas of the applied operators [19].

The tournament selection acts in the following way: first, it randomly chooses four individuals from the population, and then picks the individual with the higher fitness value for using in the next generation. As for the crossover, it takes two individuals from the current generation and combines them at a random point. The uniform mutation takes an individual and selects one or more random mutation points (genes). Then, this operator replaces the values of the selected genes with a uniform random value between the upper and lower bounds defined for this gene.

After that, the new generation is formed and assessed using fitness values. In the next step of the procedure, the algorithm checks if a stop criterion is satisfied. If it is, then the algorithm stops working. Otherwise, it continues the cycle of creating new generations.

To date, the MOGA has been integrated to different computing environments, such as Matlab and Ārtap [25–27]. In this study, the MOGA was applied through the Matlab optimization toolbox.

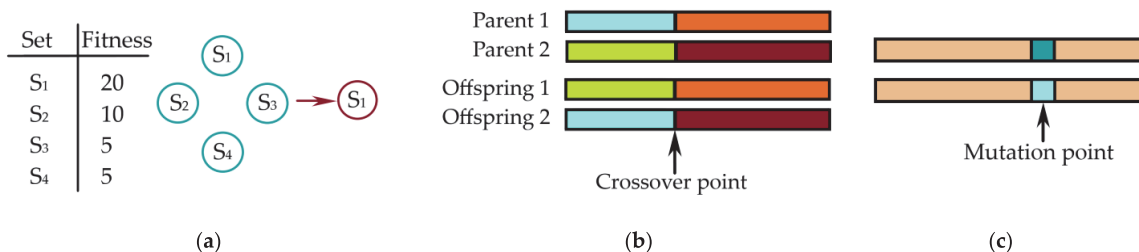


Figure 4. (a) Tournament selection; (b) single-point crossover; (c) uniform mutation.

4.2. Optimization Method

The optimization was carried out using the procedure illustrated in Figure 5. The interaction between Matlab, SolidWorks, and MagNet software programs was organized within Visual Studio as follows. The optimization cycle started with a set of parameters defined by the GA within the Matlab optimizer. Then, these parameters were used to build a 3D model using SolidWorks. Once it was complete, MagNET calculated the maximum torque and directed it together with the coupling volume to the Matlab optimizer. Using the obtained values of the objectives, the Matlab optimizer refined the parameters, and the same cycle was executed until the stop criterion had been satisfied. The number of generations and individuals defined the stop criterion. Particularly, the optimization was performed with 30 generations constituted by 50 individuals. Consequently, the cycle was repeated 1500 times.

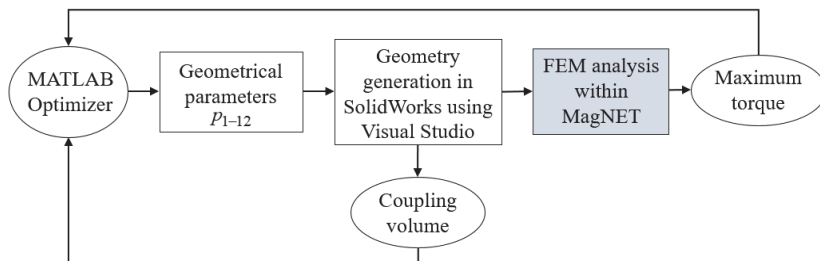


Figure 5. Optimization flowchart.

4.3. Simulation Results of the GA Optimization

The optimal design and the magnetic flux density distribution are presented in Figure 6. The figure shows that the coupling members were deeply saturated. For the driving member body, the average value of flux density $|B|$ was near 0.83 T, and for the driven member it was slightly lower—about 0.78 T. The obtained values of the maximum magnetic torque and the volume are reported in Table 2. A significant reduction in the volume can be noticed from the table. However, no difference greater than 2% was observed in the torque value.

Overall, the GA showed constructive results; however, the execution time was quite high. Fifty hours were required to resolve the optimization problem.

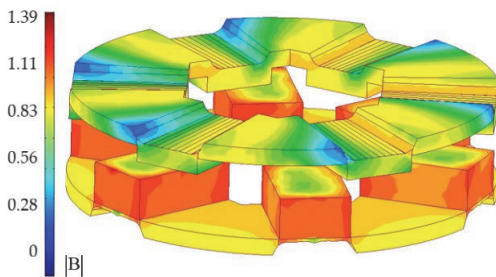


Figure 6. GA optimal design with the distribution of magnetic flux density.

Table 2. Simulation results of genetic algorithm (GA) optimization.

| Objective | Initial Design | GA |
|---------------|-----------------------------------|-----------------------------------|
| τ_{\max} | $73.0 \times 10^{-3} \text{ Nm}$ | $74.5 \times 10^{-3} \text{ Nm}$ |
| V | $2.31 \times 10^{-6} \text{ m}^3$ | $1.91 \times 10^{-6} \text{ m}^3$ |

5. Optimization Using Taguchi Method

5.1. Taguchi Methodology

The Taguchi method is a statistical method that discovers the parameter space to find a design with better performance. The parameter space in Taguchi’s terminology is called the orthogonal array. Essentially, the orthogonal array is a matrix that includes various combinations of optimization parameters. Each combination is called an experiment. The experiments should be carried out in a real test or simulation to obtain values of optimization objectives. A major advantage of the Taguchi method is that the procedure of forming the orthogonal array ensures the minimization of experiment quantity.

In the Taguchi method, once the orthogonal array is formed, the experiments are carried out, values of optimization objectives are obtained, and analysis of the results starts. Essentially, this analysis intends to reveal the effect of the optimization parameters and their levels on the objectives using average peak-to-peak values of the objectives.

5.2. Conducting the Taguchi Experiments

Within this study, a standard L50 orthogonal array was used. It included fifty experiments that involve eleven parameters with five levels and one parameter with two levels. The parameters and their levels are listed in Table 3.

Table 3. Optimization parameters and their levels.

| Parameter | Level 1 | Level 2 | Level 3 | Level 4 | Level 5 |
|-----------|---------|---------|---------|---------|---------|
| 1 | 0.8 | 1 | - | - | - |
| 2–12 | 0.6 | 0.7 | 0.8 | 0.9 | 1 |

The experiments were carried out using MagNET software. The obtained values of the magnetic torque and the volume were organized into the cost function:

$$f = \frac{\tau}{V} \tag{5}$$

To find the best combination of parameters levels, the mean values were calculated and analyzed. The mean values of the objectives and the cost function were as follows.

$$m_v = \frac{1}{50} \sum_{k=1}^{50} V_i = 1.98 \cdot 10^{-6} \text{m}^3, m_\tau = \frac{1}{50} \sum_{k=1}^{50} \tau_i = 75.0 \cdot 10^{-3} \text{Nm},$$

$$m_f = \frac{1}{50} \sum_{k=1}^{50} f_k = 3.79 \tag{6}$$

Then, the average peak-to-peak values of the cost function were calculated for each factor at each level:

$$m_{ij}(f) = \frac{1}{n} \cdot \sum f(i, j), \tag{7}$$

where i is the parameter number, j is the level number, n represents the number of experiments, and $f(i, j)$ denotes the value of the objective function for experiments that involved the parameter i at the level j . Figure 7 shows the average peak-to-peak values depending on the parameters and parameters' levels.

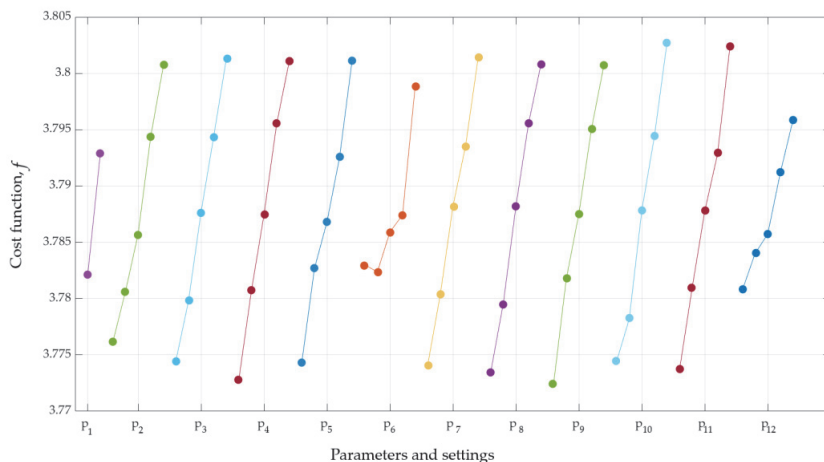


Figure 7. Parameter effects on the objective function.

As can be seen, the parameters combination [p₁₂, p₁₅] $i = 2 \dots 12$ gives the minimum value of the cost function. The optimal design provided the value of the magnetic torque of $75.0 \cdot 10^{-3}$ Nm and the value of the volume $1.91 \cdot 10^{-6}$ m³.

The last step of the Taguchi optimization is the analysis of variance (ANOVA). Using the sum of squares ss , the effect of each parameter on the objective function was computed:

$$ss_{ij} = n \cdot \sum (m_{ij} - m_f)^2, \tag{8}$$

It can be seen from Table 4 that the influence of the parameters on the cost function was nearly equal. Only the parameters p₆ and p₁₂ made the exception. This might be because the saturation of the disks near these points was the smallest for all the designs.

5.3. Simulation Results of the Taguchi Optimization

The optimal design of the coupling was obtained by the Taguchi method. The corresponding geometry and the magnetic flux distribution are shown in Figure 8. Closer inspection of the figure reveals that the bodies of the driving and driven member were highly saturated. For the driving member body, the average value of flux density $|B|$ was near 0.86 T, and for the driven member, it was slightly lower—about 0.8 T. Table 5 compares the magnetic torque and volume values of the initial and optimal designs. Using

the Taguchi optimization method allowed us to reduce the volume by 17% and to enhance the torque by 2.2% compared to the initial value.

Table 4. Effects of different parameters on the cost function.

| Variable | Sum of Squares | Factor Effect (%) | Variable | Sum of Squares | Factor Effect (%) |
|----------|----------------|-------------------|----------|----------------|-------------------|
| 1 | 0.0001 | 0.5 | 7 | 0.0023 | 10.0 |
| 2 | 0.0019 | 8.7 | 8 | 0.0025 | 10.9 |
| 3 | 0.0023 | 10.1 | 9 | 0.0025 | 10.7 |
| 4 | 0.0025 | 11.1 | 10 | 0.0027 | 11.7 |
| 5 | 0.0021 | 8.9 | 11 | 0.0024 | 10.5 |
| 6 | 0.0008 | 3.8 | 12 | 0.0007 | 3.1 |

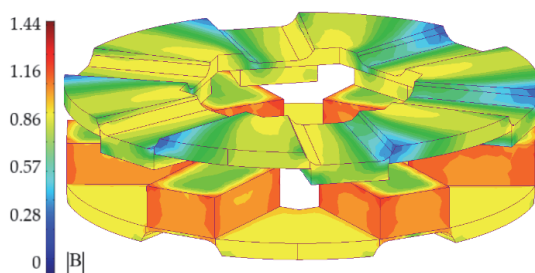


Figure 8. Taguchi optimal design with the distribution of magnetic flux density.

Table 5. Simulation results of Taguchi optimization.

| Objective | Initial Design | Taguchi Design |
|--------------|--------------------------------------|--------------------------------------|
| τ_{max} | 73.0×10^{-3} Nm | 75.0×10^{-3} Nm |
| V | 2.31×10^{-6} m ³ | 1.91×10^{-6} m ³ |

6. Comparison of the Simulation Results of the GA Optimization and the Taguchi Optimization

The designed PM couplings were compared in terms of the volume, magnetic torque, and magnetic torque density. The highlighted characteristics of the couplings are listed in Table 6. It is apparent from this table that the optimal designs showed a considerable improvement in the magnetic torque density—more than 20%. Similarly, the volume of the coupling disks was significantly reduced using both optimization methods. However, only a slight increase in torque was found after optimization—about 2%.

Table 6. Simulation results of GA and Taguchi optimization.

| Objective | Initial Design | GA Design | Taguchi Design |
|----------------|--------------------------------------|--------------------------------------|--------------------------------------|
| τ_{max} | 73.0×10^{-3} Nm | 74.5×10^{-3} Nm | 75.0×10^{-3} Nm |
| V | 2.31×10^{-6} m ³ | 1.91×10^{-6} m ³ | 1.91×10^{-6} m ³ |
| τ_{max}/V | 31.6 kN·m/m ³ | 39.0 kN·m/m ³ | 39.3 kN·m/m ³ |

The 3D models of the initial and optimal designs are presented in Figure 9. Additionally, Table 7 provides the thickness values of the disks at the optimization parameters points locations. A comparison of the GA and Taguchi designs reveals that the obtained geometry and volume of the PM coupling were identical. Similarly, the maximum value of the magnetic torque, as well as the magnetic torque density, were quite close for both designs.

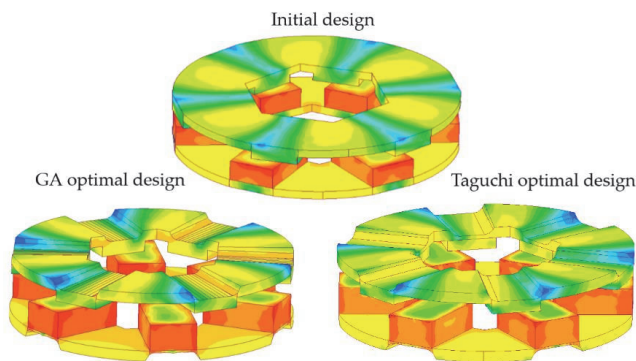


Figure 9. Comparison of initial and optimal design geometries.

Table 7. Discs thicknesses values for initial and optimal designs.

| Parameter Number | Initial Design | GA Design | Taguchi Design |
|------------------|----------------|-----------|----------------|
| 1 | 1.2 mm | 0.21 mm | 0.2 mm |
| 2 | 1.2 mm | 0.2 mm | 0.2 mm |
| 3 | 1.2 mm | 0.2 mm | 0.2 mm |
| 4 | 1.2 mm | 0.2 mm | 0.2 mm |
| 5 | 1.2 mm | 0.4 mm | 0.2 mm |
| 6 | 1.2 mm | 0.2 mm | 0.2 mm |
| 7 | 1.2 mm | 0.5 mm | 0.2 mm |
| 8 | 1.2 mm | 0.2 mm | 0.2 mm |
| 9 | 1.2 mm | 0.2 mm | 0.2 mm |
| 10 | 1.2 mm | 0.2 mm | 0.2 mm |
| 11 | 1.2 mm | 0.2 mm | 0.2 mm |
| 12 | 1.2 mm | 0.6 mm | 0.2 mm |

To provide a more comprehensive comparison of the coupling designs, the dependence of the magnetic torque on the deviation angle θ was explored. Figure 10 illustrates the approximated results of the simulations. As can be seen from the figure, the torque curves of the optimal and initial designs were quite close. Yet, the variation of the torque in the Taguchi design was more stable in the region of θ change from 0° to 5° .

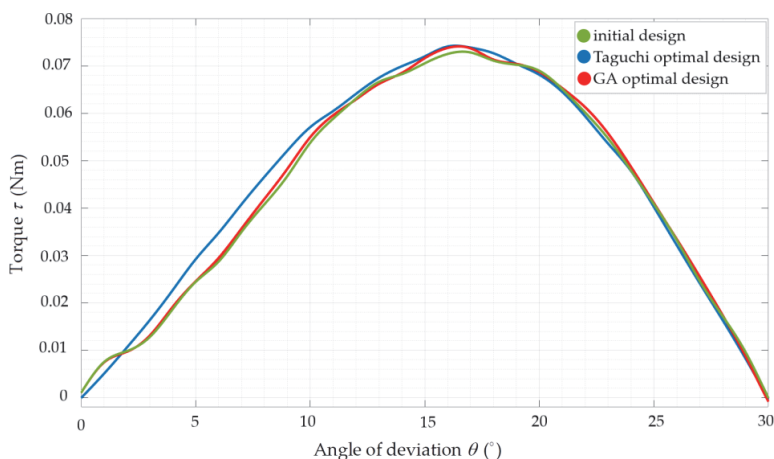


Figure 10. Comparison of three designs in terms of magnetic torque versus angle of deviation.

Moreover, the Taguchi optimization method was considerably more effective in terms of time consumption. Particularly, the GA optimization was performed within 50 hours, while the Taguchi method required just 1.5 hours of calculations. Therefore, these results taken together indicate that the Taguchi optimization had better performance compared to the GA in the scope of PM coupling optimization.

7. Experimental Setup

7.1. Test Bench

To validate the performance of the coupling, an experimental setup was designed. First, the initial design of the coupling was printed from electrical steel with 6.5% silicon content by selective laser melting printing [28]. Similarly, the Taguchi optimal design was manufactured. Three-dimensional printed prototypes are presented in Figure 11.



Figure 11. (a) Prototype of the initial design of the coupling; (b) prototype of the optimized design on the coupling.

The second step was to construct a test bench with an adjustable air gap and ability to measure the torque in various relative positions of the coupling members. Figure 12 illustrates the experimental design of the coupling together with the designed setup for the test. The driving and driven disks were inserted into two shafts which hold them in a certain position. The shafts were supported by a pair of angular contact ball bearings. The bed components were designed in such a way that the air gap could be regulated. Particularly, the following values of the air gap could be selected: 1, 1.5, 2 . . . 3.

Moreover, a mechanism was proposed to vary the angle of deviation between the driving and driven member. As shown in Figure 12, the mechanism included three elements: two disks with holes and one stick. The green disk was placed on the driving member shaft and could be rotated. The beige disk was placed on the support and fixed. The green disk was divided into 36 sectors with the step of 10° . The beige disk was divided into 12 sectors with the step of 11° . In each sector of both disks, a hole was placed to adjust the angle θ with the step 1° using the stick. All components were printed from PLA material using a 3D-printing machine.

The implemented setup was prepared for measuring the torque on the driven member shaft. Utilizing the scale provided the measurement basis for the setup (see Figure 13). In this test, the rotation of the driving member shaft induced torque on the driven member shaft. The last one had the arm, which was in contact with the scales. Essentially, the scales

here acted as a measuring device of the force produced by the arm F_R . This force had a particular relation with the torque described by Equation (9).

$$\tau = F_R \times r, \tag{9}$$

$$r = r \cdot \sin(\varphi), F_R = mg, \varphi = \pi/2 \Rightarrow \tau = F_R \cdot r,$$

where the constant r is the length of the arm, θ represents the angle of deviation between coupling members, and φ implies for the angle between vectors r and F_R .

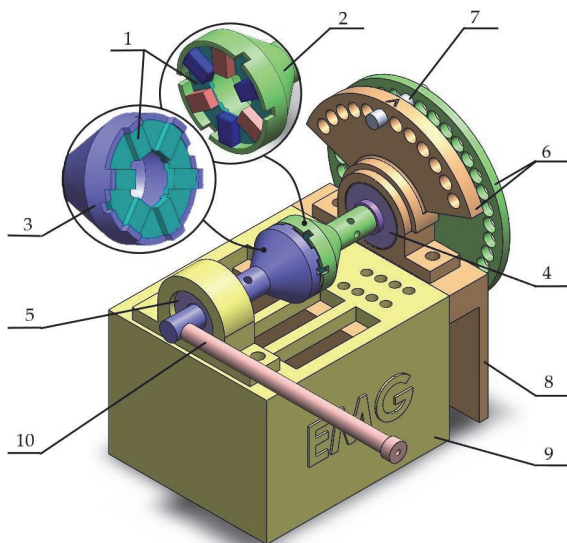


Figure 12. First view of the experimental setup. 1—PM coupling; 2—driving member shaft; 3—driven member shaft; 4 and 5—bearings; 6—mechanism for the angle θ variation; 7—stick for fixing the angle θ ; 8 and 9—bed components; 10—arm.

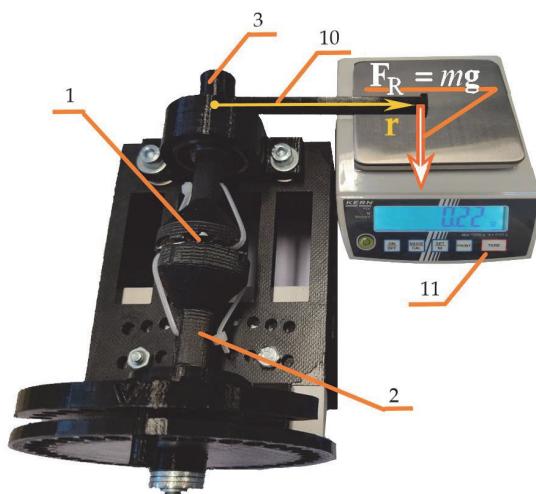


Figure 13. The measurement setup.

7.2. Experimental Results

To certify the optimization results, the initial and optimal designs were tested and compared. Each design was tested four times, and the means of the torque values were used for further analysis. Figure 14 provides the experimental data on the initial and optimal designs together with the data approximation. Particularly, the graph shows the relation of the torque, induced on the driven member shaft, and the angle θ . It can be seen that the curves were quite close within the change of the deviation angle from 0° to 17° . Yet, there was a slight difference in torque values of initial and optimal designs at the point of the torque maximum ($\theta = 17^\circ$).

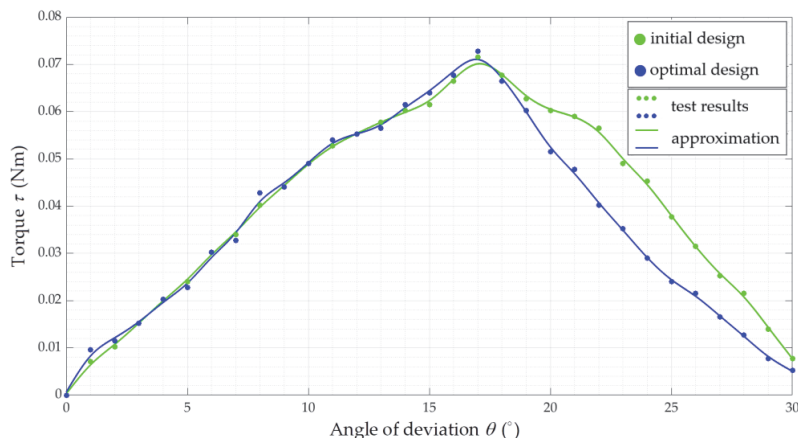


Figure 14. Test results for the initial and optimal designs of the coupling.

Additionally, Figure 15 summarizes the results obtained from the simulation and the experiments. The figure shows that the simulation and test curves were adjacent within the change of θ from 0° to 7° . However, around $\theta = 7^\circ \dots 17^\circ$, the torque, obtained from the test, was slightly lower. Moreover, it should be noted that the experimental curves appeared to be steep which indicated the rapid torque change. An explanation might be that the measured torque was not only dependent on the coupling design but also experienced the influence from the setup structure and the bearings. Additionally, the accuracy of the scales, used for measuring the torque, was not high enough.

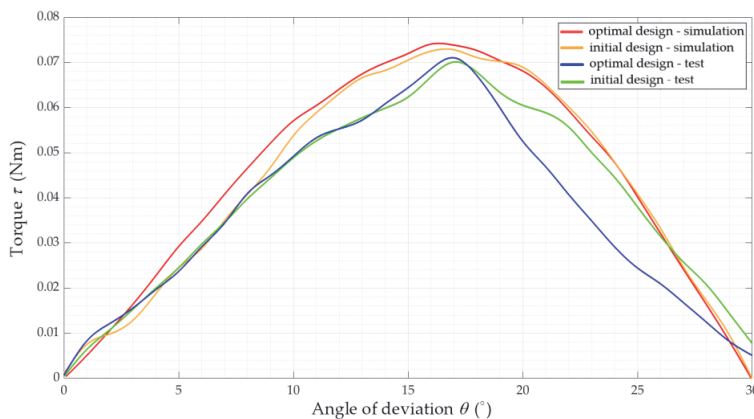


Figure 15. Comparison of simulation and experimental results for the initial and optimal designs of the coupling.

To provide a comprehensive comparison of the designs, Table 8 presents the torque-to-volume ratio according to the experiment. The table demonstrates that the optimal design achieved considerably higher performance compared to the initial design. Particularly, the difference in the torque-to-volume ration was above 20%.

Table 8. Test results of GA and Taguchi optimization.

| Specification | Initial Design | Taguchi Design |
|-----------------|---|---|
| τ_{\max} | $71.0 \times 10^{-3} \text{ Nm}$ | $72.0 \times 10^{-3} \text{ Nm}$ |
| V | $2.31 \times 10^{-6} \text{ m}^3$ | $1.91 \times 10^{-6} \text{ m}^3$ |
| τ_{\max}/V | $30.7 \text{ kN}\cdot\text{m}/\text{m}^3$ | $37.7 \text{ kN}\cdot\text{m}/\text{m}^3$ |

8. Discussion and Conclusions

This study presented the optimization of the PM coupling shapes with the following objectives: minimization of the coupling volume and maximization of the transmitted torque. For this optimization problem, two methodological approaches were employed: the DOM accompanied by the GA and Taguchi optimization method. The results of the PM coupling optimization using both approaches were impressive. The DOM and the Taguchi method led to identical geometry and the same reduction in the coupling volume. Consequently, the increase in the magnetic torque density was also quite high for both optimized designs.

Compared to the DOM-GA, the key advantage of the Taguchi method was the significant reduction in the execution time. Taking into account that the obtained results of the optimization by both methods were the same, the overall performance of the Taguchi method optimization was concluded to be higher. However, the major limitation of the Taguchi approach is the incapability to solve multi-objective problems with a high number of the optimization parameters and complex relations between the optimization objectives, constraints, and parameters. Therefore, the findings of this study are not generalizable to all optimization problems. Still, considering the obtained results, the Taguchi optimization method offers a reasonable alternative to the time-consuming DOM-GA for certain optimization problems.

Another portion of this study was dedicated to the performance validation of the initial and Taguchi optimal design of the coupling. For this purpose, the experimental setup was constructed, and both designs were tested. The experiments showed that the couplings achieved relatively similar torque values, while the torque density was improved. These experiments confirmed that the coupling design obtained from the Taguchi optimization had a comparable performance with the simulation results. Yet, to obtain a better accuracy of the torque measurements, further experimental tests need to be carried out using more precise measurement devices.

This study suggests that the capabilities of the Taguchi optimization method can be examined within the optimization of other electromagnetic devices. For example, further research will focus on the design optimization of a switched reluctance motor using the Taguchi optimization method.

Author Contributions: Conceptualization, methodology, software, validation, formal analysis, and writing—original draft preparation, E.A.; writing—review and editing, resources, and funding acquisition, A.K.; project administration, A.B. and T.V.; supervision, A.B., T.V., A.R., and H.H.; investigation, data curation, and visualization, H.H., H.T., and A.R. All authors have read and agreed to the published version of the manuscript.

Funding: The research was supported by the Estonian Research Council under grant PSG137 “Additive Manufacturing of Electrical Machines”.

Data Availability Statement: Data are contained within the article.

Conflicts of Interest: The authors declare no conflict of interest.

References

1. El-Wakeel, A.S. Design optimization of PM couplings using hybrid Particle Swarm Optimization-Simplex Method (PSO-SM) Algorithm. *Electr. Power Syst. Res.* **2014**, *116*, 29–35. [\[CrossRef\]](#)
2. Andriushchenko, E.; Kaska, J.; Kallaste, A.; Belahcen, A.; Vaimann, T.; Rassõlkin, A. Design Optimization of Permanent Magnet Clutch with Ārtap Framework. *TechRxiv* **2021**, in press.
3. Charpentier, J.F.; Lemarquand, G. Optimal design of cylindrical air-gap synchronous permanent magnet couplings. *IEEE Trans. Magn.* **1999**, *35*, 1037–1046. [\[CrossRef\]](#)
4. Hornreich, R.M.; Shtrikman, S. Optimal design of synchronous torque couplers. *IEEE Trans. Magn.* **1978**, *14*, 800–802. [\[CrossRef\]](#)
5. Zhang, B.; Wan, Y.; Li, Y.; Feng, G. Optimized design research on adjustable-speed permanent magnet coupling. In Proceedings of the IEEE International Conference on Industrial Technology, Cape Town, Western Cape, South Africa, 25–28 February 2013; pp. 380–385.
6. Buchanan, C.; Gardner, L. Metal 3D printing in construction: A review of methods, research, applications, opportunities and challenges. *Eng. Struct.* **2019**, *180*, 332–348. [\[CrossRef\]](#)
7. Frazier, W.E. Metal additive manufacturing: A review. *J. Mat. Eng. Perform.* **2014**, *23*, 1917–1928. [\[CrossRef\]](#)
8. Zhang, Z.Y.; Jhong, K.J.; Cheng, C.W.; Huang, P.W.; Tsai, M.C.; Lee, W.H. Metal 3D printing of synchronous reluctance motor. In Proceedings of the IEEE International Conference on Industrial Technology, Taipei, Taiwan, 14–17 March 2016; pp. 1125–1128.
9. Wrobel, R.; Mecrow, B. A Comprehensive Review of Additive Manufacturing in Construction of Electrical Machines. *IEEE Trans. Energy Convers.* **2020**, *35*, 1054–1064. [\[CrossRef\]](#)
10. Lei, G.; Zhu, J.; Guo, Y.; Liu, C.; Ma, B. A review of design optimization methods for electrical machines. *Energies* **2017**, *10*, 1962. [\[CrossRef\]](#)
11. Duan, Y.; Ionel, D.M. A review of recent developments in electrical machine design optimization methods with a permanent magnet synchronous motor benchmark study. In Proceedings of the IEEE Energy Conversion Congress and Exposition: Energy Conversion Innovation for a Clean Energy Future, ECCE 2011, Rostock, Germany, 24–26 August 2011; pp. 3694–3701.
12. López-Torres, C.; Espinosa, A.G.; Riba, J.R.; Romeral, L. Design and optimization for vehicle driving cycle of rare-earth-free SynRM based on coupled lumped thermal and magnetic networks. *IEEE Trans. Veh. Technol.* **2018**, *67*, 196–205. [\[CrossRef\]](#)
13. Babetto, C.; Bacco, G.; Bianchi, N. Synchronous Reluctance Machine Optimization for High-Speed Applications. *IEEE Trans. Energy Convers.* **2018**, *33*, 1266–1273. [\[CrossRef\]](#)
14. Cupertino, F.; Pellegrino, G.; Gerada, C. Design of synchronous reluctance motors with multiobjective optimization algorithms. *IEEE Trans. Ind. Appl.* **2014**, *50*, 3617–3627. [\[CrossRef\]](#)
15. Pellegrino, G.; Cupertino, F.; Gerada, C. Automatic Design of Synchronous Reluctance Motors Focusing on Barrier Shape Optimization. *IEEE Trans. Ind. Appl.* **2015**, *51*, 1465–1474. [\[CrossRef\]](#)
16. Andriushchenko, E.A.; Kallaste, A.; Belahcen, A.; Heidari, H.; Vaimann, T.; Rassõlkin, A. Design Optimization of Permanent Magnet Clutch. In Proceedings of the International Conference on Electrical Machines (ICEM), Gothenburg, Sweden, 23–26 August 2020.
17. Jensen, M.T. Reducing the Run-Time Complexity of Multiobjective EAs: The NSGA-II and Other Algorithms. *IEEE Trans. Evol. Comput.* **2003**, *7*, 503–515. [\[CrossRef\]](#)
18. Smith, J.E.; Fogarty, T.C. Operator and parameter adaptation in genetic algorithms. *Soft Comput.* **1997**, *1*, 81–87. [\[CrossRef\]](#)
19. Lamont, G.B.; Coello, C.A.C.; Van Veldhuizen, D.A. *Evolutionary Algorithms for Solving Multi-Objective Problems*; Springer: New York, NY, USA, 2007.
20. Hwang, C.C.; Lyu, L.Y.; Liu, C.T.; Li, P.L. Optimal design of an SPM motor using genetic algorithms and Taguchi method. *IEEE Trans. Magn.* **2008**, *44*, 4325–4328. [\[CrossRef\]](#)
21. Sorgdrager, A.; Wang, R.J.; Grobler, A. Taguchi method in electrical machine design. *SAIEE Africa Res. J.* **2017**, *108*, 150–164. [\[CrossRef\]](#)
22. Yang, B.Y.; Hwang, K.Y.; Rhee, S.B.; Kim, D.K.; Kwon, B.I. Optimization of novel flux barrier in interior permanent magnet-type brushless dc motor based on modified Taguchi method. *J. Appl. Phys.* **2009**, *105*, 07F106. [\[CrossRef\]](#)
23. Ashabani, M.; Mohamed, Y.A.R.I.; Milimonfared, J. Optimum design of tubular permanent-magnet motors for thrust characteristics improvement by combined taguchineural network approach. *IEEE Trans. Magn.* **2010**, *46*, 4092–4100. [\[CrossRef\]](#)
24. Ferreira, C.; Vaidya, J. Torque analysis of permanent magnet coupling using 2d and 3d finite elements methods. *IEEE Trans. Magn.* **1989**, *25*, 3080–3082. [\[CrossRef\]](#)
25. Panek, D.; Orosz, T.; Karban, P. Ārtap: Robust Design Optimization Framework for Engineering Applications. In Proceedings of the 3rd International Conference on Intelligent Computing in Data Sciences, ICDS 2019, Marrakech, Morocco, 28–30 October 2019.
26. Kaska, J.; Orosz, T.; Karban, P.; Doležel, I.; Pechanek, R.; Panek, D. Optimization of Reluctance Motor with Printed Rotor. In Proceedings of the COMPUMAG 2019—22nd International Conference on the Computation of Electromagnetic Fields, Paris, France, 15–19 July 2019.
27. Karban, P.; Pánek, D.; Orosz, T.; Petrášová, I.; Doležel, I. FEM based robust design optimization with Agros and Ārtap. *Comput. Math. Appl.* **2020**, *81*, 618–633. [\[CrossRef\]](#)
28. Tiismus, H.; Kallaste, A.; Vaimann, T.; Rassõlkin, A.; Belahcen, A. Axial Synchronous Magnetic Coupling Modeling and Printing with Selective Laser Melting. In Proceedings of the 2019 IEEE 60th International Scientific Conference on Power and Electrical Engineering of Riga Technical University (RTUCON), Riga, Latvia, 7–9 October 2019; pp. 1–4.

Publication IV

Andriushchenko E., Kaska J., Kallaste A., Belahcen A., Vaimann T., Rassolkin A. (2021). Design optimization of a permanent magnet clutch with Artap framework. *Periodica Polytechnica Electrical Engineering and Computer Science*, 65(2), pp. 106–112, 2021.

Design Optimization of Permanent Magnet Clutch with Ārtap Framework

Ekaterina Andriushchenko^{1*}, Jan Kaska², Ants Kallaste¹, Anouar Belahcen³, Toomas Vaimann¹, Anton Rassõlkin¹

¹ Department of Electrical Power Engineering and Mechatronics, School of Engineering, Tallinn University of Technology, Ehitajate tee 5, 19086 Tallinn, Estonia

² Department of Electrical and Computational Engineering, Faculty of Electrical Engineering, University of West Bohemia, Univerzitní 2732/8, 301 00 Pilsen, Czech Republic

³ Department of Electrical Engineering and Automation, School of Electrical Engineering, Aalto University, Otakaari 1B, 02150 Espoo, Finland

* Corresponding author, e-mail: ekandr@taltech.ee

Received: 09 August 2020, Accepted: 14 September 2020, Published online: 09 March 2021

Abstract

So far, Permanent Magnet (PM) clutches have been broadly used as torque transmission devices. With the aim of effective utilization of materials and energy in the manufacturing of PM clutches, design optimization has been widely applied. Generally, PM clutches are optimized applying linear dimensions as optimization parameters. On the contrary, optimization of PM clutch shapes has not been done extensively. Therefore, this paper performs optimization of PM clutch shapes with the following objectives: maximum tangential attraction force and minimum volume of utilized materials. To form optimal shapes, the points on the clutch surface are chosen as optimization parameters. The optimization is carried out using Ārtap framework in connection with COMSOL software, where the 3D model of the clutch has been created. After the optimization, the tangential attraction force has increased by 13 % and the volume of the clutch has been reduced by 24 %. Although the obtained shapes appear to be highly intricate, it does not pose an obstacle for modern manufacturing techniques.

Keywords

electromagnetic coupling, optimization, additive manufacturing, Ārtap framework, NSGA-II

1 Introduction

The electrical drive systems have an undeniable influence on the energy conservation, environment and sustainable development of the world [1–3]. As an important component of electrical drive systems, Permanent Magnet (PM) clutch always has been an object of research interest.

PM clutches are reliable devices, which can transmit torque in the hazardous environment [4–6]. Extensive implementation of PM clutches is based on their unique features. Particularly, a lack of physical contact between driving and driven member allows transmitting torque over a separator, which is often necessary for biological and food processing applications. Moreover, the friction between the members is eliminated, that helps to avoid mechanical failures, decreases vibration and offers easier maintenance [7, 8].

The main issue in PM clutch design is the optimal usage of magnetic and non-magnetic materials. For many years, researchers have successfully applied design optimization to address this issue [9–14]. Most of research works have focused on minimizing the usage of magnetic and non-magnetic materials [13, 14]. However, linear dimensions have been mainly used as optimization parameters due to limited production capacities [15, 16]. However, manufacturing of geometrically complex objects has become possible employing modern techniques (e.g. additive manufacturing) [17–21]. Therefore, few studies have attempted to obtain more intricate designs. In [22], the authors have searched for optimal shapes of clutch disks using 2D finite element analysis (FEM). However, to find shapes more accurately, it is essential to carry out 3D design

optimization. 3D design optimization takes into account the flux distribution all over the body. Consequently, this research optimizes a PM clutch design in 3D intending to obtain a low mass of non-magnetic material and high transmitted torque [23–25].

Besides, this study uses Ārtap framework along with COMSOL to carry out the optimization [26]. Due to high computational complexity, the problem is solved using HPC (High-Performance Computing) with the automatic parallelization functionality of Ārtap. Ārtap [27] is an MIT (Massachusetts Institute of Technology) licensed robust design optimization framework, which provides a user-friendly interface along with a good set of numerical solvers and optimization algorithms. Moreover, using Ārtap is highly beneficial due to its integrated FEM solver (Agros [28, 29]), and its interconnection with several finite element (FE) solvers (COMSOL and others [27, 30]).

To optimize a PM clutch, this study applies the Non-dominated Sorting Genetic Algorithm II (NSGA-II) solver. NSGA-II is a fast sorting and elite multi-objective genetic algorithm, which is becoming a key instrument in the optimization of electrical machines and devices [31, 32]. NSGA-II is highly flexible algorithm, able to find a global minimum and can deal with non-analytic formulation of optimization problems.

2 Design optimization of the PM clutch

2.1 Operation principle of the PM clutch

This study considered a PM clutch constituted of two components: driving and driven disks with teeth (see Fig. 1). The material of both disks and the driven disk teeth were set as printed steel. The teeth of the driving member of the clutch were Permanent Magnets N52 (Sintered Nd-Fe-B). When the members are coupled, attraction force appears between the magnetic and steel teeth and contains two components: axial force F_z and tangential force F_r . The axial force is a force that attracts clutch members to each other.

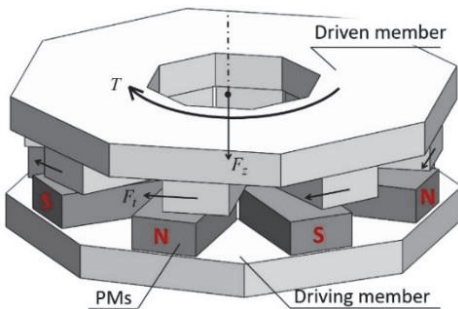


Fig. 1 Initial design of the clutch

The tangential force is a force that tries to align the teeth of the driving and driven member face to face by changing the position of the driven member. This force is associated with the torque being transmitted [33]. The transmitted torque depends on the angle of deviation of the clutch members relative to each other $\delta\theta$, magnetic flux density B , and magnetic field intensity H [4]:

$$T = \frac{\delta \int_V \int_0^H \mathbf{B} d\mathbf{H} dV}{\delta\theta} \quad (1)$$

Then, the relation between the torque and tangential force can be expressed by the following equation:

$$T = F_t \cdot R_m, \quad (2)$$

where R_m is the mean radius at which the force acts.

2.2 Design model of the PM clutch

The objectives of the PM clutch optimization were maximum tangential attraction force and minimum volume of printed steel material. The optimization started with creating the PM clutch model using COMSOL software. The clutch disks had eight symmetrical segments. Therefore, only one-eighth of the problem was modelled using periodic boundary conditions. Besides, the clutch was optimized in the position where the angular deflection was equal to $\pi/16$ and the tangential force reached a maximum (see Fig. 2). In addition, Fig. 2 presents the mesh used in the optimization. The number of elements of the mesh was approximately 50,000. It is important to highlight that the number of elements was changing during optimization. Particularly, the more complex geometry was formed, the more mesh elements were used.

The mathematical model of the clutch in COMSOL was based on the expression:

$$-\nabla \cdot (\mu \nabla \psi_m - \mathbf{B}_r) = 0, \quad (3)$$

where ψ_m is the magnetic scalar potential, \mathbf{B}_r is the remanent magnetic flux density and μ is the material

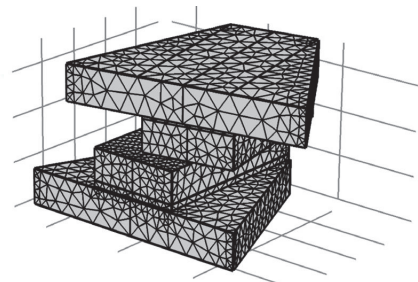


Fig. 2 Meshed design model of the clutch at $\pi/16$ angular deflection

permeability. Applying the magnetic scalar potential significantly reduces computational complexity of the design model.

Equation (3) was derived from the following relations:

$$\nabla \times \mathbf{H} = \mathbf{J}_f \rightarrow \nabla \times \mathbf{H} = \mathbf{0} \rightarrow \mathbf{H} = -\nabla \psi_m, \nabla \cdot \mathbf{B} = \nabla \cdot (\mu \mathbf{H} + \mathbf{B}_f) = 0. \quad (4)$$

Then, the Maxwell tensor was used to calculate the tangential attraction force.

In order to ensure geometrical continuity and symmetry, the magnetic scalar potential values on one side were set equal to the negative values of the magnetic scalar potential on the other side. Additionally, the mesh was identical on both sides of the one-eighth part of the model.

The utilized printed steel was nonlinear material, which means that its permeability μ changing with changes in magnetic field intensity (see Fig. 3). The magnetization curve of the printed steel was acquired from a test of a sample [34]. The sample was made of electrical steel with 6.5 % silicon content produced by selective laser melting printing.

The initial geometry of the clutch is shown in Fig. 4. The dimensions of the clutch are reported in Table 1.

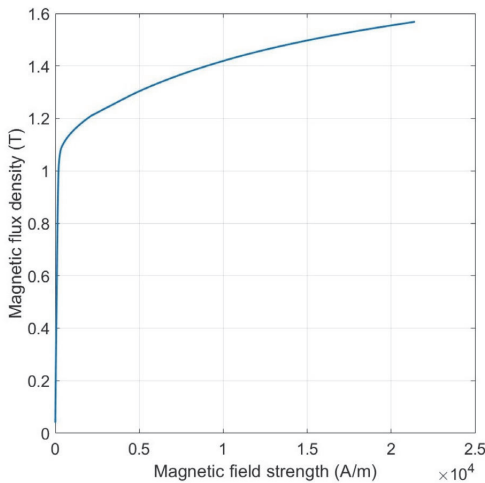


Fig. 3 B-H curve of the printed steel [19]

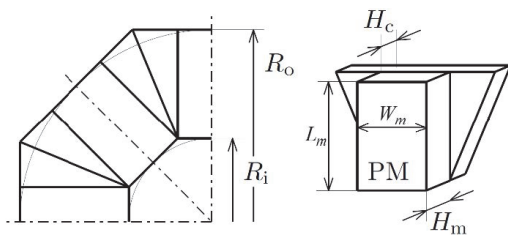


Fig. 4 Geometry of the clutch

Table 1 Clutch dimensions

| Dimension | Value |
|------------------------------|---------|
| Outer radius R_o | 32.5 mm |
| Inner radius R_i | 12.5 mm |
| Mean radius R_m | 21.5 mm |
| Thickness of the disks H_c | 4 mm |
| Thickness of the magnets | 5 mm |
| Width of the magnets | 10 mm |
| Length of the magnets | 18 mm |
| Air gap | 1 mm |

2.3 Optimization parameters

The optimization model had 56 parameters, which are presented in Fig. 5. The parameters, which correspond to the points located on the disk end faces are marked with red. The parameters, which correspond to the points located on the teeth end faces are marked with green. During optimization, the points could move in z -direction within the following limits: red points' limits were [0, 1.5] mm, green points' limits were [0, 4.5]. Both clutch members had the same parametrization. However, the shapes and sizes of the magnetic teeth were fixed.

2.4 Solving the optimization problem in Ārtap

The optimization was carried out using two interconnected programs: Ārtap and COMSOL. Within Ārtap, optimization algorithm NSGA-II was implemented, while the values of objective functions were calculated in COMSOL.

Formulation of the current optimization problem in Ārtap environment is shown in Algorithm 1. The optimization objectives and parameters were defined in the "ComsolProblem" class. The values of the objective functions were generated by COMSOL in the file named "OUT.txt".

When the problem was defined, the optimization algorithm and its setting were specified in the "solve" function (see Algorithm 2).

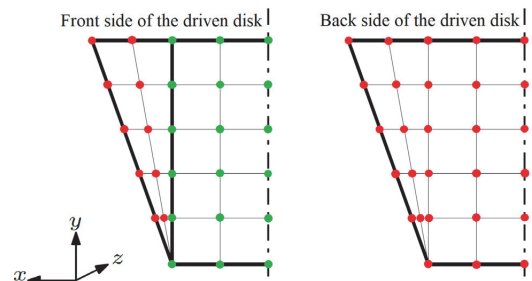


Fig. 5 Parametrization of the clutch model

Algorithm 1 Formulation of the optimization problem

```
class ConsolProblem(Problem):
    def set(self):
        self.name = "ConsolProblem"
        self.parameters = [{'name': 'b1', 'initial_value': 0, 'bounds': [0, 3e-3]},
                           {'name': 'b2', 'initial_value': 0, 'bounds': [0, 3e-3]} ... ]
        self.costs = [{'name': 'f1', 'criteria': 'minimize'},
                     {'name': 'f2', 'criteria': 'minimize'}]
        self.output_files = ["OUT.txt"]
        self.executor = CondorConsolJobExecutor(self, model_
        file="clutch2.mph", files_from_condor=["OUT.txt"])
```

Algorithm 2 Optimization algorithm and settings

```
def solve():
    problem = ConsolProblem()
    database_name = "" + os.sep + "data"
    problem.data_store = JsonDataStore(problem,
    database_name=database_name, mode="write")
    problem.options['save_data_files'] = True

    algorithm = NSGAI(problem)
    algorithm.options['max_population_number'] = 50
    algorithm.options['max_population_size'] = 50
    algorithm.options['max_processes'] = 10
    algorithm.run()
```

In this study, NSGA-II optimization algorithm was used due to its high efficiency and reliability. For NSGA-II, the settings were the following: number of generations and number of individuals in each generation. The number of individuals, as well as the number of generations, was 50, which led to 2,500 calculations. Additionally, the maximum number of parallel processes was defined to 10, since the computing cluster "Condor" was used.

3 Results

The results of the optimization are reported in the objectives plane in Fig. 6, together with the Pareto front. It can be noticed that the solutions converge to the optimal ones, which are located close to the left corner of the plot. The Pareto front is steep as long as the volume has variations around close values of the tangential attraction force. Overall, Fig. 6 confirms that the PM clutch is able to compromise a low volume with a high tangential attraction force.

Fig. 7 shows the magnetic flux density of the optimized clutch, while Fig. 8 presents the optimized shapes of the clutch in detail.

Interestingly, Fig. 7 shows quite low magnetic flux density of the optimized clutch on the bottom of driving and driven disks. A possible explanation for this might be that the limits defined for the changes of optimization parameters were too small.

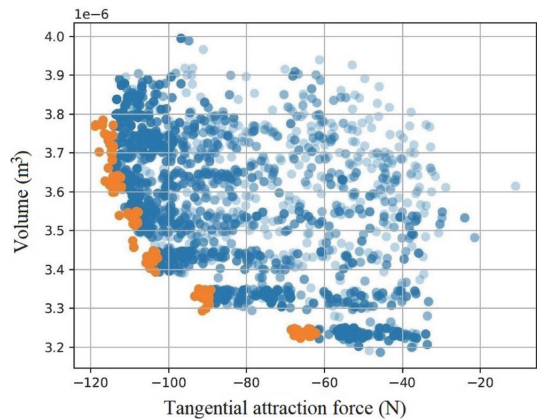


Fig. 6 Simulated individuals in the objective plane and Pareto front

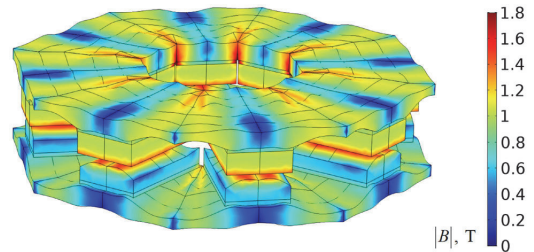


Fig. 7 Magnetic flux density of the optimized PM clutch

Table 2 illustrates the comparison of initial and optimized design in terms of the volume and tangential attraction force. From Table 2 it can be concluded, the tangential attraction force increased by 13 % and the volume was reduced by 24 %.

4 Conclusions

The current research aimed to optimize a PM clutch to achieve high transmitted torque and low volume of steel material.

After the optimization with 2,500 calculations, the volume was reduced and the tangential force increased significantly. It is worth mentioning that the intricacy of the obtained shapes of the clutch does not pose a big obstacle since modern manufacturing techniques such as additive manufacturing allow producing complex geometries [17, 34]. Nevertheless, additive manufacturing may possess several issues: geometrical imperfections and inaccuracy in material properties, which can have a negative influence on the efficient work of the clutch [9, 35]. To ensure the accuracy of geometry and material properties, robust optimization can be applied. For this purpose, further research might focus on robust optimization of the PM clutch.

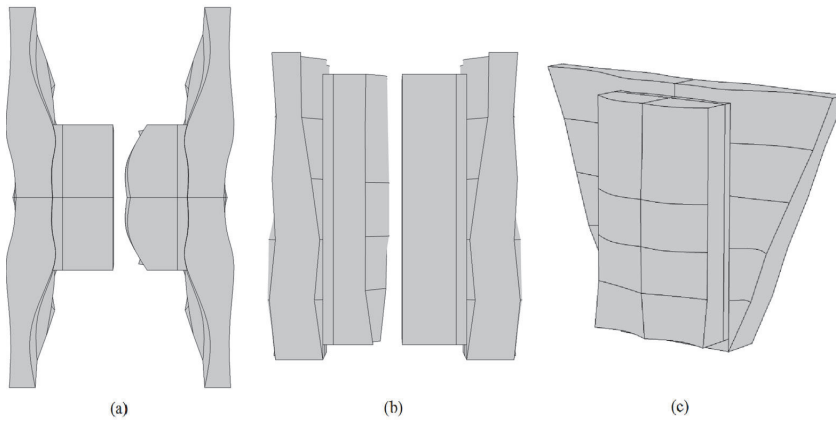


Fig. 8 Optimized shapes of the PM clutch: (a) top view of the clutch, (b) side view of the clutch, (c) driven disk

Table 2 Comparison of initial and optimal design

| Objective | Initial design | Optimal design |
|---|--------------------------------|--------------------------------|
| Volume | $4.6 \cdot 10^{-6} \text{m}^3$ | $3.5 \cdot 10^{-6} \text{m}^3$ |
| Maximum tangential attraction force F_t | 97 N | 110 N |
| Maximum axial attraction force F_a | 1056 N | 732 N |
| Torque T | 2.09 Nm | 2.37 Nm |

Besides, design optimization models, calculations and results can be downloaded from the homepage of the project [36].

Acknowledgment

The research was supported by the Estonian Research Council under grant PSG137 "Additive Manufacturing of Electrical Machines".

References

- [1] Heidari, H., Rassölkkin, A., Vaimann, T., Kallaste, A., Taheri, A., Holakooie, M. H., Belahcen, A. "A Novel Vector Control Strategy for a Six-Phase Induction Motor with Low Torque Ripples and Harmonic Currents", *Energies*, 12(6), Article No. 1102, 2019. <https://doi.org/10.3390/en12061102>
- [2] Rassölkkin, A., Belahcen, A., Kallaste, A., Vaimann, T., Lukichev, D. V., Orlova, S., Heidari, H., Asad, B., Acedo, J. P. "Life cycle analysis of electrical motor drive system based on electrical machine type", *Proceedings of the Estonian Academy of Sciences*, 69(2), pp. 162–177, 2020. <https://doi.org/10.3176/proc.2020.2.07>
- [3] Vaimann, T., Kallaste, A., Bolgov, V., Belahcen, A. "Environmental considerations in lifecycle based optimization of electrical machines", In: 2015 16th International Scientific Conference on Electric Power Engineering, Kouty nad Desnou, Czech Republic, 2015, pp. 209–214. <https://doi.org/10.1109/EPE.2015.7161057>
- [4] Ferreira, C., Vaidya, J. "Torque analysis of permanent magnet coupling using 2d and 3d finite elements methods", *IEEE Transactions on Magnetics*, 25(4), pp. 3080–3082, 1989. <https://doi.org/10.1109/20.34375>
- [5] Ravaud, R., Lemarquand, V., Lemarquand, G. "Analytical design of permanent magnet radial couplings", *IEEE Transactions on Magnetics*, 46(11), pp. 3860–3865, 2010. <https://doi.org/10.1109/TMAG.2010.2056379>
- [6] Wang, Y., Filippini, M., Bianchi, N., Alotto, P. "A Review on Magnetic Gears: Topologies, Computational Models, and Design Aspects", *IEEE Transactions on Industry Applications*, 55(5), pp. 4557–4566, 2019. <https://doi.org/10.1109/TIA.2019.2916765>
- [7] Overshott, K. J. "The comparison of the pull-out torque of permanent magnet couplings predicted theoretically with experimental measurements", *IEEE Transactions on Magnetics*, 25(5), pp. 3913–3915, 1989. <https://doi.org/10.1109/20.42475>
- [8] Weinmann, D., Wiesmann, H. J. "Application of rare earth magnets to coaxial synchronous couplings", *Journal of Magnetism and Magnetic Materials*, 9(1–3), pp. 179–181, 1978. [https://doi.org/10.1016/0304-8853\(78\)90047-1](https://doi.org/10.1016/0304-8853(78)90047-1)
- [9] Lei, G., Zhu, J., Guo, Y., Liu, C., Ma, B. "A review of design optimization methods for electrical machines", *Energies*, 10(12), Article No. 1962, 2017. <https://doi.org/10.3390/en10121962>
- [10] Duan, Y., Ionel, D. M. "A review of recent developments in electrical machine design optimization methods with a permanent magnet synchronous motor benchmark study", In: *IEEE Energy Conversion Congress and Exposition: Energy Conversion Innovation for a Clean Energy Future*, Phoenix, AZ, USA, 2011, pp. 3694–3701. <https://doi.org/10.1109/ECCE.2011.6064270>

- [11] Pabut, O., Eerme, M., Kallaste, A., Vaimann, T. "Multi-criteria design optimization of ultra large diameter permanent magnet generator", *Elektronika ir Elektrotechnika*, 21(3), pp. 42–48, 2015. <https://doi.org/10.5755/j01.eec.21.3.10278>
- [12] Wang, A., Wang, J., Wu, B., Shi, C. "Structural optimization of the permanent magnet drive based on artificial neural network and particle swarm optimization", In: 2011 3rd International Conference on Intelligent Human-Machine Systems and Cybernetics, Hangzhou, China, 2011, pp. 70–74. <https://doi.org/10.1109/IHMSC.2011.87>
- [13] El-Wakeel, A. S. "Design optimization of PM couplings using hybrid Particle Swarm Optimization-Simplex Method (PSO-SM) Algorithm", *Electric Power Systems Research*, 116, pp. 29–35, 2014. <https://doi.org/10.1016/j.epsr.2014.05.003>
- [14] Zhang, B., Wan, Y., Li, Y., Feng, G. "Optimized design research on adjustable-speed permanent magnet coupling", In: IEEE International Conference on Industrial Technology, Cape Town, South Africa, 2013, pp. 380–385. <https://doi.org/10.1109/ICIT.2013.6505702>
- [15] Wu, W., Lovatt, H. C., Dunlop, J. B. "Analysis and design optimisation of magnetic couplings using 3D finite element modelling", *IEEE Transactions on Magnetics*, 33(5), pp. 4083–4085, 1997. <https://doi.org/10.1109/20.619670>
- [16] Eliès, P., Lemarquand, G. "Analytical optimization of the torque of a permanent-magnet coaxial synchronous coupling", *IEEE Transactions on Magnetics*, 34(4), pp. 2267–2273, 1998. <https://doi.org/10.1109/20.703865>
- [17] Frazier, W. E. "Metal additive manufacturing: A review", *Journal of Materials Engineering and Performance*, 23(6), pp. 1917–1928, 2014. <https://doi.org/10.1007/s11665-014-0958-z>
- [18] Johnson, K., Zemba, M., Conner, B. P., Walker, J., Burden, E., Rogers, K., Cwiok, K. R., Macdonald, E., Cortes, P. "Digital Manufacturing of Pathologically-Complex 3D Printed Antennas", *IEEE Access*, 7, pp. 39378–39389, 2019. <https://doi.org/10.1109/ACCESS.2019.2906868>
- [19] Kruth, J. P., Leu, M. C., Nakagawa, T. "Progress in additive manufacturing and rapid prototyping", *CIRP Annals - Manufacturing Technologies*, 47(2), pp. 525–540, 1998. [https://doi.org/10.1016/S0007-8506\(07\)63240-5](https://doi.org/10.1016/S0007-8506(07)63240-5)
- [20] Keresztes, Z., Pammer, D., Szabo, J. P. "EBSD examination of argon ion bombarded Ti-6Al-4V samples produced with DMLS technology", *Periodica Polytechnica Mechanical Engineering*, 63(3), pp. 195–200, 2019. <https://doi.org/10.3311/PPme.13821>
- [21] Tiismus, H., Kallaste, A., Rassõlkin, A., Vaimann, T. "Preliminary Analysis of Soft Magnetic Material Properties for Additive Manufacturing of Electrical Machines", *Key Engineering Materials*, 799, pp. 270–275, 2019. <https://doi.org/10.4028/www.scientific.net/KEM.799.270>
- [22] Andriushchenko, E. A., Kallaste, A., Belahcen, A., Heidari, H., Vaimann, T., Rassõlkin, A. "Design Optimization of Permanent Magnet Clutch", In: 2020 International Conference on Electrical Machines, Gothenburg, Sweden, 2020. <https://doi.org/10.1109/ICEM49940.2020.9270726>
- [23] Lubin, T., Fontchastagner, J., Mezani, S., Rezzoug, A. "Comparison of transient performances for synchronous and eddy-current torque couplers", In: 2016 22nd International Conference on Electrical Machines (ICEM), Lausanne, Switzerland, 2016, pp. 695–701. <https://doi.org/10.1109/ICELMACH.2016.7732602>
- [24] Zerroul, A., Hadjout, L., Ouazir, Y., Bensaidane, H., Benbekai, A., Chaouch, O. "3D Analytical Model to Compute the Electromagnetic Torque of Axial Flux Magnetic Coupler with a Rectangular-Shaped Magnet", In: 2018 3rd International Conference on Electrical Sciences and Technologies in Maghreb, Algiers, Algeria, 2019. <https://doi.org/10.1109/CISTEM.2018.8613547>
- [25] Meng, Z., Lu, W., Meng, Z., Sun, Y., Zhu, H. "Research on modelling and simulation for dynamic characteristics of magnetic shaft coupling", *International Journal of Engineering Systems Modelling and Simulation*, 9(2), pp. 78–85, 2017. <https://doi.org/10.1504/IJESMS.2017.083226>
- [26] Kaska, J., Orosz, T., Karban, P., Doležel, I., Pechanek, R., Panek, D., "Optimization of Reluctance Motor with Printed Rotor", In: 22nd International Conference on the Computation of Electromagnetic Fields, Paris, France, 2019. <https://doi.org/10.1109/COMPUMAG45669.2019.9032792>
- [27] Panek, D., Orosz, T., Karban, P. "Artap: Robust Design Optimization Framework for Engineering Applications", In: 2019 3rd International Conference on Intelligent Computing in Data Sciences, Marrakech, Morocco, 2019. <https://doi.org/10.1109/ICDS47004.2019.8942318>
- [28] Pánek, D., Karban, P., Orosz, T., Doležel, I. "Comparison of simplified techniques for solving selected coupled electroheat problems", *International Journal for Computation and Mathematics in Electrical and Electronic Engineering*, 39(1), pp. 220–230, 2020. <https://doi.org/10.1108/COMPEL-06-2019-0244>
- [29] Karban, P., Pánek, D., Orosz, T., Petrášová, I., Doležel, I. "FEM based robust design optimization with Agros and Artap", *Computers and Mathematics with Applications*, 81, pp. 618–633, 2021. <https://doi.org/10.1016/j.camwa.2020.02.010>
- [30] Karban, P., Panek, D., Orosz, T., Doležel, I. "Semi-analytical Solution for a Multi-objective TEAM Benchmark Problem", *Periodica Polytechnica Engineering and Computer Science*, 2020.
- [31] Deb, K., Pratap, A., Agarwal, S., Meyarivan, T. "A fast and elitist multiobjective genetic algorithm: NSGA-II", *IEEE Transactions on Evolutionary Computation*, 6(2), pp. 182–197, 2002. <https://doi.org/10.1109/4235.996017>
- [32] Coello Coello, C. A., Lamont, G. B., Van Veldhuizen, D. A. "Evolutionary Algorithms for Solving Multi-Objective Problems", Springer, New York, NY, USA, 2007. <https://doi.org/10.1007/978-0-387-36797-2>
- [33] Tong, W. "Mechanical Design of Electric Motors", CRC Press, Boca Raton, FL, USA, 2014. <https://doi.org/10.1201/b16863>
- [34] Tiismus, H., Kallaste, A., Vaimann, T., Rassõlkin, A., Belahcen, A. "Axial Synchronous Magnetic Coupling Modeling and Printing with Selective Laser Melting", presented at 2019 IEEE 60th International Scientific Conference on Power and Electrical Engineering of Riga Technical University, Riga, Latvia, Oct, 7–9, 2019. <https://doi.org/10.1109/RTUCON48111.2019.8982344>

- [35] Buchanan, C., Gardner, L. "Metal 3D printing in construction: A review of methods, research, applications, opportunities and challenges", *Engineering Structures*, 180, pp. 332–348, 2019.
<https://doi.org/10.1016/j.engstruct.2018.11.045>
- [36] Orosz, T. "Artap", [online] Available at: <https://github.com/artap-framework/artap/tree/master/examples/Problems%20from%20PP%20special%20issue> [Accessed: 08 August 2020]

Publication V

Andriushchenko E., Kallaste A., Heidari H., Belahcen A., Vaimann T., Rassolkin A. (2020). Design optimization of permanent magnet clutch. 2020 International Conference on Electrical Machines (ICEM), pp. 436–440, 2020.

Design Optimization of Permanent Magnet Clutch

E. A. Andriushchenko, A. Kallaste, A. Belahcen, H. Heidari, T. Vaimann, A. Rassõlkin

Abstract – Design optimization of permanent magnet clutches can be an effective solution for minimization of the volume at a given torque output. This study proposes an optimization method for permanent magnet clutch, which allows obtaining a complex and detailed design. Design and optimization model of the clutch, optimization method and algorithm are comprehensively discussed. Optimization using 2D finite element analysis, combined with a genetic algorithm is demonstrated. The obtained optimal shapes reduced the volume of clutch discs by 31% while the maximum integral attraction force met the limit.

Index Terms – electromagnetic coupling, design optimization, genetic algorithms.

I. INTRODUCTION

PERMANENT MAGNET (PM) clutches have been widely applied for torque transition between two shafts without mechanical contact. The lack of mechanical contact denotes the air-gap between driving and driven member. This design feature brings several advantages to PM clutches over mechanical clutches [1], [2]. Firstly, the lack of friction reduces the risk of mechanical failures, reduces vibration and proposes easier maintenance. Additionally, the isolation of the driving and driven members is desired for a list of applications [3]–[5]. For instance, they are highly suitable for usage in a damaging, corrosive environment. Additionally, biological and food processing equipment such as mixers or agitators often requires torque to be transmitted through a separator.

One of the key requirements for clutches is a minimum volume of magnetic and non-magnetic materials with the desired torque output. These requirements can be satisfied by means of design optimization of PM clutches. So far, a considerable amount of literature has been published on design optimization of electromagnetic devices [6]–[8]. Besides, several studies have optimized design of PM clutch with different approaches [9], [10]. Up to now, most researchers have carried out optimizations using only linear dimensions as decision variables, for instance, diameters of discs or thickness of magnets [5]. However, it may be beneficial to exploit the designs that are more precise by defining optimal shapes instead of dimensions, since modern

manufacturing techniques allow obtaining highly complex structures. For instance, additive manufacturing provides a wide range of opportunities to more sophisticated design production. Therefore, this paper is focused on the optimization of a PM clutch shapes with the aim of obtaining the lowest weight while keeping the torque above the defined limits. As a first approximation, only shapes of the iron disks are considered in this study.

This paper begins by formulating the operation principle of the clutch and defining the design and optimization models. Later on, Section II. continues with the optimization method and algorithm description. Towards the end, results of the optimization are reported and discussed.

II. DESIGN OPTIMIZATION

A. Design model

The first step in any optimization is to create a design model. In this study, the design model of the clutch was made in program Finite Element Method Magnetics (FEMM). Fig. 1 illustrates the initial design of the clutch (a) and the model of the clutch (b), where magnets are highlighted in beige colour. In principle, the clutch consists of driving and driven member. The driving member possesses PM teeth placed on the disc made from printed steel. The magnets are magnetized as it is shown in Fig. 1. On the other hand, the driven member is fully made from printed steel. Working principle of PM clutch is based on attraction force between magnetic and steel teeth. The attraction force is a vector that includes two components: axial attraction force F_z and tangential attraction force F_t . The axial attraction force allows two members to couple and move synchronously. The angle between the members and subsequent tangential attraction force are responsible for transmitted torque. This is due to the fact that the tangential attraction force arises between the members when one member spins relative to the other one. When this force reaches the maximum value, the driven member shifts to another stable position, where its teeth are aligned with the magnetic teeth of the driving member. However, if the torque on the driving member exceeds the maximum value that clutch can handle, the driven member slips. Consequently, the maximum value of the tangential attraction force defines the torque that the clutch is able to transmit [4], [11]. Therefore, the considered clutch was optimized with respect to the transmitted torque.

For a given system, the dimensions of the initial design are reported in Table I. As a first approximation, the volume of the clutch was reduced by means of the reduction of the volume of discs, particularly, by optimizing the discs

This research work has been supported by Estonian Ministry of Education and Research (Project PSG137).

E. Andriushchenko, A. Kallaste, H. Heidari, T. Vaimann and A. Rassõlkin are with the Department of Electrical Power Engineering and Mechatronics, Tallinn University of Technology, Estonia (e-mail: ekandr@taltech.ee)

A. Belahcen is with Department of Electrical Engineering and Automation, Aalto University, Espoo, Finland and with the Department of Electrical Power Engineering and Mechatronics, Tallinn University of Technology, Estonia (e-mail: anouar.belahcen@aalto.fi)

shapes.

The flux distribution in discs in the radial direction was not changing significantly. Therefore, it was acceptable to optimize only a cross-section of a circle type (A-A) and use an obtained optimal geometry along the radial direction. In order to simplify the model for making 2D analysis, the cross-section was considered with straightened air gap. To simulate the geometrical continuity of each disk, periodic boundary conditions were implemented on the sides of each disk. They are shown as red and green lines in Fig. 1. The clutch was placed in the air box. The length of the disks L was calculated as the length of the circle with a diameter of D_m . Consequently, the shift in this design model represented the angular deflection between clutch halves. Particularly, the used shift value was equal to 5 mm and denoted the position when the attraction force between the halves of the clutch was maximum. The members of the clutch were separated by the air gap equal to 1 mm.

B. Materials

As it was mentioned before, the driving part teeth were permanent magnets, while the material of the driven member was printed steel [12]. Fig. 2 illustrates B-H magnetization curve, which characterises the magnetic properties of the utilized material. Particularly, the properties were obtained from the sample made from the gas-atomized pre-alloyed powder of Fe-Si by selective laser melting printing.

Sintered Nd-Fe-B (N52) magnets were utilized in the optimized clutch since these magnets are the strongest permanent magnets available in today's market [13]–[15].

C. Optimization model

The first step in optimization is to constitute an optimization model. An optimization model includes objective functions, constraints and decision variables [16]–[18].

In order to obtain optimal shapes of the discs, the points on the discs' end faces were chosen as decision variables (see Fig. 3). Particularly, by changing the position of each point in z and z' -direction, different complex shapes could

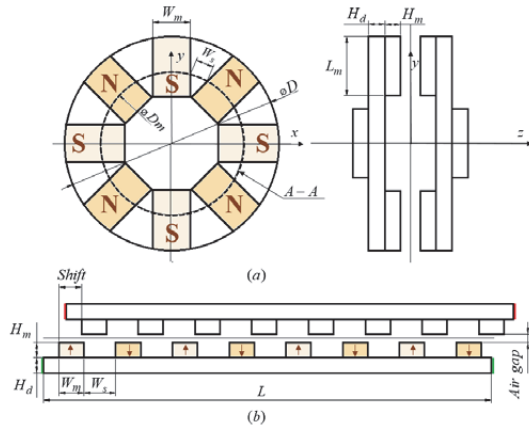


Fig. 1. Initial design (a) and model (b) of the clutch.

TABLE I
MAIN DATA OF THE CLUTCH UNDER OPTIMIZATION

| Dimension | Symbol / formula | Value |
|-----------------------------------|---------------------|---------|
| Outer diameter | D | 65 mm |
| Diameter in the middle of magnets | D_m | 44.6 mm |
| Clutch length in developed view | $L = \pi \cdot D_m$ | 140 mm |
| Magnet length | L_m | 20 mm |
| Magnet height | H_m | 5 mm |
| Magnet width | W_m | 10 mm |
| Space between magnets | W_s | 7.5 mm |
| Discs height | H_d | 4 mm |

be formed. Only six points on each disc were satisfactory ($p_i, i=1\dots12$), for the reason that flux lines were symmetric with respect to the axes of clutch's teeth (t_{11}, t_{21}). The variation limits of decision variables p_{1-6} in z -direction and p_{7-12} in z' -direction were $[0, 3.5]$.

The objective function of the optimization model was the volume of the discs. The integral tangential attraction force F_t was used as a constraint. During the optimization, the force was kept above 95% of the initial value with a maximum reduction of the volume. The values of objective and constraint were calculated in FEMM. The initial values of objective and constraint are reported in Table II.

D. Optimization method and algorithm

Optimization method can be described as a strategy or procedure within which an optimization model is optimized. Optimization method applied in this problem is called a direct optimization method since it uses design model accompanying by optimization algorithm [16], [19].

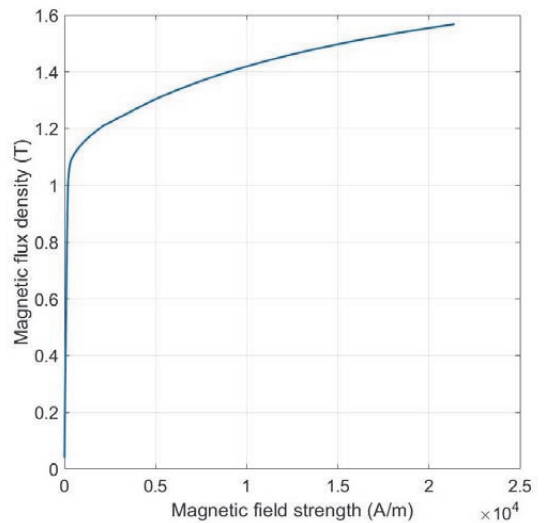


Fig. 2. B-H magnetization curve for printed steel.

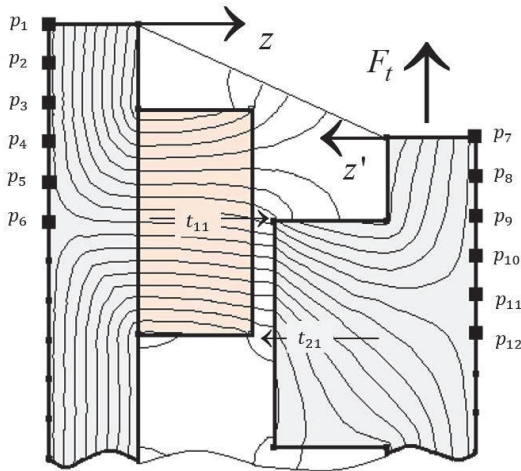


Fig. 3. Decision variables mapped on design model.

The considered optimization model had a high number of decision variables – twelve. Generally, it is rather difficult to optimize this kind of a model [16], [20]. Therefore, in order to prevent the overloading of the applied algorithm and reduce execution time, the optimization was made in two steps. More specifically, the shapes of the driving and driven disc were optimized one after another.

The optimization models were as follows:

$$\begin{aligned} \min: & \quad V_1(p_1, \dots, p_6); \\ \text{s.t.} & \quad F_{t_1}(p_1, \dots, p_6) \geq [F_{t_1}], \quad [F_{t_1}] = 119 \text{ N}; \end{aligned} \quad (1)$$

$$\begin{aligned} \min: & \quad V_2(p_7, \dots, p_{12}); \\ \text{s.t.} & \quad F_{t_2}(p_7, \dots, p_{12}) \geq [F_{t_2}], \quad [F_{t_2}] = 117 \text{ N}. \end{aligned} \quad (2)$$

Fig. 4 shows the applied optimization method in detail and provides the settings of the algorithm. The objective and constraint were calculated in the design model and optimization algorithm was proposing decision variables.

The algorithm used here was a single-objective genetic algorithm (GA) [21], [22]. Nowadays, GAs are widely applied due to the high number of advantages such as [23]:

- 1) ability to find a global minimum,
- 2) ability to handle non-analytic problem definition,
- 3) possibility to be adjusted to a particular problem,
- 4) robustness to noisy evaluation functions.

GA includes several operators that justify the flexibility of the algorithm as long as can be easily adjusted to a particular problem. To name, crossover, mutation, selection

TABLE II
INITIAL SPECIFICATIONS OF THE CLUTCH

| Specification | Symbol/formula | Value |
|--|----------------|-----------------------|
| The maximum integral tangential attraction force | F_t | 124 N |
| Driving disc volume | V_1 | 11200 mm ³ |
| Driven disc volume | V_2 | 11200 mm ³ |

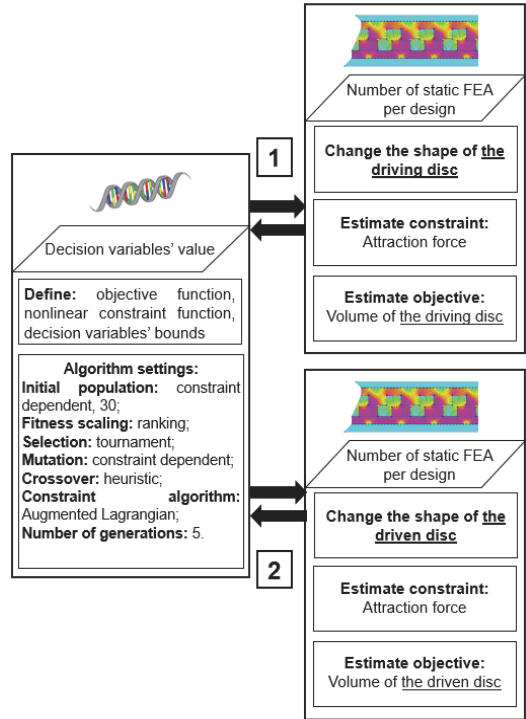


Fig. 4. Scheme of applied optimization method.

and fitness scaling are the operators. Fitness scaling is used to calculate the performance of each individual (decision variables set). The function of selection is to choose the best individuals. Further, the selected individuals constitute a new generation together with crossover fraction, which is generated by the operator crossover. This operator is applied to two individuals in order to create a new one. Finally, the operator that provides diversity and broadens the search space is mutation. It is important to mention that GA can be directly applied only to unconstrained optimization. Therefore, it is necessary to use additional techniques, such as constraint-handling methods, that can keep solutions in the feasible region [24], [25]. It is worth mentioning that algorithm settings, i.e. operators' functions, have a direct effect on optimality of the results. Therefore, for a defined problem, algorithm settings were chosen according to the common settings used in electrical devices optimization [26]–[28].

As it is shown in Fig. 4, the augmented Lagrangian was applied to handle the constraint. This method combines the objective function with constraint function using the Lagrangian [29]. Consequently, the final formulation of the problem was as follows:

$$V_i - \lambda_i \cdot s_i \cdot \log(s_i - [F_{t_i}] + F_{t_i}), \quad (3)$$

where the elements $\lambda_i > 0$ are known as Lagrange multiplier estimates and the components $s_i > 0$ are known as shifts and $s_i = \mu \cdot \lambda_i$, $\mu > 0$.

The number of individuals was 300 ($=30 \cdot 5 \cdot 2$), where 30 is the size of each generation and 5 is the number of generations. Consequently, it required 300 evaluations of the optimization model that resulted in 4 hours of calculations.

III. RESULTS

Fig. 5 shows the optimal geometry of the clutch and presents the optimal values of decision variables. Overall, the volume of the driving disc was reduced significantly by 36%, while the maximum value of the integral tangential attraction force met the limit $F_T=119$ N. The second step of optimization demonstrated considerable changes in the driven disc volume as well (25%). Overall, there was a significant difference (31%) between initial and optimal design volumes. What is interesting about the results is that there were no changes in the attraction force after the driven disc optimization. Therefore, it may be assumed that the geometry of the driving disc had a stronger effect on the attraction force.

In addition, the dependence of the integral attraction force on the increase in the shift was built (see Fig. 6). In Fig. 6, blue line illustrates the attraction force in initial design configuration, red line demonstrates the force after the driving disc optimization, and black line denotes the final optimized design configuration. As it was noticed before, the maximum integral attraction force did not experience radical changes after optimization. This effect remained the same way during changing of the shift.

IV. CONCLUSION

The purpose of the current study was to optimize PM clutch shapes in order to obtain the lowest weight while keeping the torque above the defined limits.

The problem had a single-objective optimization model, where the volume of clutch's discs was the objective and the tangential attraction force was considered as a constraint. The applied method was based on the interaction between the design model and the genetic algorithm. The optimization was made in two steps, i.e. the driving and driven disc were optimized separately. It allowed preventing the overloading of the applied algorithm and reducing execution time.

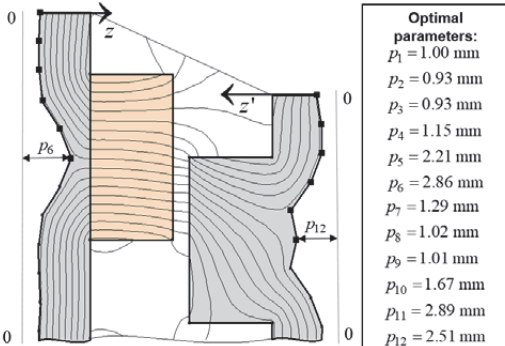


Fig. 5. Optimized geometry and optimal values of parameters.

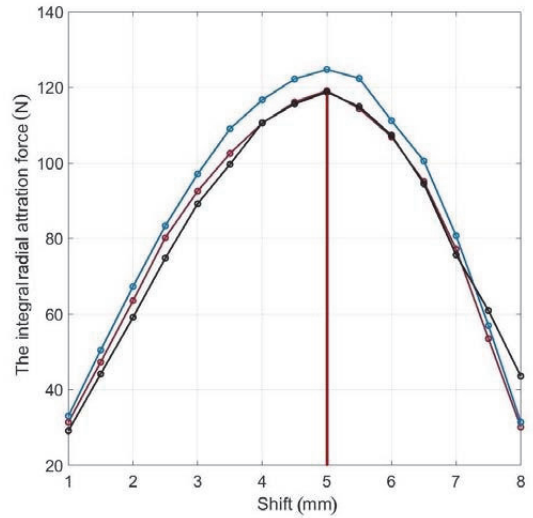


Fig. 6. Optimization results. Blue: the initial design. Red: the driving disc optimization. Black: the final optimized design.

The result of this optimization was the significant reduction in the volume of the discs (31%), while the tangential attraction force experienced a small change from the initial value.

The present study lays the groundwork for future research into PM clutches optimization. Specifically, a natural progression of this work is to obtain optimal shapes of the permanent magnets, teeth, and discs in 3D.

V. REFERENCES

- [1] R. Ravaut, V. Lemarquand, and G. Lemarquand, "Analytical design of permanent magnet radial couplings," *IEEE Trans. Magn.*, vol. 46, no. 11, pp. 3860–3865, 2010.
- [2] C. Ferreira, J. Vaidya, and S. Corporation, "Torque Analysis of Permanent Magnet Coupling Using 2D and 3D Finite Elements Methods," vol. 25, no. 4, pp. 3080–3082, 1989.
- [3] D. Weinmann and H. J. Wiesmann, "Application of rare earth magnets to coaxial synchronous couplings," *J. Magn. Magn. Mater.*, vol. 9, no. 1–3, pp. 179–181, Oct. 1978.
- [4] K. J. Overshott, "The comparison of the pull-out torque of permanent magnet couplings predicted theoretically with experimental measurements," *IEEE Trans. Magn.*, vol. 25, no. 5, pp. 3913–3915, 1989.
- [5] W. Wu, H. C. Lovatt, and J. B. Dunlop, "Analysis and design optimisation of magnetic couplings using 3D finite element modelling," *IEEE Trans. Magn.*, vol. 33, no. 5 PART 2, pp. 4083–4085, 1997.
- [6] C. López-Torres, A. G. Espinosa, J. R. Riba, and L. Romeral, "Design and optimization for vehicle driving cycle of rare-earth-free SynRM based on coupled lumped thermal and magnetic networks," *IEEE Trans. Veh. Technol.*, 2018.
- [7] G. Lo Calzo and M. Galea, "Design Optimization of a High-Speed Synchronous," *IEEE Trans. Ind. Appl.*, vol. 54, no. 1, pp. 233–243, 2018.
- [8] C. Babetto, G. Bacco, and N. Bianchi, "Synchronous Reluctance Machine Optimization for High-Speed Applications," *IEEE Trans. Energy Convers.*, vol. 33, no. 3, pp. 1266–1273, Sep. 2018.
- [9] R. M. Hornreich and S. Shtrikman, "Optimal design of synchronous torque couplers," *IEEE Trans. Magn.*, vol. 14, no. 5, pp. 800–802, 1978.
- [10] P. Eliès and G. Lemarquand, "Analytical optimization of the torque of a permanent-magnet coaxial synchronous coupling," *IEEE Trans. Magn.*, vol. 34, no. 4 PART 2, pp. 2267–2273, 1998.

- [11] W. Tong, Mechanical design of electric motors. 2014.
- [12] H. Tiismus, A. Kallaste, T. Vaimann, A. Rassolkin, and A. Belahcen, "Axial Synchronous Magnetic Coupling Modeling and Printing with Selective Laser Melting," 2020, pp. 1–4.
- [13] H. Nakamura, K. Hirota, M. Shimao, T. Minowa, and M. Honshima, "Magnetic properties of extremely small Nd-Fe-B sintered magnets," in *IEEE Transactions on Magnetism*, 2005, vol. 41, no. 10, pp. 3844–3846.
- [14] Y. Matsuura, "Recent development of Nd-Fe-B sintered magnets and their applications," *J. Magn. Magn. Mater.*, vol. 303, no. 2 SPEC. ISS., pp. 344–347, Aug. 2006.
- [15] K. Hono and H. Sepehri-Amin, "Strategy for high-coercivity Nd-Fe-B magnets," *Scr. Mater.*, vol. 67, no. 6, pp. 530–535, Sep. 2012.
- [16] G. Lei, J. Zhu, Y. Guo, C. Liu, and B. Ma, "A review of design optimization methods for electrical machines," *Energies*, vol. 10, no. 12, 2017.
- [17] R. C. Eberhart and Y. Shi, "Particle swarm optimization: Developments, applications and resources," in *Proceedings of the IEEE Conference on Evolutionary Computation, ICEC*, 2001, vol. 1, pp. 81–86.
- [18] P. Ponomarev, I. Petrov, N. Bianchi, and J. Pyrhonen, "Selection of Geometric Design Variables for Fine Numerical Optimizations of Electrical Machines," *IEEE Trans. Magn.*, vol. 51, no. 12, Dec. 2015.
- [19] D. S. Weile and E. Michielssen, "Genetic algorithm optimization applied to electromagnetics: A review," *IEEE Trans. Antennas Propag.*, vol. 45, no. 3, pp. 343–353, 1997.
- [20] G. Lei, J. Zhu, and Y. Guo, *Multidisciplinary Design Optimization Methods for Electrical Machines and Drive Systems*. 2016.
- [21] K. Deb, A. Pratap, S. Agarwal, and T. Meyarivan, "A fast and elitist multiobjective genetic algorithm: NSGA-II," *IEEE Trans. Evol. Comput.*, vol. 6, no. 2, pp. 182–197, Apr. 2002.
- [22] G. B. L. Carlos A. Coello Coello, David A. Van Veldhuizen, *Evolutionary Algorithms for Solving Multi-Objective Problems*. Springer US, 2007.
- [23] B. Xin, L. Chen, J. Chen, H. Ishibuchi, K. Hirota, and B. Liu, "Interactive multiobjective optimization: A review of the state-of-the-art," *IEEE Access*, vol. 6, Institute of Electrical and Electronics Engineers Inc., pp. 41256–41279, 17-Jul-2018.
- [24] A. Golchha and S. G. Qureshi, "Non-Dominated Sorting Genetic Algorithm-II-A Succinct Survey," *Int. J. Comput. Sci. Inf. Technol.*, vol. 6, no. 1, pp. 252–255, 2015.
- [25] A. Jayswal and Preeti, "An exact II penalty function method for multi-dimensional first-order PDE constrained control optimization problem," *Eur. J. Control*, 2019.
- [26] G. Lei, K. R. Shao, Y. Guo, J. Zhu, and J. D. Lavers, "Improved sequential optimization method for high dimensional electromagnetic device optimization," in *IEEE Transactions on Magnetism*, 2009, vol. 45, no. 10, pp. 3993–3996.
- [27] G. Lei, K. R. Shao, Y. Guo, J. Zhu, and J. D. Lavers, "Sequential optimization method for the design of electromagnetic device," in *IEEE Transactions on Magnetism*, 2008, vol. 44, no. 11 PART 2, pp. 3217–3220.
- [28] K. T. Alfriend, S. R. Vadali, P. Gurfil, J. P. How, and L. S. Breger, "The Basics of Analytical Mechanics, Optimization, Control and Estimation," in *Spacecraft Formation Flying*, Elsevier, 2010, pp. 39–57.
- [29] A. R. Conn, N. Gould, and P. L. Toint, "A globally convergent Lagrangian barrier algorithm for optimization with general inequality constraints and simple bounds," *Math. Comput.*, vol. 66, no. 217, pp. 261–289, Jan. 1997.

University of Technology, Department of Electrical Power Engineering and Mechatronics. He is holding the position of Head of Electrical Machines Research Group. He is the member of IEEE and Estonian Society of Moritz Hermann Jacobi.

His main research interest is design of electrical machines.

Anour Belahcen was born in Essaouira, Morocco, in 1963. He received the BSc degree in physics from the University Sidi Mohamed Ben Abdellah, Fes, Morocco, in 1988 and the MSc (Tech.) and Doctor (Tech.) degrees from Helsinki University of Technology, Finland, in 1998, and 2004, respectively. He is the professor of electrical machines at Tallinn University of Technology, Estonia and in 2013 he became Professor of Energy and Power at Aalto University, Finland.

His research interest are modeling of electrical machines, magnetic materials, coupled magnetic and mechanical problems and magnetostriction.

Hamidreza Heidari was born in Zanjan, Iran, in 1989. He received the B.Sc. and M.Sc. degrees in electronic engineering from the University of Zanjan, Zanjan, Iran. He is currently working toward the Ph.D. degree in electrical engineering with Tallinn University of Technology.

His current research interests include analysis and control of electric machines.

Toomas Vaimann received his BSc, MSc and PhD degrees in electrical engineering from Tallinn University of Technology, Estonia, in 2007, 2009 and 2014 respectively. He is currently a senior researcher in Tallinn University of Technology, Department of Electrical Power Engineering and Mechatronics. He has been working in several companies as an electrical engineer. He is the member of IEEE, Estonian Society of Moritz Hermann Jacobi and Estonian Society for Electrical Power Engineering.

His main research interest is the diagnostics of electrical machines.

Anton Rassolkin received the Ph. D. degree in electric drives and power electronics from Tallinn University of Technology in 2014. He works as a Research Scientist at the Department of Electrical Power Engineering and Mechatronics at Tallinn University of Technology.

His main research interests are in the field of electric drives and their control systems as well as in the fields of electrical machines and electric transportation.

VI. BIOGRAPHIES

Ekaterina Andriushchenko received her BSc and MSc degrees in mechanical engineering from Peter the Great St. Petersburg Polytechnic University, Russia, in 2013 and 2019 respectively. She is currently working toward the Ph.D. degree in electrical engineering with Tallinn University of Technology.

Her current research interest is design optimization of electrical machines.

Ants Kallaste received his BSc, MSc and PhD degrees in electrical engineering from Tallinn University of Technology, Estonia, in 2004, 2006 and 2013 respectively. He is currently a senior researcher in Tallinn

Curriculum vitae

Personal data

Name: Ekaterina Andriushchenko
Date of birth: 15/01/1996
Place of birth: Russia
Citizenship: Russian

Contact data

E-mail: katarina.and96@gmail.com

Education

2019–now PhD, Tallinn University of Technology (Electrical Power Engineering and Mechatronics)
2017–2019 MSC, at Peter the Great St. Petersburg Polytechnic University (Institute of Machinery, Materials, and Transport)
2013–2017 BSC, at Peter the Great St. Petersburg Polytechnic University (Institute of Machinery, Materials, and Transport)

Language competence

English Fluent
Russian Native
German Intermediate

Elulookirjeldus

Isikuandmed

Nimi: Ekaterina Andriushchenko
Sünniaeg: 15/01/1996
Sünnikoht: Venemaa
Kodakondsus: Vene

Kontaktandmed

E-post: katarina.and96@gmail.com

Hariduskäik

2019–... PhD, Tallinna Tehnikaülikool (Elektroenergeetika ja mehhatroonika)
2017–2019 MSC, Peeter suure nimeline polütehniline ülikool (Masinate, materjalide ja transpordi instituut)
2013–2017 BSC, Peeter suure nimeline polütehniline ülikool (Masinate, materjalide ja transpordi instituut)

Keelteoskus

Vene keel Emakeel
Inglise keel Kõrgtase
Saksakeel Algtase

ISSN 2585-6901 (PDF)
ISBN 978-9949-83-984-1 (PDF)